Multi-Disciplinary Applications of Oceanographic Geophysical Data Collection

Dax Christian Soule

A dissertation
submitted in partial fulfillment of the
requirements for the degree of

Doctor of Philosophy
University of Washington
2016

Reading Committee:
Professor William Wilcock
Professor Emeritus Russell McDuff
Professor Kenneth Creager

Program Authorized to Offer Degree:
School of Oceanography

University of Washington

Abstract

Multi-Disciplinary Applications of Oceanographic Geophysical Data Collection

Dax Christian Soule

Co-chairs of the Supervisory Committee:

Professor William Wilcock
School of Oceanography

Professor Emeritus Russell McDuff
School of Oceanography

Geophysical data and methods are a key source for information about geologic features beneath the seafloor that are difficult to sample directly. Our knowledge of the Earth's structure has largely relied on our ability to apply classical physics to study the Earth's through the transmission of seismic and electromagnetic waves. As our data collection capabilities have benefited from technological advancements in connectivity, bandwidth, power usage, battery life and data storage, the scope of questions that can be addressed using seismology and other techniques is broadening. Larger data sets and increased bandwidth offer opportunities to explore multiple questions with individual data streams. This dissertation explores using seismology and other sources of time series data both as tools for exploring novel science questions but also as tools for teaching Earth science to students as they develop Science, Technology, Engineering, and Mathematics (STEM) skills. These analyses (1) create a model of crustal thickness and lower crustal velocities for crustal ages of 0.1-1.2 Ma on the Endeavour Segment of the Juan de Fuca Ridge by inverting travel times of crustal paths and non-ridge-crossing wide-angle Moho reflections obtained from a three-dimensional tomographic experiment; (2) use fin whale calls

recorded by a seafloor seismic network on the Endeavour segment of the Juan de Fuca Ridge to create over 150 whale tracks using new techniques and identify four characteristic inter-pulse intervals (IPIs) that indicate group size and swimming speed and direction; and (3) engage students in analysis of data collected by networks of environmental sensors, which are used to study various natural phenomena, such as nutrient loading, climate change, and stream discharge to compare approaches to implementation in an undergraduate time-series analysis course. These results demonstrate the utility of seafloor networks as both instruments of primary data collection and teaching tools.

TABLE OF CONTENTS

Page

LIST OF FIGURES

Figure Number Page

LIST OF TABLES

ACKNOWLEDGEMENTS

First and foremost I thank my advisors William Wilcock and Russell McDuff for their support and guidance. A graduate degree is a long journey and it takes many types of nurturing for any student to reach their full potential. William, thank you for being so generous with your time. You have challenged me in ways that I will benefit from for the rest of my life. Your high standards, your work ethic, your creativity, and your impeccable sincerity are qualities that I will model each and every day. Russ, thank you for all the care and support you have given. Your dedication to service, your kindness and your willingness to help me find the pathway to my own brilliance are gifts that I can only hope to one day give the students that I will mentor. Your willingness to be my advocate has made all the difference in the world. The two of you have given me a learning environment that has allowed me to thrive.

Texas A&M University was where this all started. My career change was born of a deep desire to have the opportunity to do something that I cared about. My father's encouragement and many levels of support as I made the transition back into an academic life was crucial. The Geology and Geophysics department gave me opportunities for which I will always be grateful. Mark Everett, Richard Carlson and Phillip Rabinowitz all took an interest in my development from the moment I set foot back on campus and played an active roll in making opportunities possible. These opportunities are the genesis of my career and I will spend the rest of my life trying to emulate their willingness to engage and the students I have the privilege work with.

I would like to thank Rebekka Gougis-Darner, the entire EDDIE community, and Mikelle Nuwer. Your willingness to open your doors and share opportunities with me has provided a pathway for exploring my passions. Rebekka, your insights on how students learn and how to

develop an educational manuscript will be tools that I employ for the rest of my career. Mikelle, your mentorship has been among the most important parts of my graduate career and I look forward to many years of collaboration.

I cannot thank enough my officemates Michelle Weirathmueller and Robert Weekly, and the rest of my Oceanography cohort whose friendships have buoyed me through the ups and downs of graduate school. Among the only types of real wealth a person may possess is the friendship of his peers and in this regard I am a very wealthy man.

Many thanks also to Doug Toomey, Emily Hooft, Ken Creager, Paul Johnson, and David Butterfield whose insight and assistance have proven invaluable. Doug and Emily, your willingness to invest your time, share your code and provide guidance at every step along the way made my tomography project possible. Ken, you taught me almost every seismology class I took here at UW and your helpfulness throughout my graduate career is something that I have come to count on. Paul, your fire for science is something that I hope to emulate. I am very grateful to have had the opportunity to work with you. David, I really appreciate the feedback you have given in our meetings both here and at NOAA. Your input as a non-seismologist shaped how I presented these results.

I would like to thank the captains and crews of the *R/V Langseth*, without whom data collection could never have happened. Thank you to the National Science Foundation for funding this research. I would also like to thank the School of Oceanography administrative staff for making science happen everyday.

Most of all I would like to thank my wife Michelle Soule. We met almost as soon I arrived in Seattle and you have supported my dreams each and every day. You have lived the graduate

school life every bit as much as I have and this accomplishment is just as much yours as it is mine. Thank you for being my partner in life. I love you.

Chapter 1:

Introduction and Organization of the Dissertation

The goal of this dissertation is to connect two separate studies that use seismic networks with a third study that uses digital data as a pedagogical tool in the classroom. The first research study of this dissertation used ocean bottom seismometers to make a 3-D tomographic image of the ocean crust along a mid-ocean ridge spreading center in order understand magma transport along the ridge axis and the extend that hydrothermal fluids reach the lower crust. The second research study used a seafloor seismic network to identify and locate fin whale vocalizations in order to better understand the relationship between their swimming and vocalization behaviors. Both studies relied on state of the art data analysis techniques and cutting edge technology. My desire to communicate these concepts broadly motivated a third research study in science education, which assesses techniques for using time series data to teach basic analytical skills to undergraduate students.

In Chapter 2, a model of crustal thickness and lower crustal velocities is obtained for crustal ages of 0.1-1.2 Ma on the Endeavour Segment of the Juan de Fuca Ridge by inverting travel times of crustal paths and non-ridge-crossing wide-angle Moho reflections obtained from a three-dimensional tomographic experiment (published in Geophysical Research Letters, June, 2016). The analysis of this data set involved extensive work with time-series data and utilized ~120,000 analyst-identified seismic arrivals. Making travel time "picks" is an iterative process that requires an analyst to identify changes in amplitude and frequency caused by a heterogeneous subsurface environment. The final result employed a wide range of statistical

concepts to optimize our preferred model and a variety of graphical methods to display and analyze the data set.

In Chapter 3, fin whale calls recorded from 2003-2004 by a seafloor seismic network on the Endeavour segment of the Juan de Fuca Ridge were analyzed in a completely novel manner to determine tracks and calling patterns (published in *Journal of the Acoustical Society of America*, March 2013). The methods employed in the fin whale study relied on the ability to detect events on a seismic record based on their spectra and utilized the spectrogram to both display fin whale calls and distinguish them from earthquakes. Because I was applying seismic localization techniques to a marine mammal problem, I was given many opportunities to present the concepts used to pick arrivals, model our results and demonstrate statistical significance in the findings to an audience that extended beyond the seismic community. These conversations revealed many conceptual gaps related to how sounds propagate through liquids and solids and how frequency and amplitude can vary in response to both range and the material properties through which they pass. Presenting my findings to the marine mammal research community developed our ability to present waveform data to audiences with no experience and lack a conceptual comfort with the relationship between the time and frequency domain. This led to my development of these topics from an educational perspective through the development of an EDDIE (Environmental Data-Driven Inquiry and Exploration) module focused on the relationship between data presented in both the time and frequency domain.

In Chapter 4, EDDIE modules are used to engage students in analysis of data collected by networks of environmental sensors to study various natural phenomena such as nutrient loading, climate change, and stream discharge. We compared two approaches to EDDIE module implementation in an undergraduate time-series analysis course. Course goals were to use high-

frequency and long-term environmental datasets to improve quantitative literacy, develop data manipulation and analysis skills, construct scientific knowledge about natural phenomena, and highlight the inherent variability in real data. In this context we developed a new EDDIE module that uses seismic data to address the conceptual gaps we encountered presenting our Chapter 3 results. The Spectral Seismology module makes a conceptual presentation of waveforms and filters in order to help students go beyond the basic terminology used to describe waveforms and relate a signal presented in the time domain to its conjugate in the frequency domain.

Chapter 5 summarizes the key findings of this work, and considers how these studies could be followed with future work.

Chapter 2:

Near-Axis crustal structure and thickness of the Endeavour Segment, Juan de Fuca Ridge

Dax C. Soule[1], William S. D. Wilcock[1], Douglas R. Toomey[2], Emilie E. E. Hooft[2], and Robert T. Weekly[1,3]

[1]School of Oceanography, University of Washington, Seattle WA 98115
[2]Department of Geological Sciences, University of Oregon, Eugene, OR 97403-1272
[3]Now at Incorporated Research Institutions for Seismology Data Management Center, Seattle, WA 98105

2.0 Abstract

A model of crustal thickness and lower crustal velocities is obtained for crustal ages of 0.1-1.2 Ma on the Endeavour Segment of the Juan de Fuca Ridge by inverting travel times of crustal paths and non-ridge-crossing wide-angle Moho reflections obtained from a three-dimensional tomographic experiment. The crust is thicker by 0.5-1 km beneath a 200-m-high plateau that extends across the segment center. This feature is consistent with the influence of the proposed Heckle melt anomaly on the spreading center. The history of ridge propagation on the Cobb overlapping spreading center may also have influenced the formation of the plateau. The sharp boundaries of the plateau and crustal thickness anomaly suggest that melt transport is predominantly upward in the crust. Lower crustal velocities are lower at the ends of the segment, likely due to increased hydrothermal alteration in regions influenced by overlapping spreading centers, and possibly increased magmatic differentiation.

2.1 Introduction

2.1.1 Mid-Ocean Ridges

At mid-ocean ridges, measurements of crustal thickness are an important tool for understanding the magmatic and volcanic processes that form oceanic crust. Amongst the geophysical tools available to estimate crustal thickness and structure, seismic tomography using crustal arrivals and Moho reflections (*Pg* and *PmP* phases, respectively) is well-suited to distinguish variations in crustal thickness from variations in the seismic velocities of the lower crust. As such this method provides reliable constraints on magma flux from the mantle to crust, the composition and temperature of the lower crust, and by inference patterns of magma redistribution within the crust.

At the slow-spreading Mid-Atlantic Ridge (MAR), both seismic [*Hooft et al., 2000, Tolstoy et al., 1993; Dunn et al.,* 2005] and gravity [*Lin et al.,* 1990; *Detrick et al.,* 1995] studies show that magmatic and volcanic accretion is spatially variable with the thickest crust found near the center of each ridge segment coincident with the shallowest bathymetry. The seismic images further show that crustal thickness variations result primarily from differences in lower crustal thickness [*Hooft et al., 2000, Mutter and Mutter*, 1993*, Tolstoy et al., 1993*]. These patterns are consistent with competing accretionary models, where either buoyant mantle flow [*Lin and Phipps Morgan,* 1992] or melt migration processes [*Magde et al.*, 1997] focus mantle-derived melt toward the segment center. Previous seismic studies also infer that some melt supplied to the segment centers is redistributed along axis in the upper crust by brittle diking events; however, to what degree the upper and lower crust at segment ends are formed by along-axis transport of magma, versus vertical delivery from the mantle, remains an open question [*Hooft et al.,* 2000; *Dunn et al.,* 2005; *Magde et al.,* 2000].

Along the fast-spreading East Pacific Rise (EPR) at 8-10°N, melt delivery from the mantle to the crust is effectively continuous throughout tectonically-defined ridge segments [*Toomey et al.,* 2007]. At the segment scale, the primary feature in crustal thickness maps is a broad band of thickened crust that forms behind the wake of the 9°03' overlapping spreading center (OSC) [*Canales et al.,* 2003]. Between tectonic offsets, centers of melt delivery from the mantle to the crust are spaced at intervals of ~25 km [*Toomey et al.,* 2007], effectively defining volcanic or third-order segmentation of the ridge. Seismic studies of the mantle, lower crust, and mid-crustal axial magma chamber all conclude that along-axis transport of melt at mantle or crustal depths is unlikely at the scale of a tectonically-defined ridge segment. To what degree melt is redistributed at the scale of third-order or volcanic-scale segmentation is unknown, although detailed studies of the AMC reflector near 9˚50'N suggest that vertical transport of melt in the lower crust likely resupplies the upper crustal magma chamber [*Aghaei et al.,* 2014; *Carbotte et al.*, 2013].

2.1.2 Regional Setting

In this paper, we use seismic tomography to examine the variations in off-axis crustal thickness and lower crustal velocity at the Endeavour segment of the Juan de Fuca Ridge (Figure 2.1). This is an intermediate spreading-rate ridge which has some characteristics of both slow- and fast-spreading ridges. The central portion of the ridge is underlain by a mid-crustal magma chamber similar to that seen at the EPR [*Van Ark et al.,* 2007]. Somewhat like the MAR although more muted, there are variations in elevation along the spreading axis; the segment center comprises a plateau which extends out to crustal ages of ~0.71 Ma and is elevated ~200 m relative to adjacent regions [*Carbotte et al.*, 2008]. The segment is bounded by OSCs that are similar to those seen on the EPR. Although there is a considerable amount of melt stored at mantle depths beneath the

OSCs [*VanderBeek et al.*, 2014], the limbs are not in most places underlain by a crustal magma chamber [*Carbotte et al.*, 2006; *Van Ark et al.*, 2007]. Along axis variations in upper crustal structure show similarities to both the MAR and EPR [*Weekly et al*., 2014]. The Endeavour thus, represents a good site to further investigate the roles of axial magmatic systems and ridge segmentation in shaping the volcanic structure of oceanic crust.

2.2 Experiment and Methods

2.2.1 Survey Design

In 2009 we conducted a seismic tomography experiment on the Endeavour segment of the Juan de Fuca Ridge using 64 ocean bottom seismographs (OBSs) to record ~5,500 airgun shots from the 36-element, 6600 in^3 array of the *R/V Marcus G. Langseth* (Figure 2.1). *Weekly et al.* [2014] inverted 93,000 crustal *P*-wave (*Pg*) arrivals for the segment-scale isotropic and anisotropic velocity structure of the upper oceanic crust. The models are characterized by low velocities at the segment ends relative to the segment center that were interpreted in terms of increased fracturing in the upper crust created near the OSCs and possibly less hydrothermal infilling of porosity. More recently *Morgan et al.* [2016] have used full-waveform inversions to improve the resolution of shallow upper crustal structure in the central portion of the experiment footprint.

In this study, the goal is characterize lower crustal structure and thickness off axis using wide-angle, Moho-reflected *P*-wave arrivals (*PmP*); future work will expand these models to the ridge axis where axial crustal magma bodies complicate the analysis. Approximately 19,000 *PmP* arrival times were iteratively handpicked for non-ridge crossing paths with reflection points at crustal ages of 0.1 – 1.2 Ma. Uncertainties were visually estimated on the basis of the signal-to-noise ratio and trace-to-trace coherency. In the Supporting Information, Text S1 and Figures

S1-S3, we provide details of our process for picking *PmP* arrivals and show examples of record sections with *PmP* picks.

2.2.2 Modeling

The starting velocity model for our inversion is a three-dimensional isotropic model obtained by inverting the *Pg* dataset of *Weekly et al.* [2014]; to obtain this starting model we used an inversion strategy similar to theirs, except that we do not include the effects of upper crustal anisotropy and we use a creeping strategy as opposed to jumping [*Shaw and Orcutt, 1985*]. The results of this creeping inversion yield an upper crustal model in which all signal that can be attributed to upper crustal structure has been accounted for prior to inverting for lower crustal structure. Velocities in this model at 5.6 km depth, the largest depth sampled anywhere by *Pg* in the model of *Weekly et al.* [2014], are extended downward to create a starting model for the *PmP* inversion (Figure 2.2a). A Moho interface is draped from a smoothed version of the seafloor at 6.8 km depth. The *Pg* and *PmP* arrivals were then inverted jointly using the method of *Dunn et al.* [2005] and a jumping strategy [*Shaw and Orcutt*, *1985*]. Including the *Pg* arrival times ensures that the inversion retains the upper crustal structure required by the *Pg* data while the *PmP* arrival times constrain the lower crustal velocity and crustal thickness

The inverse method [*Dunn et al.,* 2005] iteratively solves for perturbations to the starting crustal isotropic slowness and crustal thickness model by minimizing the variance of the travel time misfit and imposing smoothing and dampening terms with user-defined weights. We used perturbational nodes for slowness of 1 km and 0.25 km in the horizontal and vertical directions, respectively, and 2.5 km on the Moho interface. We systematically explored different choices of smoothing parameters to find the smoothest model with an acceptable fit to the travel time data and employed inversions of synthetic data to demonstrate that the primary features are well

resolved. Our preferred model fits the data to its uncertainties (see Supporting Information, Figure S4) and is insensitive to the starting model (see Supporting Information, Figure S5).

2.3 Results

2.3.1 Crustal Thickness

Figure 2.3 shows maps of crustal thickness and lower crustal velocity anomalies obtained from tomographic inversion of *Pg* and *PmP* data. The mean crustal thickness in resolved regions is 6.8 km, and the range is 5.9 km - 7.7 km. The most prominent feature of the model is a region of thicker crust beneath the central Endeavour that coincides with the bathymetric plateau (Figure 2.3a, areas 1 and 2). In addition crust is thicker in smaller regions to the southeast of the plateau (area 3) and to the north just west of the Endeavour Ridge.

The boundaries of the thicker crust, in the center of the segment, correspond closely with edges of the bathymetric plateau; while wide angle reflections do not have good horizontal resolution, modeling that tested the sensitivity of the inversion to the sharpness of the transition suggest that the data are consistent with a sharp transition in crustal thickness at the edges of the plateau (see Supporting Information, Figures S6-S8). Well off-axis, the average crustal thickness beneath the plateau (areas 1 and 2 on Figure 2.2a) is ~0.5-1 km greater than adjacent sites away from the plateau (areas 4 and 5). Crustal thickness beneath the plateau is asymmetric; the thickness on the Juan de Fuca plate is about 0.3 km greater than on the Pacific plate. In addition, there appears to be a decrease in crustal thickness beneath the plateau towards the ridge axis.

2.3.2 Lower Crustal Velocity

Lower crustal velocities are not imaged directly beneath the ridge axis but are depressed in a band that extends about 3-5 km to either side (Figure 2.3b-d). As for the upper crust

[*Weekly et al.*, 2014], velocities in the lower crust are elevated in the segment center in an area that includes the bathymetric plateau and extends about 10 km to the south. Average velocities in the segment center (areas 1 and 2 on Figure 2.2a) are ~0.15 km/s higher than those found near the segment ends (area 4). This leads to a noticeable correlation between lower crustal velocities and crustal thickness (Figure 2.2b). Lower crustal velocities are also slightly asymmetric across the central Endeavour with average velocities ~0.1 km/s higher on the Juan de Fuca plate. The correlation between crustal thickness and lower crustal velocity beneath the plateau is the opposite of what would be expected if the inversion mapped some of the increased *PmP* travel times from thicker crust into velocity; synthetic inversions confirm that there is little tradeoff between crustal thickness and velocity in this region (see Supporting Information, Figures 2.4-2.11).

2.4 Discussion

2.4.1 Crustal Thickness

The observation of thicker crust beneath the plateau is consistent with the results of *Carbotte et al.* [2008], who estimated a similar crustal thickness increase beneath the plateau from the analysis of vertically incident Moho reflections in a multichannel seismic profile. However, unlike this earlier study, we see no evidence for thicker crust extending beyond the western limit of the plateau towards the Heckle seamount chain. As reported by *Carbotte et al.* [2008], the crustal thicknesses are consistent with the central plateau being isostatically supported by a thicker crust. For example, assuming a lower crustal density of 2950 kg m^{-3} [*Carlson and Miller*, 2004] and a mantle density of 3300 kg m^{-3} [*McKenzie et al.*, 2005], the ~200-m-high plateau would be isostatically compensated by an increase in lower crustal thickness of ~1.1 km [e.g., *Turcotte and Schubert*, 2002]. This is a reasonable match to the upper limit of the observed

crustal thickening but given the uncertainties in parameters, the seismic data cannot rule out an isostatic contribution from crustal density changes [e.g., *Toomey and Hooft,* 2008].

Carbotte et al. [2008] attribute the thicker crust beneath the plateau to enhanced mantle melt production resulting from the Juan de Fuca Ridge overriding the melting anomaly that created the Heckle Seamount chain. They note that the onset of thicker crust at 0.71 Ma coincided with a lengthening of the Endeavour segment and a temporary reversal of the long-term northward propagation of the Cobb OSC. The sharp western and eastern boundaries of the plateau and the absence of thicker crust west of the plateau imply that the Heckle melt anomaly transitioned quickly from supporting the growth of off-axis seamounts to feeding the spreading center.

If the plateau is the result of a Heckle melting anomaly, our data suggest that the influence of the anomaly is waning because crustal thickness beneath the plateau decreases substantially towards the ridge axis. Our inversion excludes *PmP* travel times for ridge crossing paths, which reduces the number of Moho reflections near the ridge axis, but synthetic inversions with the same ray geometry and travel times based on a uniform thickness crust beneath the plateau, show only a small decrease in apparent crustal thickness towards the ridge axis (Supporting Information, Figure 2.11a) suggesting that the observed crustal thinning is not an artifact of uneven ray coverage. *Carbotte et al.* [2008] suggest that renewed northward propagation of the Cobb OSC in the past 100,000 years as the Northern Symmetric Segment lengthens [*Johnson et al.,* 1983, *Shoberg et al.*, 1991] is consistent with a waning influence of the Heckle melt anomaly. In addition the chemistry of basalts along the Endeavour has been interpreted in terms of a failing rift that is underlain by diminishing mantle melting [*Karsten et al.,* 1986]. Our results are consistent with these interpretations, but other interpretations are possible, as discussed below.

It is difficult to explain the across-axis asymmetry in crustal thickness beneath the plateau in terms of the migration of the Heckle melt anomaly. The westward migration of the spreading axis toward a mantle heterogeneity is predicted to produce increased melting beneath the Pacific plate [*Davis and Karsten*, 1986]. *Carbotte et al*. [2008] identify a small recent eastward jump of the Endeavour spreading axis based on across-axis asymmetry in the width of the Brunhes magnetic anomaly, which they interpret as evidence that the Heckle melt anomaly has moved east of the ridge axis. However, this is a recent event and the asymmetry in crustal thickness is most pronounced on the outer flanks of the plateau.

It is possible that the asymmetry reflects across axis differences in the structure of the Moho. If the Moho transition zone is thicker beneath the Pacific Plate and first-arriving *PmP* picks tend to be for reflection near the top of the transition zone then the crustal thicknesses may be biased shallower beneath the Pacific plate. The *PmP* arrivals are harder to pick for paths on the Pacific Plate and the RMS travel time residuals for the inversion are markedly larger for paths traversing area 1 than area 2 (23.5 ms versus 18.2 ms, Supporting Information Figure 2.7f, h). This might indicate that the Moho structure is more complex beneath the Pacific side of the plateau.

Alternatively the propagation history of the Cobb OSC may have led to the formation of an asymmetric plateau. *VanderBeek et al.* (2014) argue that the advancing limb of an OSC taps melt that ponds beneath the overlap basin, leading to thickened crust in its wake. At the Endeavour, the onset time and position of the plateau coincide with the northernmost advance of the North Symmetric segment prior to the Brunhes-Matuyama reversal [*Carbotte et al.*, 2008] (Figure 2.1). According to this model the subsequent southward growth of the Endeavour segment would have generated thicker crust in the vicinity of the plateau by tapping mantle melt that was asymmetrically concentrated beneath the Juan de Fuca Plate. This mechanism could

have acted in concert with the capture of the Heckle melt anomaly. However, we note that *Dziak et al.* [2006] argue that the seamount chains to the west of the Endeavour coincide with strike slip faults associated with southward reorganization of the Juan-de-Fuca / Pacific / North American triple junction, an explanation that does not require that the Heckle seamount chain results from a small melting anomaly fixed within the mantle reference frame. Thus, it is possible to produce chains of seamounts and a near-axis bathymetric plateau without invoking a mantle melt anomaly.

The characteristics of the plateau support a model in which along-axis melt transport is inefficient in the lower crust. The axial magma chamber that is present at the segment center can presumably feed diking events that propagate to the segment ends [*Van Ark et al.*, 2007] and there is evidence of recent diking events on the northern Endeavour propagating southward, presumably in the upper to mid-crust, from a melt source near Endeavour Seamount [*Hooft et al.*, 2010; *Weekly et al.*, 2013]. However, the sharp northern and southern edges of the plateau and of the crustal thickness variations that appear to support it isostatically suggests the temperatures of the lower crust away from the plateau are insufficient for ductile flow to transfer lower crustal material to the segment ends. On the basis of our results, we infer that melt transport at lower crustal levels is predominantly in the vertical direction. Similar inferences have been made for both the Mid-Atlantic ridge [*Hooft et al.,* 2000] and the East Pacific Rise [*Carbotte et al.,* 2013].

2.4.2 Lower Crustal Velocity

The near and off-axis lower crustal velocity model is consistent with the results from the EPR, which show that the axial magmatic system in the lower crust solidifies and cools within a few kilometers of the ridge axis [*Dunn et al.*, 2000]. Although our velocity model does not extend to the ridge axis, velocities generally decrease toward the ridge by about 0.2 km/s,

relative to velocities at a distance of ~5 km off-axis. This imaged velocity anomaly can be explained by a temperature change of ~200°C [*Christensen*, 1979], relative to lower crustal temperatures well off axis. Thus while we have not imaged the axial magmatic system, we can infer that its cross-axis width is less than 10 km

Ridge-parallel velocity variations in the lower crust well off-axis may be related to variations in hydrothermal alteration. *Weekly et al.* [2014] interpreted lower velocities in the upper and middle crust at the segment ends in terms of increased porosity due to enhanced fracturing associated with deformation in the overlapping spreading centers. It is unlikely that porosity can explain the lower crustal velocity variations; a porosity change approaching 1% is required generate the observed velocity variation of 0.15 km/s but the overburden pressure in the lower crust likely limits maximum porosities to <0.5% [*Carlson and Herrick*, 1990; *Iturrino et al.*, 1991]. A more likely explanation is that the presence or absence of talc and/or serpentine in the microcracks of olivine crystals has a substantial effect on the elastic properties of Gabbro [*Carlson et al.*, 2009]. Thus, the lower velocities at the segment ends are likely a result of enhanced hydrothermal alteration promoted by increased fracturing of the upper crust. Likewise, at the segment center the velocities we observe are higher than 7 km/sec which may indicate that alteration is less than typical for lower crustal gabbros [*Carlson and Miller,* 2004].

An alternative explanation for the higher lower crustal velocities near the segment center is that they are related to compositional variations [*Toomey and Hooft*, 2008]. If the lower crust near the segment center has undergone less differentiation than at the segment ends it will have higher velocities [*Iturrino et al.*, 1991]. It will also have lower densities that might contribute to the isostatic compensation of the plateau. We note that at the Lau back arc basin, *Arai and Dunn* [2014] also observe a positive correlation between lower crustal velocity and crustal thickness

which they attribute to variable influences of water released from the subducting slab. However, the slope of their fit is larger from ours (~0.4 s^{-1} versus ~0.15 s^{-1}), which supports a different causative mechanism.

Two smaller areas of thicker crust are also present within our model. The first connects to the southeast corner of the plateau and coincides with a region of disturbed topography that formed during the northward propagation of the Northern Symmetric segment prior the Brunhes-Matuyama reversal [*Carbotte et al.*, 2008]. It may thus be a region of crustal thickening that formed behind the tip of the propagator [*Canales et al.*, 2003; *Marjanović et al.,* 2011, *VanderBeek et al.*, 2014]. Crustal velocities in this region are relatively low, which is consistent with a region of differentiated magmas as is often observed near propagating ridge tips [e.g., *Sempere et al.*, 1984].

The second smaller area of thicker crust lies within the overlap basin of the West-Valley Endeavour OSC and is immediately north of a region of thin crust near the spreading axis that cuts into the plateau. The thin crust coincides with a region of intense ongoing seismicity that is interpreted as a region of extension at the southernmost limit of the West Valley propagator [*Weekly et al.*, 2013]. The thicker crust to the north is harder to explain – it is beneath the advancing part of the overlap basin rather than behind it as the OSC models predict [*Marjanović et al.,* 2011, *VanderBeek et al.*, 2014] and is south of the region of enhanced mantle melt concentrations imaged beneath the center of the OSC [*VanderBeek et al.*, 2014].

2.5 Conclusions

We present the results of a tomographic inversion for crustal thickness and lower crustal velocities on the Endeavour segment of the Juan de Fuca Ridge using Moho reflections for paths that do not cross the ridge axis. Our results confirm that a 200-m high bathymetric plateau

extending out to crustal ages of 0.71 Ma is underlain by a region of crust that is thicker by 0.5-1.0 km with higher apparent thicknesses on the east flank. The crustal thickness increases may be sufficient to support the plateau isostatically but the seismic data cannot rule out a contribution from crustal density variations. The symmetric component of crustal thickness beneath the plateau can be explained by the spreading center overriding the Heckle melting anomaly [*Carbotte et al.*, 2008]. Alternatively, the asymmetry and perhaps some of the symmetric component may result from the history of ridge propagation in the Cobb OSC [*VanderBeek et al.*, 2014]. The sharp boundaries of the plateau suggest that the lower crust is too cool near the segment ends for ductile flow to even out crustal thickness and that melt transport within the crust is primarily vertical as previously inferred at the Mid-Atlantic Ridge and East Pacific Rise. Gradients in crustal velocity near the ridge axis suggest that the axial magmatic system cools within a few kilometers of the ridge axis as is observed at the EPR [*Dunn et al.*, 2000]. Depressed lower crustal velocities in crust created at the ends of the segment are most likely a result of a combination of enhanced hydrothermal alteration and compositions that are more differentiated.

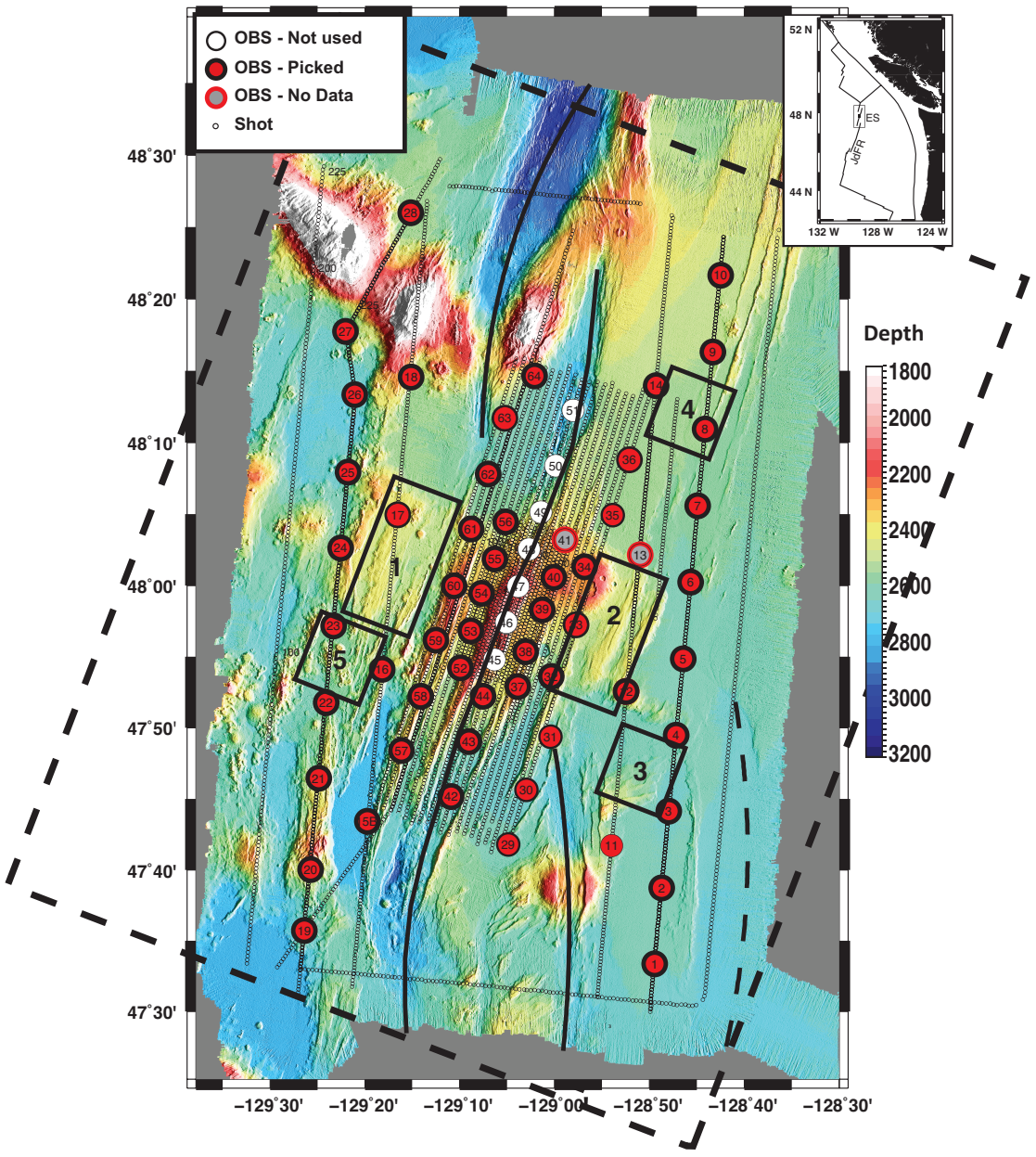

Figure 2.1 – Bathymetric map of the Endeavour Segment of the Juan de Fuca Ridge showing the configuration of the tomography experiment with shots shown as small open circles and OBSs as large circles labeled with the site number and colored red for OBSs used in this study, white for

OBS not used, and grey for OBSs that did not return data. The dashed box shows the bounds of the X-Y grid used for the inversions. Also shown are the locations of plate boundaries (solid lines), a relict propagating rift of the Cobb OSC (dashed line) and 5 numbered boxes that bound areas used to calculate average crustal velocities in Figure 2.2. Areas 1 and 2 cover off-axis portions of central Endeavour plateau on the Pacific and Juan de Fuca plates, respectively, area 3 overlies an area impacted by the Cobb OSC, and areas 4 and 5 are representative areas of crust off the plateau on the Pacific and Juan de Fuca plates, respectively. The inset figure shows the location of the study area in relation to the coast of the Pacific Northwest and plate boundaries with labels as follows: JdFR – Juan de Fuca Ridge, ES – Endeavour Segment.

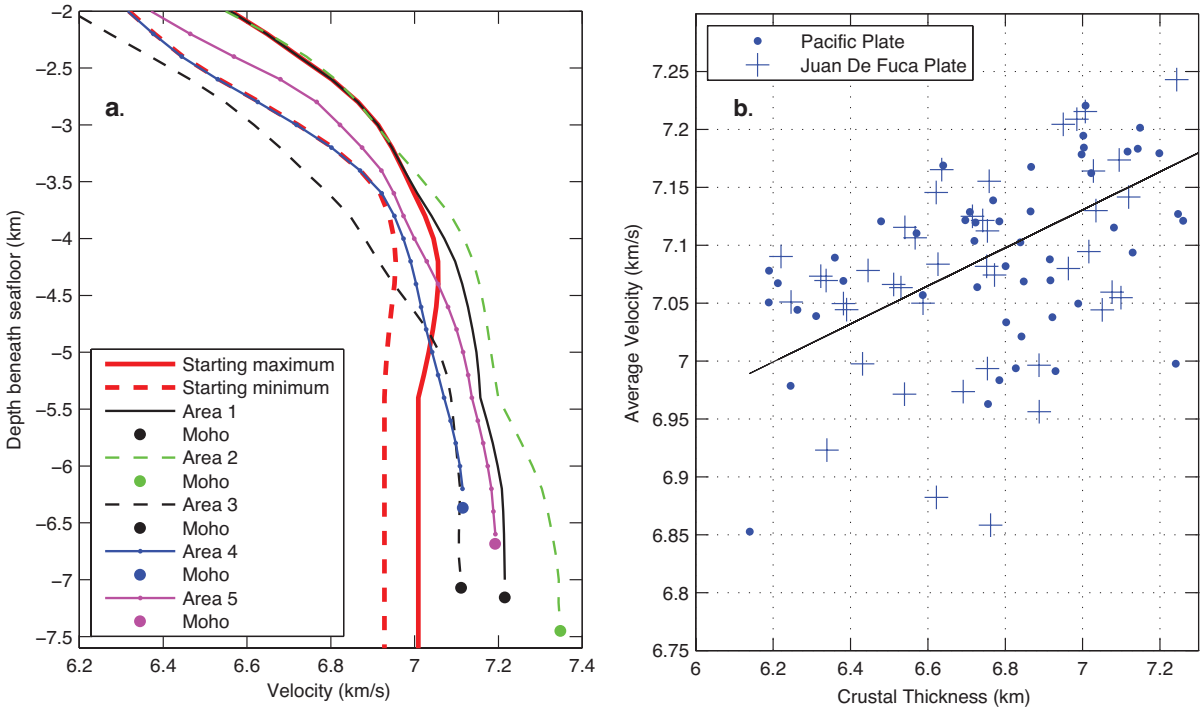

Figure 2.2 – (a.) Vertical velocity profiles for the mid- to lower crust showing the minimum and maximum velocities in the starting model (bold red dashed and solid lines, respectively) and horizontal averaged velocity in the preferred model for areas 1 (black solid), 2 (green dashed), 3 (faint black dashed), 4 (blue solid with dots) and 5 (magenta solid with dots) (see Figure 1). These profiles have gradients that are pretty typical for normal oceanic crust. Also shown by terminal dots are mean crustal thickness in each area which are 7.2 km for area 1, 7.5 km for area 2, 7.1 km for area 3, 6.4 km for area 4 and 6.7 km for area 5. (b.) Average velocity over the lower 2 km of crust plotted versus crustal thickness for the Pacific plate (dots) and Juan de Fuca plate (pluses). Averages were obtained for 5 km by 5 km grid squares and are limited to regions with ray coverage ≥10 km from the spreading axis. There is a noticeable positive correlation between lower crustal velocities and crustal thickness (black line, $R^2 = 0.4$).

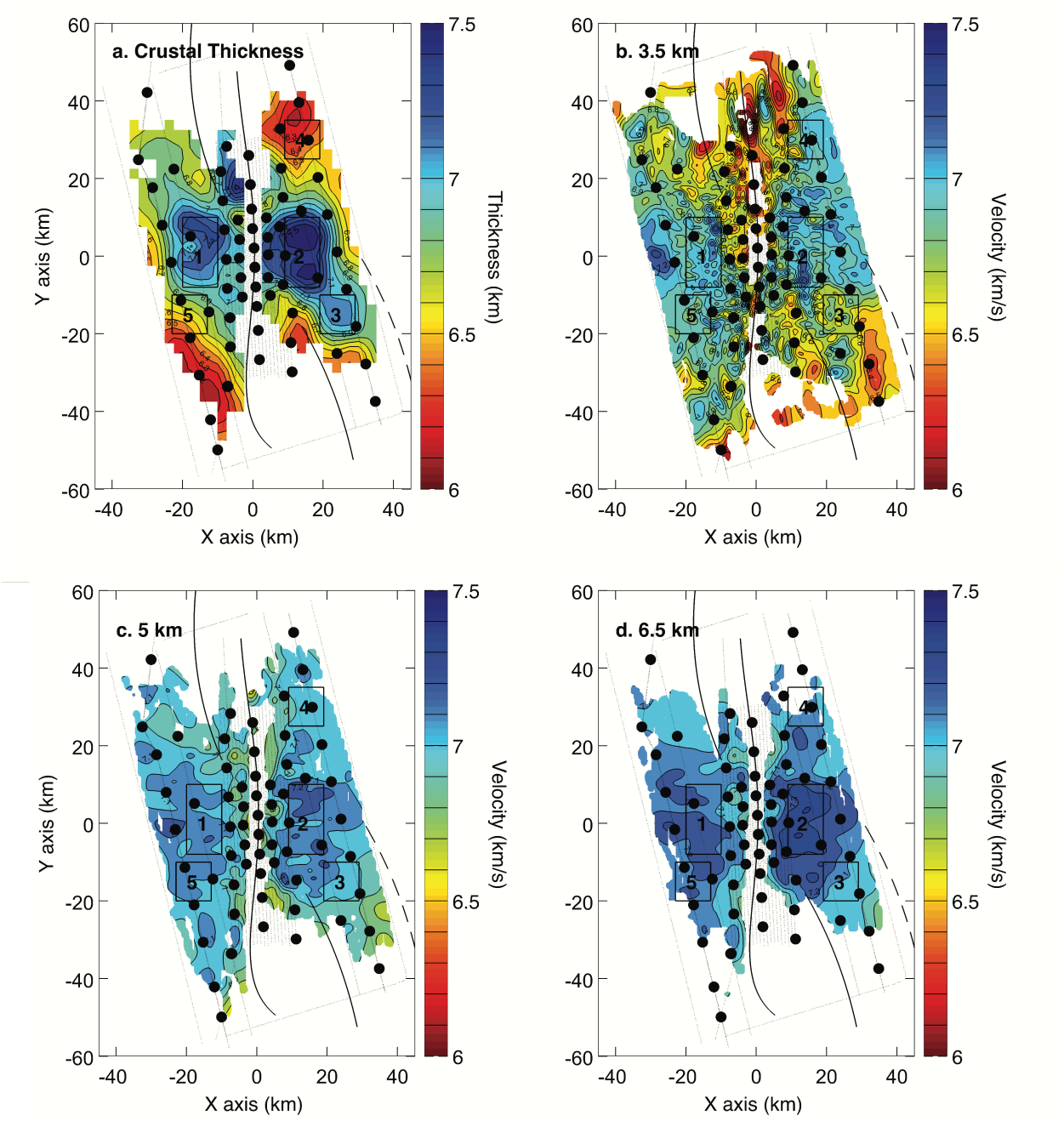

Figure 2.3 – Contour plots showing (a) crustal thickness and crustal velocity at (b) 3.5 km (c) 5 km and (d) 6.5 km depth for the preferred inversion with masking in regions with no ray coverage. Also shown are the plate boundaries (solid black lines), the relict propagator (dashed

black line), the locations of OBSs (filled black circles) and shots (dots), and the five areas used to calculate the averaged vertical profiles shown in Figure 2.2 (numbered boxes).

2.6 Supporting Information[1]

2.6.1 Introduction

Our supporting information details the analytical process we used to arrive at and validate our final model. In this supporting document we provide details of the process we used for picking the seismic arrivals, provide plots of the data residuals, show additional inversions that demonstrate that our results are insensitive to our starting models, and describe tests of the inversion's ability to discriminate between changes in crustal thickness and lower crustal velocity beneath the plateau that are based on inversions of synthetic arrival times.

2.6.2 *Picking*

We used an iterative approach to compile our catalogue of *PmP* travel times. Initially the joint inversion of *Pg* and *PmP* times only included *PmP* picks along the ridge-parallel refraction profiles on the outer portions of the experiment footprint (Figure 2.1). Picks with large residuals were inspected to eliminate mis-picks and the data re-inverted. Using the predicted arrivals from the latest inversion as a guide, we then incrementally added picks to the inversion for paths between refraction profiles, for shots and receivers on the outer lines of the dense shooting grid, and finally for all remaining non-ridge-crossing shot-receiver pairs. At each step mis-picks were eliminated and the data re-inverted.

Secondary *PmP* arrivals can be challenging to pick and we adopted two approaches to improving the consistency of picks. First, because complex bathymetry distorts the timing of arrivals in a conventional record section plotted with a reduction velocity (Figure S1a), we picked *PmP* on record sections that were flattened on the predicted time of the *Pg* arrival for the

[1] This was published as an online supplement.

model of *Weekly et al.* (2014) (Figure S1b). Second, we picked the second cycle of the *PmP* waveform and then applied a correction to adjust it to the time of the first arrival. The second cycle of both *Pg* and *PmP* waveforms in our data set have much larger amplitudes than the first (Figure S2). Because the onset of the *PmP* waveform is often obscured by the *Pg* waveform, it is easier to pick the onset of the second cycle of the *PmP* arrival and apply a time correction that we estimated from inspecting waveforms to be -0.05 s for the filtered data.

The primary source of uncertainty in *PmP* picks arises from the uncertainty in visually identifying the onset time of a secondary phase [*Barclay et. al.,* 1998]. We assigned uncertainties of 15 ms or 30 ms to each pick (Figure S2) based on a subjective assessment of the signal to noise, the consistency of waveforms between adjacent traces and whether the *PmP* appeared to be interacting with the *Pg* arrival.

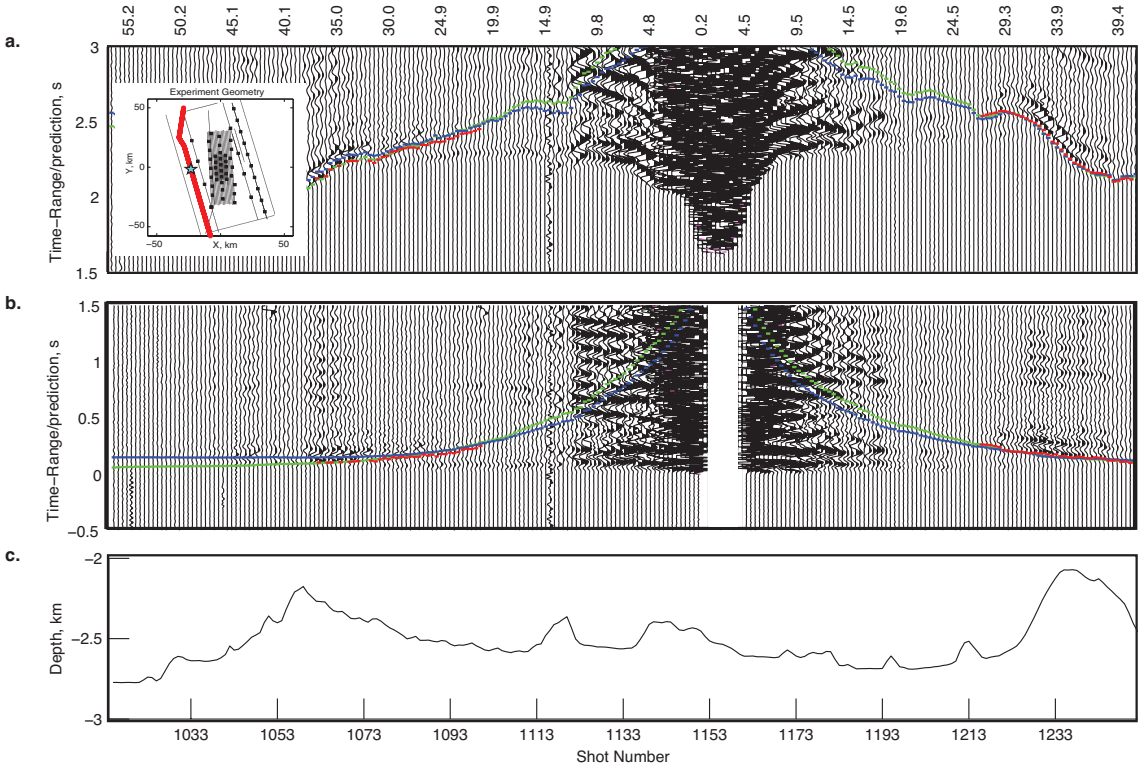

Figure 2.4. Record section plotted for OBS 24 (Figure 1) for a ridge-parallel refraction profile on the Pacific plate with (a) a reduction velocity of 6.8 km/s and (b) times zeroed at the predicted Pg arrival time for the model of *Weekly et al.* [2014] and (c) the bathymetric profile along the refraction line. Record section are plotted after applying a 5-40 Hz bandpass filter and show the picked PmP times (bold red ticks) and predicted times for our preferred model (green ticks). Labels on the top show the range of shots in kilometers. The inset map on (a) shows the experiment geometry with the location of the OBS (blue star) and the shots along the profile (reds line). The effect of flattening the profile on the predicted Pg arrival times is to eliminate the complex patterns of PmP arrival times that result from bathymetry along the profile.

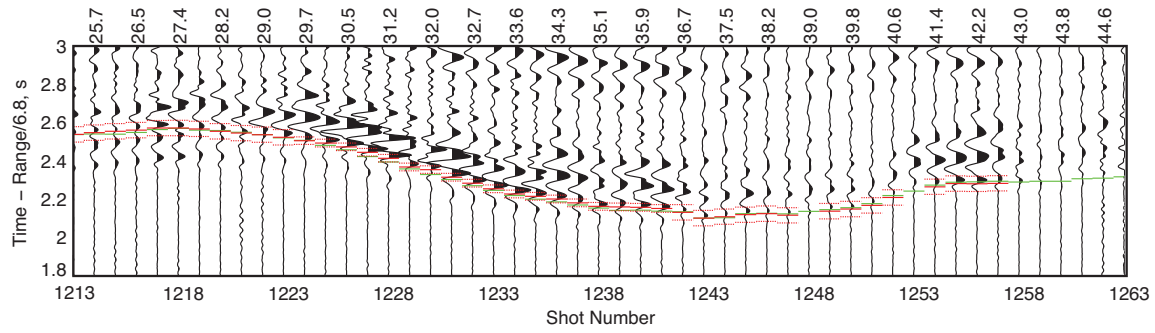

Figure 2.5. Portion of the record section shown in Figure 2.4a showing examples of picks with uncertainties estimated at 15 ms (shots 1222-1241) and 30 ms (shots 1213-1221 and 1242-1263) (dotted red ticks). Higher uncertainties are assigned to picks with lower signal to noise, overlapping Pg and PmP, and less consistency in the shape of waveforms between adjacent traces.

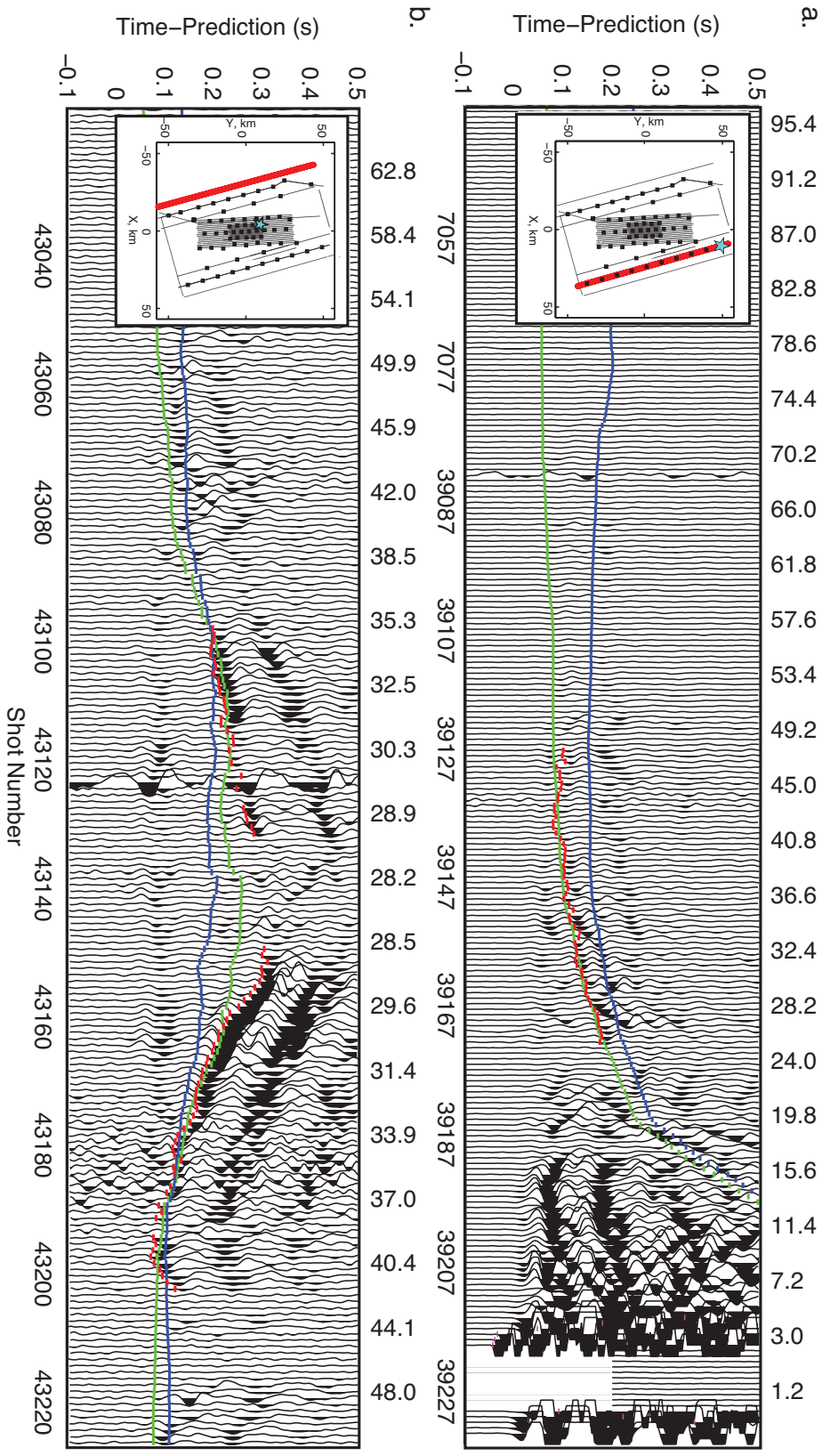
a.
b.
Time−Prediction (s)
Time−Prediction (s)
−0.1
0
0.1
0.2
0.3
0.4
0.5
Y, km
X, km
−50
0
50
7057
7077
39087
39107
39127
39147
39167
39187
39207
39227
95.4
91.2
87.0
82.8
78.6
74.4
70.2
66.0
61.8
57.6
53.4
49.2
45.0
40.8
36.6
32.4
28.2
24.0
19.8
15.6
11.4
7.2
3.0
1.2
43040
43060
43080
43100
43120
43140
43160
43180
43200
43220
62.8
58.4
54.1
49.9
45.9
42.0
38.5
35.3
32.5
30.3
28.9
28.2
28.5
29.6
31.4
33.9
37.0
40.4
44.1
48.0
Shot Number

Figure 2.6. Example record sections for (a) a conventional refraction profile recorded by OBS 10 on the Juan de Fuca plate to the east of the central plateau with *PmP* arrivals reflecting in regions of normal seafloor depth and (b) a fan of shots from the westernmost shooting line recorded by OBS 56 just west of the ridge axis on the Pacific Plate with some *PmP* arrivals reflecting beneath the plateau. Traces are plotted with times relative to the predicted Pg arrival time of *Weekly et al.* [2014] showing PmP travel time picks (bold red ticks) and PmP predictions of the starting (blue line) and preferred (green line) model. Labels on the top of the sections show the shot-receiver ranges in kilometers. A 5-40 Hz bandpass filter has been applied to traces in each record section. Inset figures show the source receiver-geometries with red lines for the shots and a light blue star for the OBS.

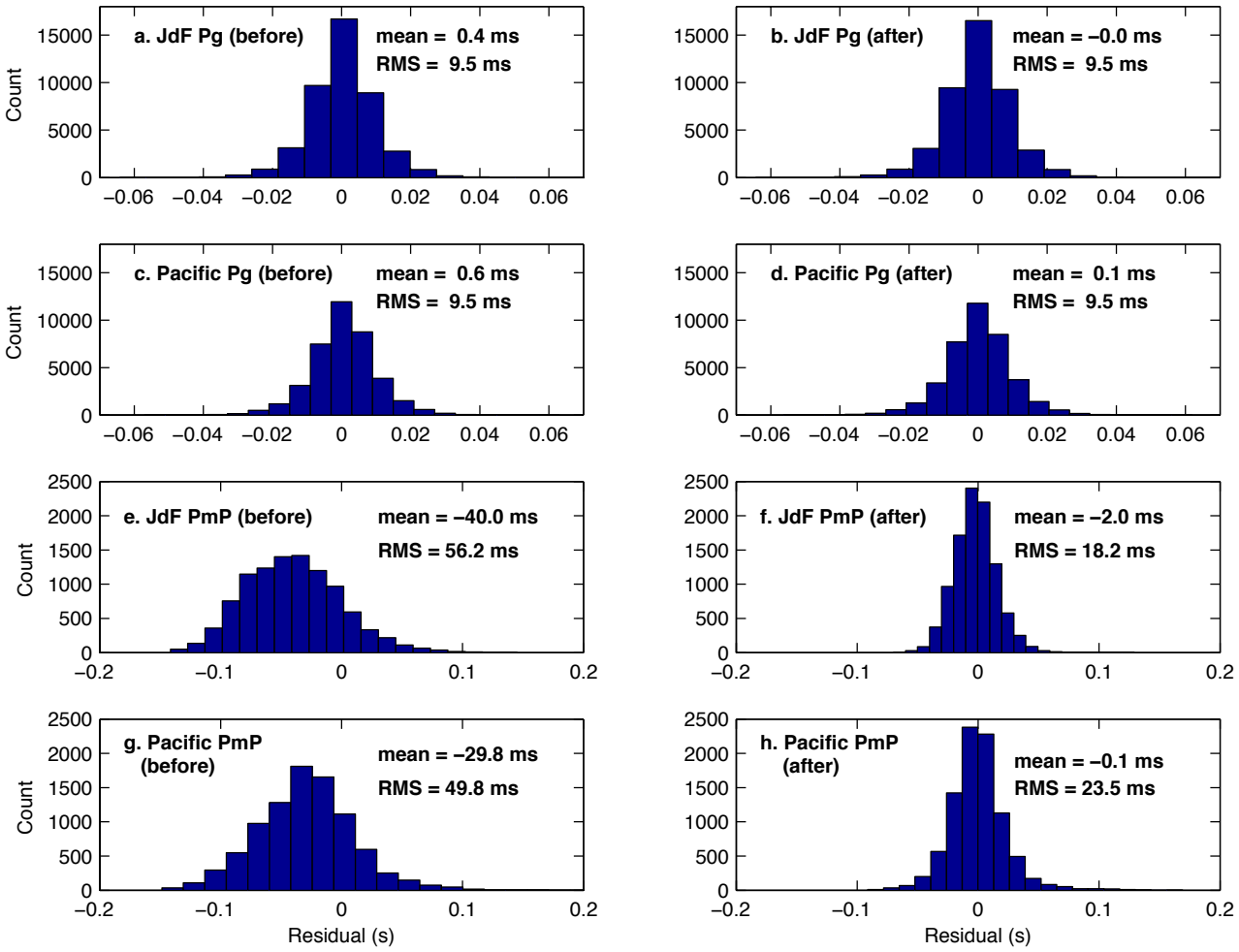

Figure 2.7. Histograms of travel time residuals labeled with the mean and root mean squared (RMS) value. (a-d) *Pg* residuals before and after the inversion for (a-b) the Juan de Fuca (JdF) and (c-d) Pacific plates. There is only a very slight change in residuals because the starting model is based on an inversion of *Pg* arrivals and so the upper crustal structure changes only very slightly. (e-h) *PmP* residuals before and after the inversion for (e-f) the Juan de Fuca and (g-h) Pacific plates.

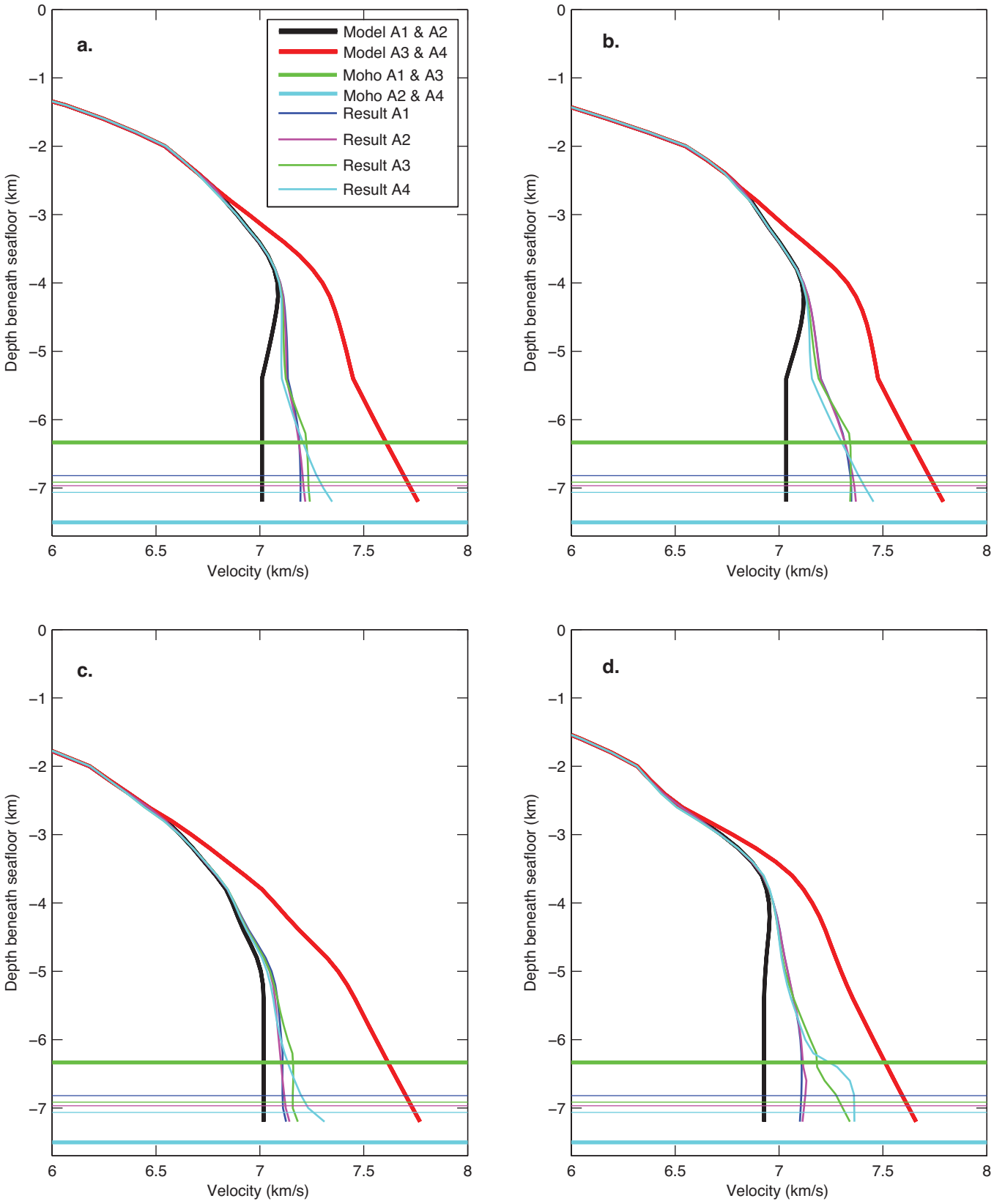
a.
b.
c.
d.
Model A1 & A2
Model A3 & A4
Moho A1 & A3
Moho A2 & A4
Result A1
Result A2
Result A3
Result A4
Depth beneath seafloor (km)
Velocity (km/s)
0
−1
−2
−3
−4
−5
−6
−7
6
6.5
7
7.5
8

Figure 2.8. Results of inverting the data assuming 4 alternative starting models that bracket the inverted lower crustal velocities and Moho thickness. Model A1 has low starting velocities in the lower crust and a thin crust (6.3 km); model A2 has low lower-crustal velocities and a thick crust (7.5 km); model A3 has high lower-crustal velocities and a thin crust; and model A4 has high lower-crustal velocities and a thick crust. (a) Average vertical velocity profiles and crustal thicknesses (horizontal lines) in area 1 (Figure 1) for the starting models and inversions showing the starting crustal velocity for models A1 and A2 (black bold line) and models A3 and A4 (red bold line), starting crustal thickness for models A1 and A3 (green bold line) and models A2 and A4 (cyan bold) and the crustal velocity and thickness that results from inverting models A1 to A4 (blue, purple, green and cyan lines, respectively). (b) As for (a) except for area 2. (c) As for (a) except for area 3. (d) As for (a) except for area 4. The results show that the inversion results are insensitive to the starting model.

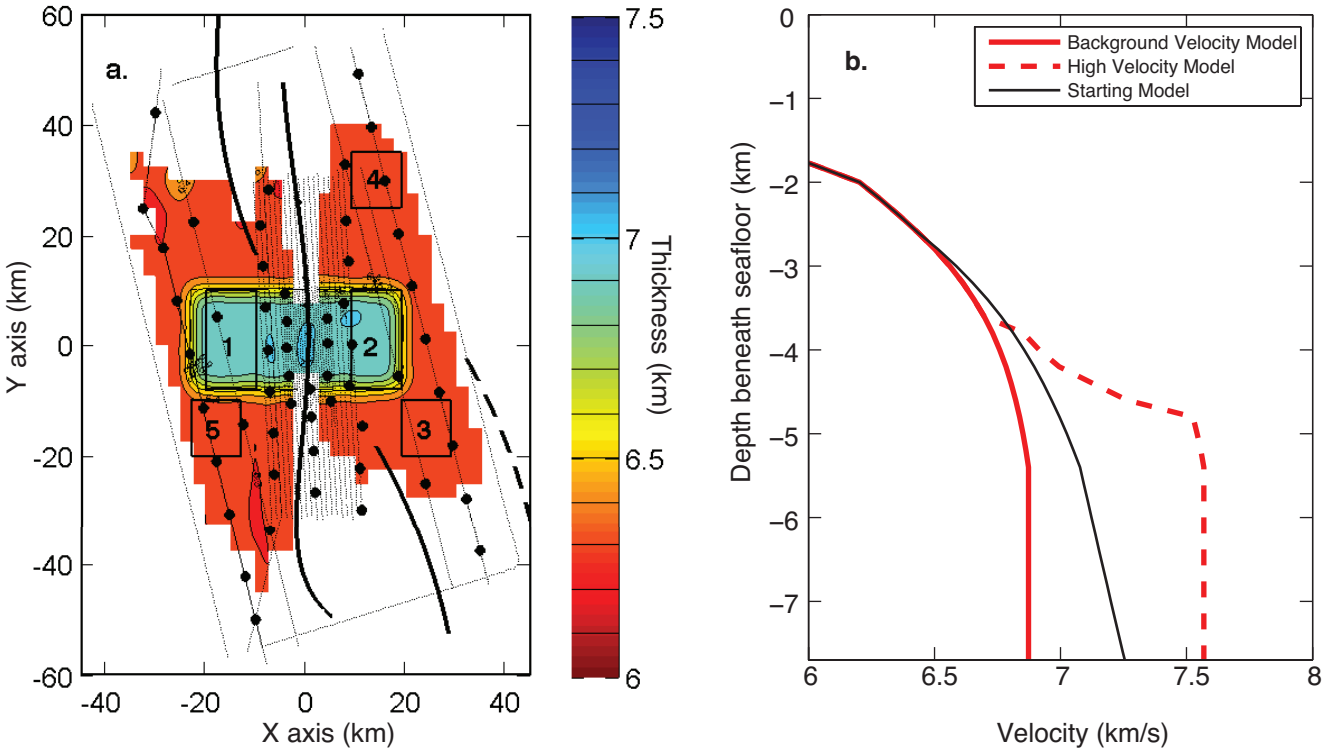

Figure 2.9. Crustal thickness and velocity models used to construct starting models for a series of synthetic inversions to evaluate the ability of the inversions to resolve thickened crust and increased velocities beneath the bathymetric plateau. (a) Crustal thickness model with a Moho keel in a 42 km by 18 km region corresponding to the bathymetric plateau (Figure 1). The crust is 7 km thick beneath the plateau and 6.3 km thick elsewhere with the transition in thickness occurring over 5 km. Note that the small irregularities in crustal thickness result because the Moho is derived from smoothed bathymetry. (b) Vertical velocity profiles in the lower crust for a background model (bold red line), a high velocity model (bold dashed red line) and a starting model for the synthetic inversions (black line). Four synthetic models were constructed: Model B1 has uniform crustal thickness of 6.3 km and the background lower crustal velocities; model

B2 has thickened crust beneath the plateau and background lower crustal velocities; model B3 has a uniform crustal thickness and elevated velocities beneath the plateau; and model B4 has thickened crust and elevated velocities beneath the plateau. Travel times were calculated for each model and used for synthetic inversions that matched the experiment geometry and preferred smoothing parameters. The starting model for each synthetic inversion has a crustal thickness of 6.7 km and crustal velocities intermediate between the background and high velocity profiles.

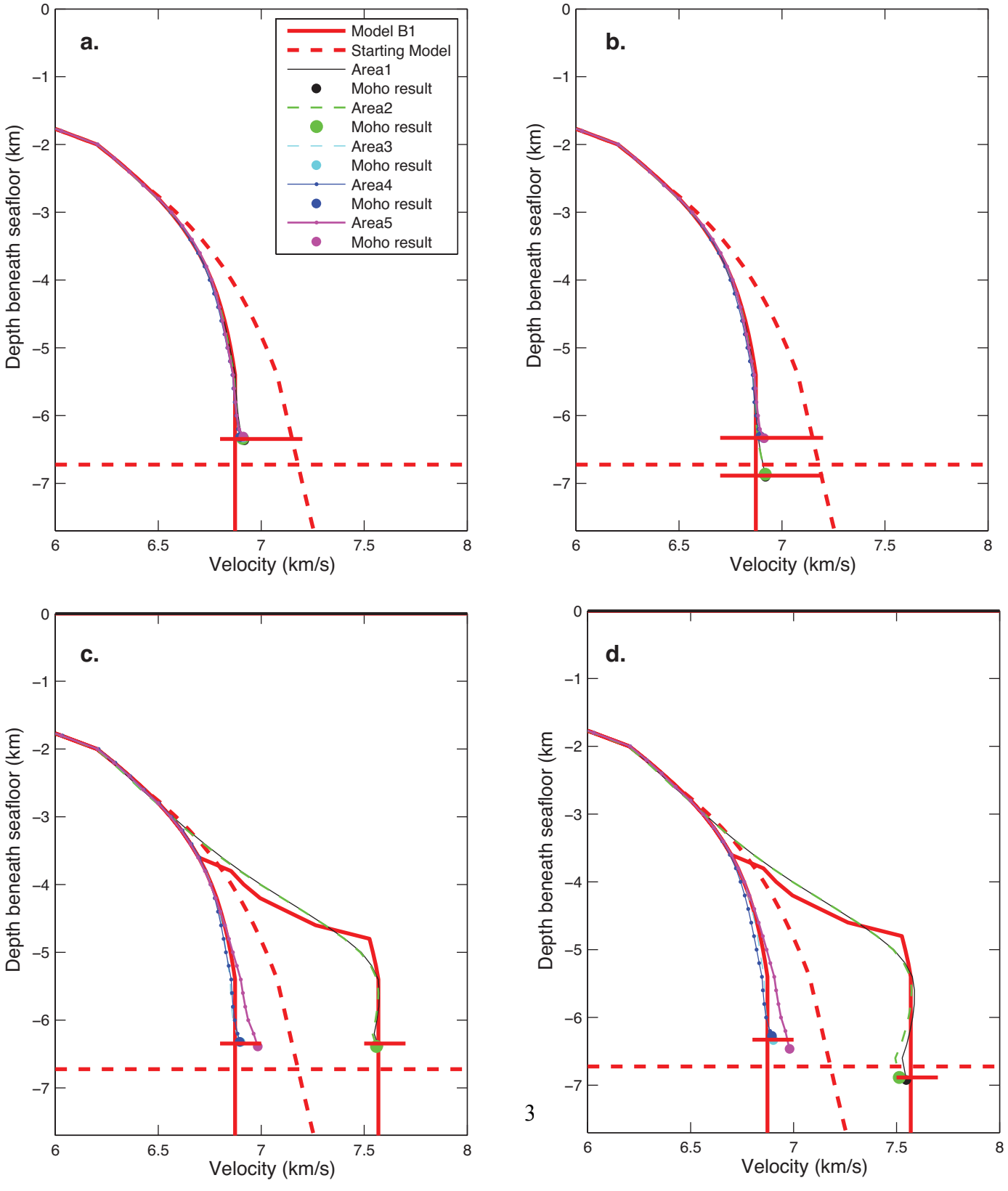
a.
b.
c.
d.
Model B1
Starting Model
Area1
Moho result
Area2
Moho result
Area3
Moho result
Area4
Moho result
Area5
Moho result
Depth beneath seafloor (km)
Velocity (km/s)
0
−1
−2
−3
−4
−5
−6
−7
6
6.5
7
7.5
8

Figure 2.10**.** Results of the synthetic inversions for the four models described in Figure 2.9 showing average velocities and crustal thickness. (a) Result of inverting for synthetic model B1 which has uniform crustal thickness and background velocities everywhere. The average models in areas 1-5 (Figure 1) reproduce the synthetic model well. Velocities are very slightly elevated (<0.05 km/s) in the lowermost crust and the crustal thickness slightly reduced, reflecting a slight influence of the starting velocity model which has higher velocities and a higher gradient than the synthetic model. (b) Result of inverting for synthetic model B2, which has a Moho keel beneath the plateau (areas 1 and 2). The model resolves the crustal thickness well and there is no significant tradeoff between increased crustal thickness and decreased lower velocities; instead, as in (a) velocities are slightly elevated in the lower crust mirroring the staring model. (c) Result of inverting for synthetic model B3 which has uniform crustal thickness and elevated velocities beneath the plateau. The model resolves velocity differences between the plateau (areas 1 and 2) and other regions (areas 3-5) well. (d) Result of inverting for synthetic model B4 which has both increased crustal thickness and elevated velocities beneath the plateau. Both the increased crustal thickness and elevated velocities are well resolved beneath the plateau (areas 1 and 2).

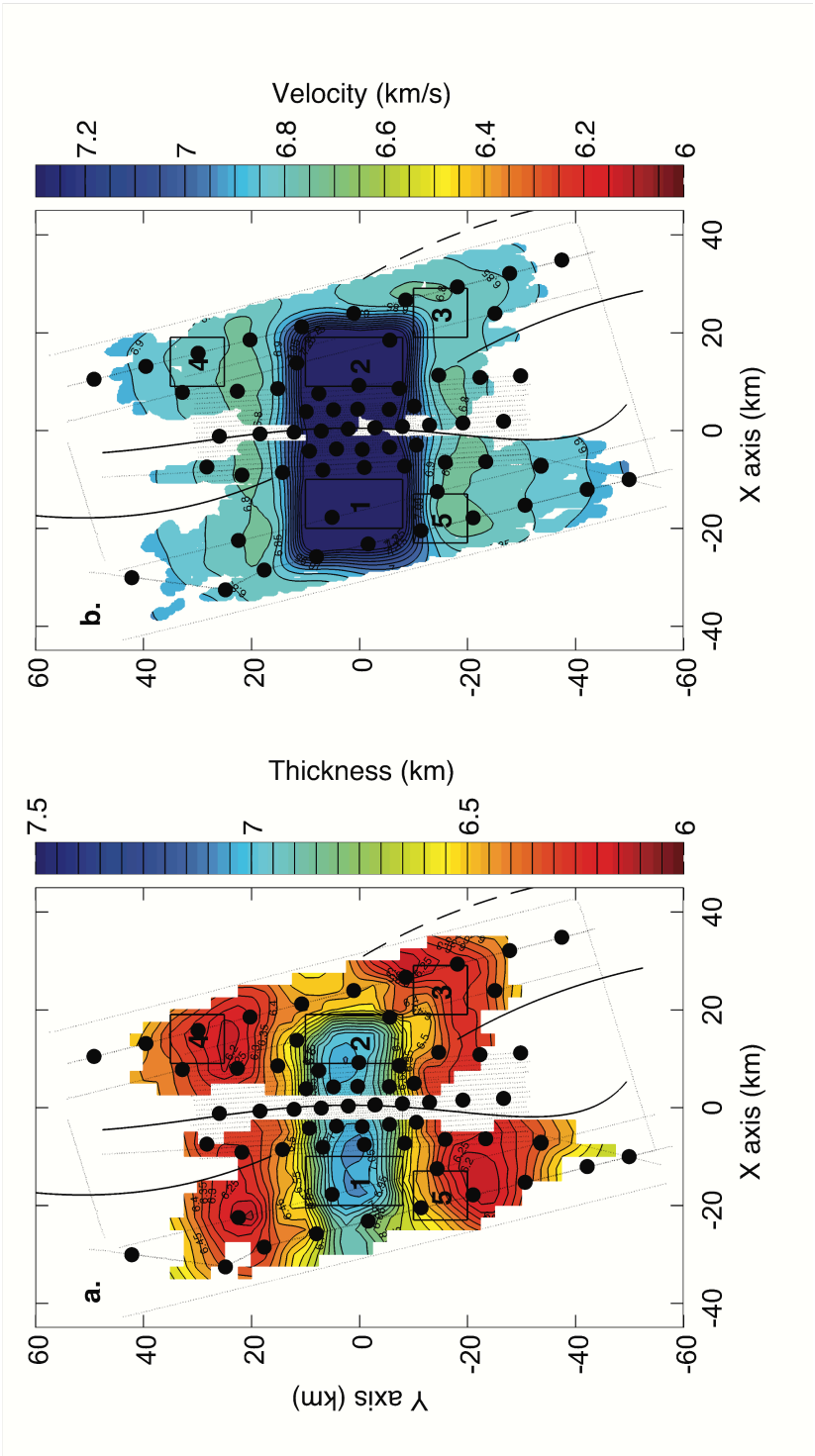

Figure 2.11. Contour plots showing (a) crustal thickness and (b) velocities at 5 km depth for the synthetic inversion of model B4.

Chapter 3:

Fin whale tracks recorded by a seismic network on the Juan de Fuca Ridge, Northeast Pacific Ocean

Dax C. Soule[1], and William S. D. Wilcock[1]

[1]School of Oceanography, University of Washington, Seattle WA 98115

3.0 Abstract

Fin whale calls recorded from 2003-2004 by a seafloor seismic network on the Endeavour segment of the Juan de Fuca Ridge were analyzed to determine tracks and calling patterns. Over 150 tracks were obtained with a total duration of ~800 hours and swimming speeds from 1-12 km/hr. The dominant inter-pulse interval (IPI) is 24 s and the IPI patterns define 4 categories; a 25 s single IPI and 24/30 s dual IPI produced by single calling whales, a 24/13 s dual IPI interpreted as two calling whales, and an irregular IPI interpreted as groups of calling whales. There are also tracks in which the IPI switches between categories. Call rates vary seasonally with all the tracks between August and April. From August-October tracks are dominated by the irregular IPI and are predominantly headed to the north, suggesting that a portion of the fin whale population does not migrate south in the fall. The other IPI categories occur primarily from November to March. These tracks have slower swimming speeds, tend to meander and are predominantly to the south. The distribution of fin whales around the network is non random with more calls near the network and to the east and north.

3.1 Introduction

3.1.1 Fin Whale Acoustics

Fin whales (*Balaenoptera physalus*) are an endangered baleen whale with a global distribution (Mizroch et al., 2009). Passive acoustic methods have been widely used to identify

their call types and calling patterns (e.g., Hatch and Clark, 2004; Watkins et al., 1987; Watkins, 1981). The most common call produced by fin whales is a down-swept 20 Hz pulse that is ~1 s in duration and typically ranges from ~18 Hz to ~23 Hz (Watkins et al., 1987; McDonald and Fox, 1999). Other calls include a 15-18 Hz narrow-band backbeat (Hatch and Clark, 2004), a higher frequency downswept pulse at frequencies up to 35 Hz (Thompson and Friedl, 1982), and a 135 Hz upsweep (Watkins et al., 1987). The number of calls fin whales produce per day has been reported to vary seasonally with more calls in winter (Sirovic et al., 2007; Watkins et al., 1987; Moore et al., 1998), diurnally with more calls at night (Watkins et al., 1987; Oleson, 2005), and inter-annually (Stafford et al., 2009). The 20-Hz calls commonly occur in stereotyped sequences or songs that are attributed to males (Croll et al., 2002) and can last for over a day (Delarue et al., 2009). Songs can be comprised of a single call repeated at a fixed interval, or doublets and triplets of closely spaced calls separated by a longer interval (Watkins et al., 1987, Oleson 2005). Songs can be used as a proxy for population identification because they vary geographically (Hatch and Clark, 2004; Delarue et al., 2009; Castellote et al., 2011) while showing little intra or inter-individual variation within a geographic region (Delarue et al., 2009).

3.1.2 Fin Whale Migratory Habits

Migratory habits of fin whales are difficult to observe and quantify due to the pelagic nature of their habitat. With hydrophones researchers can analyze seasonal variability (Delarue et al., 2009), conduct detection range modeling (Stafford et al., 2007), and examine population density (McDonald and Fox, 1999). Based on whaling data and fin whales that were tracked using radio tags, at least a portion of the Northeast Pacific population migrates southward in winter (Mizroch et al., 1984). Acoustic records indicate that a portion of the fin whale population remains in the

Northeast Pacific throughout the winter and presumably feeds during this period (Stafford et al., 2009). These results may indicate that only portions of the population migrate (Payne and Webb, 1971) and indicate the need for more information on fin whale movements.

3.1.3 Fin Whales & Seismometers

Fin whale vocalizations at frequencies near 20 Hz are detectable using ocean bottom seismometers (OBSs) designed for earthquake studies. Two previous investigations (McDonald et al., 1995; Rebull et al., 2006) used data from relatively short duration OBS experiments to demonstrate the potential of OBS networks to track fin whales. In this study fin whale tracks and calling patterns are obtained over one year with data from a local seismic network on the Endeavour segment of the Juan de Fuca ridge. The results are used to investigate patterns in calling and movement.

3.2 Methods

3.2.1 Seismic Network

This study uses data from a local seismic network that was deployed on the Endeavour Segment of the Juan de Fuca ridge located 250 km offshore of Vancouver Island in the Northeast Pacific Ocean (Figure 3.1). The central portion of the Endeavour segment is delineated by a topographic high that is cut by a 100- to 200-m-deep and 1-km wide axial valley that hosts five major hydrothermal vent fields. Depths in the region range from 2100 m to 2800 m and the ridge flanks are characterized by 300-m-high ridge parallel abyssal hills. The seafloor near and to the west of the ridge axis consists of rough basaltic topography with a thin sediment cover in the topographic lows, while to the east extensive turbidite deposits extend within about 6 km of the ridge.

The eight station seismic network (Figure 3.1) was deployed around the vent fields for three years starting in August 2003. The network aperture was 10 km along axis and 6 km across axis with a station spacing of 3 km (Wilcock et al., 2009). Seven of the stations were 3-component MBARI/ GEOSense seismometers (Stakes et al., 1998) with a flat response from 1-90 Hz that was sampled at 128 Hz. The eighth station was a 3-component MBARI Guralp broadband seismometer (Romanowicz et al., 2003) with a flat response from 2.8 mHz to 50 Hz that was sampled at 50 and 100 Hz. The stations were installed below the seafloor using remotely operated vehicles to ensure good coupling and recorded continuously with data retrieval each summer. All the stations recorded good data in the first year but in subsequent years instrument failures reduced the number of usable stations to 5-7 (Weekly et al., 2012). This study is limited to the first year of data.

3.2.2 Whale Tracking

The fin whale detection and location method is described in detail by Wilcock (2012). The ratio of root-mean-squared (RMS) amplitudes in running short-term and long-term boxcar windows is used to detect impulsive arrivals on each channel. Potentially locatable events are found by grouping arrivals detected within 2.5 s of one another on at least eight channels and four OBSs (Figure 3.2). If more than half of the arrivals have more spectral energy in the 15-35 Hz band than the 5-15 Hz band the event is identified as a whale call. Direct and multiple arrivals are picked by finding peaks in the instantaneous amplitude that exceed background noise by a factor of two and are at least 1 s away from higher peaks.

To locate whale calls a grid search is used to systematically search spatial locations with different assumptions about the number of multiples associated with each arrival. The RAY two-dimensional ray-tracing software (Bowlin et al., 1993) is used to calculate travel times using a

depth-dependent water velocity model for the region and taking into account the seafloor bathymetry along the profile between each station and grid point. The method finds the grid point that minimizes the RMS travel time residual while fitting an acceptable number of arrivals. The formal position uncertainty is typically 0.5 km for locations inside the network, increasing to up to several kilometers at the maximum location range of 15-20 km (Wilcock, 2012).

For calls more than 5-10 km outside the network, the direct arrival has a low amplitude and is often not picked; for such calls the algorithm sometimes mislocates calls by systematically assigning one too few multiples to each arrival. The algorithm can also mislocate calls if arrivals from two calling whales overlap or if the signal to noise ratio is poor. To identify tracks we inspect the locations and the seismic data manually. If a minimum of 30 locations occurring over at least half an hour form a clear track that travels a minimum resolved distance of 2.5 km, a smooth path is input manually through these locations. The smooth path is then used for a second iteration of the grid search that requires solutions to lie near the path.

3.2.3 Calling Patterns

Because the tracking algorithm does not detect and locate every call, a spectral detection method was developed to analyze the scale calling patterns along each track. Each call sequence is inspected on multiple stations and the station/channel combination with the highest signal-to-noise ratio is used to detect calls. A spectrogram is calculated with a 128 point Fourier transform, a Hanning window, and a 98% overlap (Figure 3.3a). A modified spectrogram in decibels is created by subtracting a threshold set to two standard deviations above the mean decibel level in the 15-35 Hz whale band and zeroing all negative values (Figure 3.3b). Times for possible whale arrivals are found by summing the modified spectrogram between 15 and 35 Hz at each time sample and finding peaks.

If the original spectrogram for a detection contains more energy in the 5-15 Hz band than in the 15-35 Hz band, the peak is interpreted as an earthquake and discarded. The remaining peaks are classified as whale calls if two criteria are met: (1) the amplitudes exceed a detection threshold set to 25% of the largest peak in a 10-minute window and (2) the peak is spaced 7 s from all larger peaks to eliminate multi-path arrivals. The algorithm fails when earthquake energy swamps the whale calls or during intervals with low signal-to-noise ratio, where it triggers on background noise likely caused by distant fin whales. During these periods an analyst manually adjusts the detection threshold. The performance of this method was evaluated for a subset of data comprising 2400 calls on portions of 10 tracks by comparing detections to visual identifications by the analyst; there were no false detections and only 0.7% of the calls were missed.

The weighted mean and standard deviation of the call's frequency are calculated from the modified spectrogram for each call. Backbeat calls (Hatch and Clark, 2004) are present on many tracks, but efforts to identify them automatically based on their lower frequency and smaller standard deviation of frequency proved unreliable because they showed a high level of variability. Instead, backbeats were identified manually for a representative subset of 20 whale tracks based on comparing the mean frequency and bandwidth of adjacent calls.

Following the terminology of Watkins et al. (1987), the inter-pulse interval (IPI) is calculated as the time spacing between the start of two successive calls in a sequence. Since most call sequences include notes with different frequency, the IPI is different from the inter-note interval used by some researchers which measures the time spacing between two successive calls of the same frequency (Hatch and Clark, 2004; Castellote et al., 2011). Watkins et al. (1987) define longer IPIs lasting from 1 to 20 minutes and 20 minutes to 2 hours as rests and gaps,

respectively, and groupings of IPIs separated from other groupings by at least 2 hours as bouts. To be consistent with this terminology all pairs of tracks falling within two hours of each other were examined. If the two segments had similar IPI patterns and call frequencies, and swimming speeds and directions that were consistent with each other and with the spacing between the tracks, they were merged into a single track.

For each track, histograms were created of the call frequency, IPI, rest duration and rest spacing, and an average swimming speed and meander parameter were calculated. The meander parameter is defined as the ratio of the total distance along the smoothed path to the net distance traveled; a value of one would indicate a straight path. To identify relatively straight and fast tracks a track is defined as transiting if its speed is >4 km/hr and its meander parameter is <1.25.

If the IPI histogram indicated an irregular pattern of calls, the seismic record sections were inspected to search for variations between successive calls in the relative arrival times and amplitudes at different stations that would indicate that the track was obtained during an interval when there were calls from a whale in a different location. Tracks or portions of tracks that were corrupted by off track calling were excluded from the detailed analysis of calling patterns.

Figure 4 shows results for one example whale track. This whale is tracked (Figure 3.4a) for 22 hours as it swims with an average speed of 1.3 km/hr along the ridge axis from the north to the south with a meander parameter of 1.7. The spectral characteristics of the calls from a ten-minute segment (Figure 3.4b) show mostly 19 Hz calls. Two backbeats are visible at ~240 s and ~650 s and one resting interval from ~140 to 240 s. The IPI histogram (Figure 3.4c) shows little variation from its 25 s peak, with almost all the calls from this track in the 24-26 s bins. The histogram of call frequency (Figure 3.4d) peaks at 19 Hz with all calls between 16-20 Hz (Table 3.1). The backbeat calls have lower frequencies but do not create a separate peak.

3.3 Results

The complete analysis of the seismic data from August 2003 through July 2004 yielded 154 tracks satisfying our criteria with a total duration of 785 hours. Individual tracks range in length from the minimum allowed length of 2.5 km to 55 km with durations from less than 1 hour to nearly a day. A total of 44 full tracks and 29 partial tracks comprising 27% of the total track duration occurred during intervals when fin whale calls are detected off the track.

3.3.1 Call types

The tracks contain three call types: a 18 Hz down-swept pulse with a center frequency of 17-20 Hz, a narrow-band backbeat with a center frequency of 16-17 Hz, and a higher frequency 24-Hz down-swept pulse whose frequency can vary from 21 to 30 Hz. The 18 Hz pulse is the most common call type in this data set (Figure 3.5a), comprising 81% of the calls and appearing in 98% of the tracks. Its rate of occurrence spikes from November to February and it is always associated with a backbeat. The 17 Hz backbeat call is the second most common call type comprising 10% of the calls and occurs primarily as the first call after a rest or a longer IPI. Backbeats are found on a large proportion of tracks with the 18 Hz down-swept pulse and are only found in association with this call. They do not form a separate peak in the frequency spectrogram (Figure 3.5e) but can be identified in individual tracks based on their lower frequency and bandwidth. The 24 Hz pulse forms a separate peak in the call frequency histogram and is the least common, comprising 9% of the calls and occurring on 29% of the tracks. Three tracks are comprised entirely of the 24 Hz pulse. The rate of occurrence for the 24 Hz pulse remains approximately constant from September through March.

3.3.2 Inter-pulse interval categories

Based on the pattern of the IPI, the calling can be subdivided into 4 categories: 1) 25 s single IPI; 2) 24/30 s dual IPI; 3) 24/13 s dual IPI, and 4) irregular IPI. Most tracks fall into a single calling category but 13 tracks include intervals of two IPI categories and form a fifth category of tracks termed "mixed" IPI tracks. Table I summarizes the characteristics of the track types.

The 25 s single IPI tracks account for 16% of the total number of tracks and are characterized by calls spaced uniformly 25 s apart (Figure 3.4b). The IPI histogram for all of these tracks has a sharp peak centered at 24-25s (Figure 3.5a). The frequency histogram (Figure 3.6a) has a peak at 19 Hz with all the calls between 17 and 20 Hz. Backbeat calls occur in all of these tracks, most frequently on the trailing call of rests and on the occasional longer IPIs.

The 24/30 s dual IPI tracks are the most common and account for 48% of the tracks. The IPI histogram for all of these tracks (Figure 3.6b) has a primary peak at 24 s and a secondary peak at 30 s. The overall ratio of the number of 24 s to 30 s IPIs is ~3.5 to 1 but it can vary markedly between tracks. The 30 s IPIs do not occur consecutively and for any track the number of 24 s IPIs before a 30 s IPI will typically vary from 1 to >10 with no regular pattern (Figure 3.7a). The frequency histogram (Figure 3.5b) peaks at 18 Hz with all calls between 16 and 20 Hz. Backbeats occur on all of these tracks in about twice the proportion than for the 25 s single IPI tracks and are consistently the trailing calls of both rests and 30 s IPIs.

The 24/13 s dual IPI tracks account for 10% of the tracks. The IPI histogram for these tracks (Figure 3.6c) has a primary peak at 24 s and a secondary peak at 13 s. The ratio of the number of 24 s to 13 s IPIs is ~1.5 to 1. On an individual track the 13 s IPIs are not distributed in a regular pattern but instead appear to be created by calls intermittently breaking a 25 s IPI sequence. These tracks can include all three call-types. Backbeats are relatively rare and are

primarily found as the trailing call of rests. Higher-frequency down swept pulses with frequencies from 21-24 Hz (Fig 3.7b) are found on 75% of the tracks and comprise 10% of the total calls. The 24 Hz calls tend to be found on the trailing edge of the shorter IPI (Figure 3.7b) indicating that there is a tendency for the 13-s IPI to be created by a 24 Hz call interrupting an 18 Hz caller with a longer IPI rather than vice-versa.

The irregular IPI tracks account for 18% of the total and are characterized by a broad IPI distribution weighted towards smaller IPIs (Figure 3.6d). Individual irregular IPI tracks produce a range of IPI histograms, from a single peak near the 7 s limit imposed by our call detection algorithm, to multiple peaks all under 25 s. The frequency histogram (Figure 3.5d) shows calls ranging from 16 to 30 Hz with peaks at 17, 19, and 24 Hz. This is the only track type to contain calls whose frequency exceeds 24 Hz (Fig 3.7c); 47% of the calls are categorized as 24 Hz calls (i.e., frequency ≥ 21 Hz). For individual tracks, the frequency histogram has up to five peaks and has at least two peaks for 85% of these tracks. This is the only category to include tracks composed exclusively of "24 Hz" calls.

There are 13 mixed IPI whale tracks for which the locations indicate one continuous whale track, but the calling characteristics switch, often several times, between two categories. For all but three of these the IPI switches between irregular IPI and either the 25 s single IPI or 24/30 s dual IPI. There are two tracks that switch from a 25 s single IPI to the 24/30 s dual IPI and one that switches from a 24/13 s dual IPI to 25 s single IPI. Where the irregular and 24/13 s dual IPI portions of mixed IPI tracks contain multiple frequencies, the shift to 25 s single and 24/30 dual IPI coincides with the loss of the higher frequency calls.

Histograms of the rest spacing and duration for individual tracks show a wide variety of characteristics for each category. In some tracks rests are regularly spaced with similar duration

while in others they vary. For the full data set the most frequent rest spacing is around 200 s but all spacings up to 700 s are common. Rest durations are also variable but most are <130 s and there are peaks in the histogram at 90 s and 115 s.

3.3.3 Swimming characteristics

The estimated swimming speeds of individual tracks range from 1 to 12 km/hr with a mean value of 4.3 km/hr. The mean swimming speeds for the 24/30 s and 24/13 s dual IPI tracks are very similar (4.2 ± 2.0 km/hr, n = 90) but are different from the 25 s single and irregular IPI tracks (Table 3.1). The swimming speeds for the 25 s single IPI tracks (3.0 ± 1.7 km/hr, n = 24) are significantly slower (two sample t-test, p = 0.004) while those for the irregular IPI tracks (5.9 ± 2.5 km/hr, n = 27) are significantly faster (two sample t-test, p = 0.001) (Rice, 1994).

The meander parameters vary from 1 to 8.5. The mean and standard deviation of meander parameter (1.2 ± 0.3, n = 27) is lower for the irregular IPI tracks than for the 25 s single, 24/30 s dual and 24/13 s dual IPI tracks combined (1.8 ± 2.4, n = 114). The smaller mean and standard deviation for the irregular IPI track meander parameters reflects the lack of irregular IPI tracks with high meander parameters. The tendency for the irregular IPI tracks to be faster and straighter is reflected in the relatively high percentage (60%) of those tracks that meet the requirement for a transiting track. Similarly, a small percentage (17%) of the 25 s single IPI tracks are transiting because they have slower swimming speeds.

Although 27% of the track duration is corrupted by off-track calls that are sufficiently loud to be detected by the spectral detection method, in most instances these calls are too far (> ~15 km) from the network to be located. However, there are 5 periods totaling 8 hours during which whales were calling concurrently on two tracks (Figure 3.8). There are also another ~11 hours during which time calls were located off tracks in consistent location but the number of

locations, calling duration and path lengths are too small to meet the criteria for a track. In all cases, concurrent tracks are always separated by >5 km and there is no indication that the whale movements are coordinated. Figure 8 shows one example; over a 4 hour interval a 25/30 s dual IPI track located to the north of the network heads east while a second 25-s single IPI track to the west heads south.

3.3.4 Track distribution and directionality

The distributions of track types throughout the year and their directions show distinct patterns (Figure 3.9). The irregular IPI tracks occur primarily from August to October and tend to be directed to the northwest (Figure 3.9a). The 25 s single IPI tracks are the dominant track type in November (Figure 3.9b) and all but three occur between November and January. The 24/30 s dual IPI tracks start in November and continue through April with the highest numbers from December to February (Figure 3.9c-e). The 25 s single and 24/30 s dual IPI tracks have a tendency to be oriented southward and an overall directionality towards the south-southeast. The 24/13 s dual IPI tracks occur from September to March with the highest number in December (Figure 3.9c). They also tend to be southward.

Two statistical tests were conducted to test the significance of track directionality (Table 3.1). First a one-sided binomial test (Rice, 1994) was applied to determine if the larger number of tracks headed either northwards or southwards might be expected in a random distribution. The northward directionality of the irregular IPI tracks is not quite significant at the 95% confidence level but when only the tracks in August to October are considered ($x = 16$, $n = 21$) it is significant ($p = 0.01$). The southward directionality is significant at the 95% confidence level for the 24/30 s dual IPI tracks but not for the 25 s single and 24/13 s dual IPI tracks, which may

just reflect the smaller sample sizes. The probability of a random directionality for these three categories combined (x = 43, n = 114) is 0.03.

Second random walk tests (Rayleigh, 1919) were applied to each category by summing the cumulative displacement of tracks and determining if they are consistent with a random walk with step lengths equal to the average length of the individual tracks in the category. The results show that the 25 s single and 24/30 s dual IPI tracks are inconsistent with a random walk at the 95% significance level while the irregular IPI tracks just fail to meet this significance level (Table 3.1). The 24/13 s IPI tracks cannot be distinguished from a random walk.

The spatial density of fin whale tracks around the network (Figure 3.10) appears non-random. The highest densities of calling whales are observed within and to the east and north of the network while densities to the south and particularly the southeast are markedly lower. Overall the densities in the quadrant centered to the southwest are less than half those in the northeast quadrant. Inspection of similar plots for the different track categories suggests that the observed spatial patterns are a result of non-random distributions for the single and dual IPI track categories, rather than for the irregular IPI tracks that tend to transit across the region.

3.4 Discussion

In this study 154 whale tracks lasting for nearly 800 hours were obtained over one year from a small region in the Northeast Pacific Ocean. This work builds upon earlier studies with OBS data that localized a small number of fin whale calls to obtain tracks (McDonald et al., 1995; Rebull et al., 2006). The quality of each call sequence in this survey was verified by an analyst and is comparable to calling bouts observed during focal animal follows (Watkins, 1981; Watkins et al., 1987). Although swimming speeds will be underestimated for meandering tracks because the location uncertainty for the tracking algorithm prohibits resolution of the small-scale

non-linearity, the range of swimming speeds reported here (1 to 12 km/hr) is consistent with previous observations. For example, aerial observations yield sustained near-surface swimming speeds from <1 km/hr to 10-16 km/hr (Watkins, 1981).

Given the global range of the fin whale's habitat (Watkins, 1981) and evidence that individuals cover large distances (Cotte et al., 2009), it is likely that the 154 tracks represent many individuals. The tracks are thus complementary to those obtained by tagging, which are typically limited to a small number of individuals but either cover a longer duration (Cotte et al., 2009) or provide more information such as dive profiles (Croll et al., 2002, 2001).

3.4.1 Call Types

The 18 Hz down-swept pulse and the 17 Hz backbeat are always found in association and together constitute over 90% of the calls. In a global compilation of song data backbeat calls are present in only 44% of fin whale song (Hatch and Clark, 2004). In our study backbeats appear to be in a large proportion of tracks containing the 18 Hz pulse. Hatch and Clark (2004) also report that backbeats are preferentially incorporated into fin whale song in the late summer and early fall (Hatch and Clark, 2004). This also contrasts with this study, where backbeats are most common from December through February when 24/30 s dual IPI tracks occur in large numbers and are the dominate track type.

A higher frequency downswept pulse has been reported previously in the Northeast Pacific (McDonald et al., 1995; MacDonald and Fox, 1999). McDonald and Fox (1999) note that it makes up >90% of the summer calling at high latitudes in the Northeast Pacific based on extensive unpublished data. This call described as the "20-35 Hz irregular repetition interval" has been recorded near Hawaii, where it was attributed to fin whales (Thompson and Friedl, 1982; McDonald and Fox, 1999). However, more recently the same or a very similar call has

been attributed to sei whales based on concurrent visual and acoustic observations near Hawaii (Rankin and Barlow, 2007)

In our data set the higher frequency "24 Hz pulse" constitutes about 9% of the calls and while its frequency varies, it is clearly distinguishable from the 18 Hz pulse since there are very few calls at 21 Hz (Figure 3.5e). Unlike the 18 Hz pulse which is found in all track categories, the 24 Hz pulse is only found in the 24/13 s and irregular IPI tracks. Since the 24 Hz pulse is found in association with the 18 Hz pulse in all but 3 of the 35 tracks where it is present, it would be surprising if it were from a different species. Since the 18 Hz pulse is associated with males in the breeding season (Croll et al., 2002; Watkins, 1981; Watkins et al., 1987), it might be inferred that the 24 Hz pulse does not come from mature males. If only males vocalize (Croll et al., 2002), one possibility is that the higher frequency call is produced by smaller immature males.

3.4.2 Inter-pulse interval

The spacing of calls in fin whale songs has been shown to be an effective measure of population identity that may separate stocks or groups within the species (Hatch and Clark, 2004; Castellote et al., 2011). Globally, calling bouts have IPIs ranging from 4 s to 46 s with the most common intervals between 7 s and 26 s (Watkins et al., 1987; Hatch and Clark, 2004). Examples of the dominant IPIs in other regions include a 7/11 s doublet found near Cape Cod (Watkins, 1981), a 12 s IPI found in the waters near Bermuda (Watkins, 1981) and a 12-15 s in the Western Mediterranean Sea (Castellote et al., 2011). In the Northeast Pacific, McDonald et al. (1995) reported a 19 s interval for data collected in 1990 and an IPI of ~20 s can be deduced for many of the Northeast Pacific fin whales sampled by Hatch and Clark (2004) in 1995-1996 and 2000 (see Figure 4 of that study). For our study the dominant IPI is 24 s. Since the study of McDonald et

al. (1995) was conducted only about 300 km south of the Endeavour site, one possibility is that there has been a significant change in the IPI of Northeast Pacific fin whale on a decadal a timescale.

We interpret both the 25 s single IPI and the 24/30 s dual IPI as single whales. The single IPI is seen in data from surveys in many geographic locations other than the northeast Pacific Ocean (Hatch (2004) Figure 4.5; and Watkins et al. (1987)) and its seasonal occurrence has been linked to the breeding season. The 24/30 dual IPI differs from the doublet call reported for the North Atlantic (Watkins 1981) in that the two IPIs do not alternate but occur in a more complex pattern. This type calling-pattern has not been discussed in the literature. Although there is overlap in their occurrence (Figure 3.9), the 25 s single IPI is more prevalent in November while the 24/30 s dual IPI is the dominant song type from December through the end of the calling season. The simple IPI tracks are also characterized by slower swimming speeds and a smaller proportion of tracks that are not corrupted by off-track calling (Table 3.1), suggesting that they occur when there are more calling whales in the vicinity.

We infer that the 25 s single IPI and the 24/30 s dual IPI are produced by the same population of whales. Some of the 25 s IPI tracks include a small number of larger IPIs that tend to be near 30 s IPI and the proportion of 30 s IPI varies between 24/30 s dual IPI tracks. There are two mixed IPI tracks in which the IPI appears to change in mid-track from the 25 s IPI to the 24/30 dual IPI. In one track this happens abruptly following a rest in calling and so might be attributed to two whales being mistakenly assigned to the same track but in the other, the change in IPI pattern occurs without a break in calling.

Since 75% of the 24/13 s dual IPI call sequences include 24 Hz pulses in addition to 18 Hz pulses, they must either be attributed to a single whale vocalizing at two frequencies or to a pair

of whales vocalizing at different frequencies. The latter interpretation seems more likely for three reasons. First, while fin whales can call at multiple frequencies up to 135 Hz (Watkins et al. 1987), there are no previous reports of individual fin whales generating down-swept calls at two distinct frequencies near 20 Hz. In contrast, there are published examples of calling and counter calling (Watkins, 1981; McDonald et al. 1995). Second, as noted above the 24 Hz pulse is nearly always observed as the trailing edge of the 13 s IPIs, which is consistent with the 24 Hz pulse being a counter call that interrupts this longer IPI. Third, on the one mixed IPI track that switched from 24/13 s dual IPI to 25 s single IPI, the change in IPI category coincided with the loss of the 24 Hz pulse. This can be simply explained if a whale counter calling at 24 Hz stopped calling, leaving a single whale vocalizing at 18 Hz.

If the 24/13 s dual IPI whale tracks are generated by two callers it raises interesting behavioral questions. The track characteristics including dominant IPI, speed, tortuosity, seasonal occurrence and directionality are similar to the 25 s single and 24/30 s dual IPI tracks that are attributed to the breeding display of a single male. If only male fin whales sing (Croll et al., 2002; Watkins et al., 1987), what would motivate two males to travel together calling and responding? If the 24 Hz pulse is attributed to a smaller immature whale then it can be inferred that the second whale in these tracks is sometimes a mature male and sometimes an immature whale. Since the frequency of the 24 Hz pulses in the 24/13 dual IPI tracks (Figure 3.5c) are at the lower end of the 21-30 Hz range for these calls observed in the full data set (Fig 3.5e), these calls might be interpreted as from a whale nearing maturity if the call frequency is an indication of size.

The irregular IPI histogram (Figure 3.5d) is most easily interpreted as multiple whales singing and/or responding as they swim together. The peak IPI in the histogram is at 8 s (Figure

3.6d), which is close to the minimum separation allowed for two events in the detection algorithm to avoid triggering on multiples. Inspection of the data shows that some irregular IPI tracks can have very closely spaced calls. All but 2 of the 27 irregular IPI tracks include 24 Hz pulses and the frequency histograms for individual tracks contain up to five distinct center frequencies (Table 3.1). Irregular IPI patterns with multiple frequencies are visible in several published spectrograms from the Northeast Pacific (Charif et al., 2002; McDonald and Fox, 1995; McDonald et al., 1999; Moore et al., 1998) although in some instances the number and relative position of whales is unknown. McDonald et al. (1995) used tracking to infer that an irregular IPI sequence comprised three whales calling at distinct frequencies and swimming in the same direction a few kilometers apart. McDonald and Fox (1999) infer four calling whales based on call frequency content and bearing.

In this study, the different frequency calls in the irregular IPI tracks are not resolved onto separate tracks. Given the location uncertainties, this indicates that the callers are swimming no more than one to several kilometers apart from each other. The high proportion of higher-frequency calls with mean frequencies up to 30 Hz suggests that irregular IPI tracks include many callers that are not mature males. The faster swimming speed and consistently low meander parameters of these tracks are consistent with groups of whales communicating while transiting through the experiment area.

There are ten tracks where either 25 s single or 24/30 dual IPI calling patterns switch back and forth to irregular IPI. The simple explanation is that the single whale being tracked is either joined by or was always in the company of other whales that start or stop vocalizing. The presence of irregular IPI in mixed IPI tracks implies that the 18 Hz pulses in the irregular IPI are not generated by a completely distinct subset of 18 Hz callers from those in the other track types.

3.4.3 Seasonality and Directionality of Tracks

Fin whale calling is strongly seasonal in our data set with all the tracks between August and April and the highest numbers from November to February. These seasonal variations do not require variations in the number of fin whales present in the study area, because they can be explained by seasonal changes in sound production (Watkins et al., 2000). In high latitude areas there are many observations of relatively silent fin whales during summer months (Stafford et al., 2007; Simon et al., 2010). Fin whale calling rates have been previously observed in acoustic surveys of the Northeast Pacific Ocean to be highest during the winter months (Stafford et al., 2007; Watkins et al., 2000; Simon et al., 2010), which is consistent with gestation estimates that indicate mating in this season (Watkins et al., 1987). This fits the well accepted theory that stereotyped song is a male breeding display (Croll et al., 2002; Watkins, 1981; Watkins et al., 1987).

Our data documents a systematic progression in the dominant IPI from irregular IPI in the August-October to the single IPI in November to 24/30 dual IPI throughout the winter months (Figure 3.9) that indicates changes in social behavior. We interpret the irregular IPI as a social calling pattern indicative of multiple whales traveling together (Payne and Webb, 1971). As winter progresses, and the onset of the mating period commences (Watkins et al., 1987), the track class shifts to the solitary 25 s single IPI and the 24/30 s dual IPI.

Acoustic monitoring in other studies has shown migratory movements of one whale population between two locations by comparing inter-note intervals recorded in both locations (Castellote et al., 2011). This study is limited to one location, but constrains the travel direction and variations in IPI and group size that occur over the year. The progression shown from August through April in both the classes of tracks detected and the net directionality from

northward in the fall to southward in the winter (Figure 3.9) seems to conflict partially with the conclusions from studies of both whaling data and tagged whales (Mizroch et al., 1984, 2009) that recorded systematic movement between low latitude winter grounds and high latitude summer grounds. The northward irregular IPI tracks in the fall with many 24 Hz callers may indicate that a portion of the population, possibly including immature males, does not migrate south in the fall. The southward movement of the other categories in the winter is not necessarily incompatible with a conventional migration pattern but would require that these callers swim silently northward as soon as the calling tapers down in March and April.

3.4.4 Spatial Distribution of Fin Whales

Because our location algorithm is not designed to separate overlapping calls, the observation of 5 pairs of concurrent tracks totaling 8 hours as well as 11 more hours when there are short intervals of calling located off-track may tend under-report the time when there are two separate whales or groups of whales vocalizing in the vicinity of the network. Nevertheless it appears that these tracks are relatively rare. There are 654 hours of tracks from November through February, which gives an expected number of trackable whales at any given time of 0.23. Assuming that these tracks occur randomly in time, the Poisson's distribution (Rice, 1994) predicts that two or more should be present for over 60 hours. Because concurrent tracks are much less frequent and are always well separated, our data supports previous studies that report calling whales or groups of whales to be separate from one another (Watkins, 1981).

One hypothesis that motivated this study was that fin whales might be found preferentially near the ridge axis to exploit the increased zooplankton biomass (Burd et al., 1992; Thompson et al., 1992; Burd and Thomson, 1994, 1995). The track density plot (Figure 3.10) shows a non-random distribution of tracks with more tracks near the network and to the north and east.

Variations in network aperture might lead to different sensitivity to the north and south than to the east and west. The presence of thick sediments to the east may impact the relative sensitivity to the east and west of the ridge axis because of the effects of the bottom lithology and roughness on seafloor multiples. However, it is difficult to attribute all spatial variations to sensitivity effects. For example, the density of the calls to the northeast of the network is nearly twice that to the southeast despite similar network geometry and seafloor characteristics. The mean near surface currents in the region are characterized by flow to the east and northeast associated with the Eastward North Pacific Current (Strub and James, 2002). The higher density of tracks seen within the network and to the north and east is thus not inconsistent with a source of food near the rise axis that is advected by the ocean currents. High densities of zooplankton biomass have been shown to co-occur with cetaceans in many studies (Cotte et al., 2009; Stafford et al., 2007), and while there is not an established link between vocal behavior and feeding behavior, singing males have been observed in areas of high food concentration (Croll et al., 2002) and singing whales there are generally found near non vocalizing whales (Watkins et al., 1987). A more definite test of the linkage between hydrothermally-supported zooplankton and fin whales would require measurements of zooplankton concentration in the winter and a better understanding of the linkages between vocalizing whales and whales feeding in the vicinity.

3.5 Conclusions

In this study the acoustic behavior of fin whales has been linked to their tracks over one year in a small portion of the Northeast Pacific Ocean. These results demonstrate the usefulness of seafloor seismic networks in studying fin whales. OBS networks can provide long-term

opportunistic monitoring capabilities that would be expensive to duplicate in a dedicated experiment. The primary conclusions of our study are:

- The 18 and 24 Hz pulses are distinct call types that are likely indicative of different individuals.
- The dominant IPI for the Northeast Pacific fin whale is 24 s.
- The 25 s single IPI and the 24/30 s dual IPI are probably single whales generating 18 Hz pulses.
- The 24/13 dual IPI is a previously unidentified type of track that is possibly indicative of two calling whales traveling together, one of which may use a 24 Hz pulse.
- The irregular IPI is indicative of multi-whale groups that contain a high proportion of 24 Hz pulses.
- The swimming patterns show northward movement of groups of transiting whales from August to October and a southward movement from November to April of 25 s single, 24/30 s dual and 24/13 s dual IPI tracks.

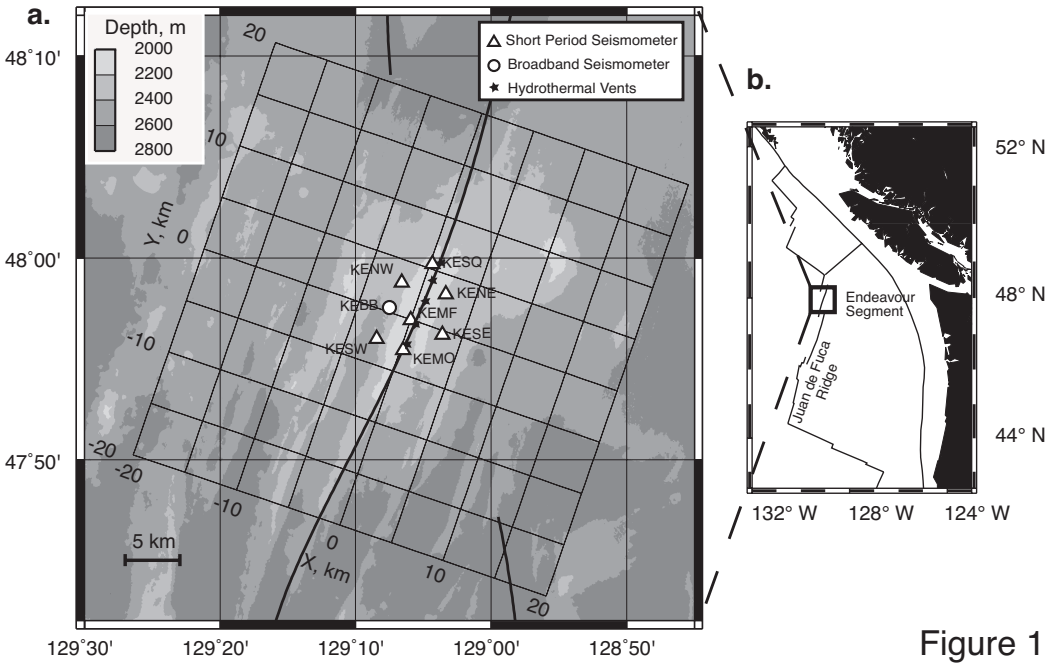

Figure 1

Figure 3.1 – (a) Bathymetric map showing the configuration of the experiment. The position of the spreading center is shown by solid bold lines and hydrothermal vent fields by black stars. The seismic network is comprised of seven short period seismometers (open triangles) and one buried broadband seismometer (open circle) which are labeled with the station name. Whales were tracked within a square x-y grid (faint lines) centered on the seismic network with the y-axis aligned with the ridge axis. (b) Regional map showing the location of the study area and tectonic plate boundaries.

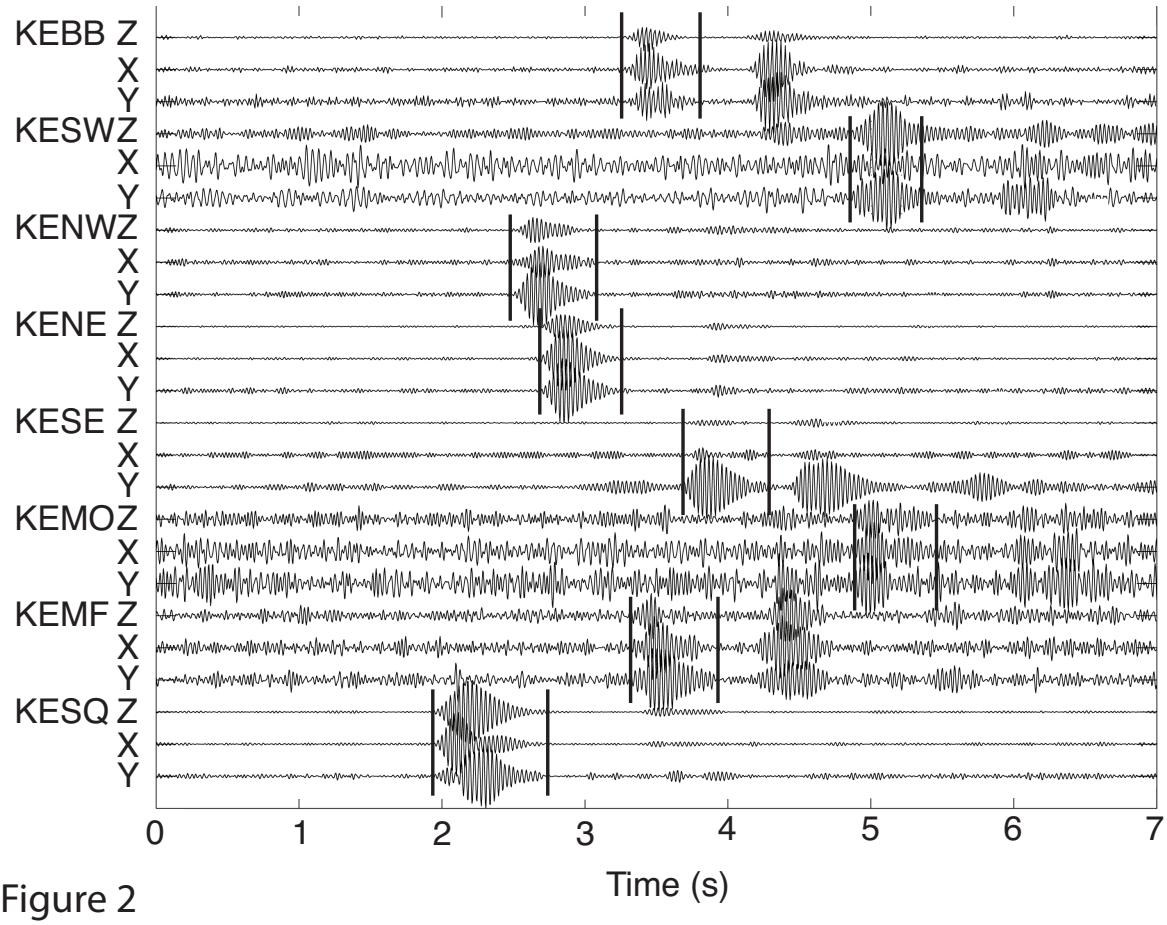

Figure 2

Figure 3.2 – Example of a call from a fin whale in the northern part of the seismic network. A high-pass 5 Hz filter has been applied and the records have been adjusted to equal maximum amplitude for each seismometer. The labels show the station name (Figure 3.1) and geophone orientation with the X and Y channels horizontal and the Z channel vertical. The direct arrivals are demarked with vertical bars and the first and sometimes second water column multiples are also often visible.

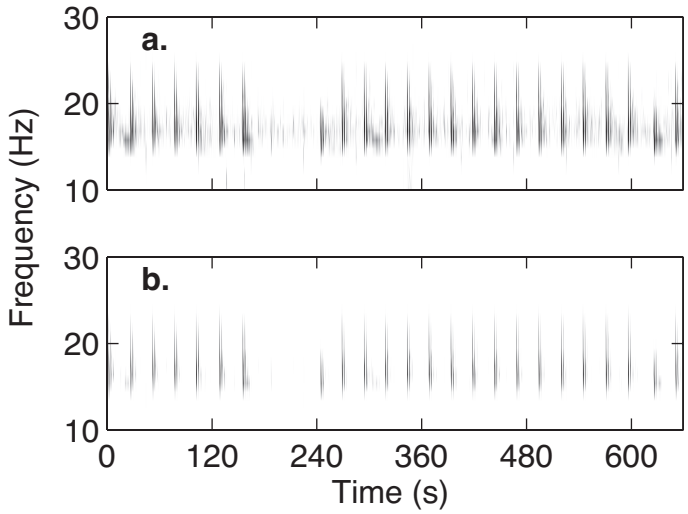

Figure 3

Figure 3.3 – (a) Example spectrogram from 24 October 2003 (128 point FFT, a Hanning window, and a 98% overlap) showing fin whale calls received on the network. (b) A modified spectrogram of the same data created by converting to decibels, subtracting a threshold set to two standard deviations above the mean decibel value in the 13-35 Hz frequency band and zeroing all negative values.

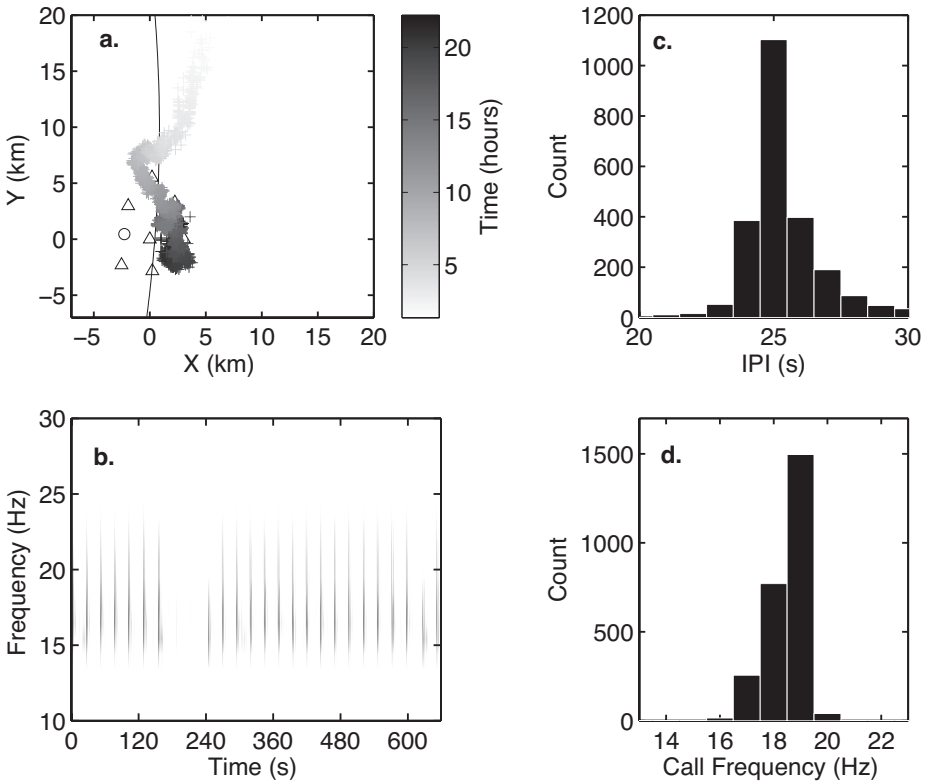

Figure 3.4 – (a) Example from 24 October 2003 of a 25 s single IPI fin whale track with locations shown by pluses shaded by time with light gray at the start of the track and dark gray at the end. The origin of the plot coincides with the center of the network and the y-axis for the plot is aligned with the mid-ocean ridge axis (Figure 3.1). The seismic stations of the network are shown by open symbols. (b) Modified Spectrogram for 650 seconds of data from the northernmost station. (c) Histogram showing distribution of inter-pulse interval (IPI) (d) Histogram showing the distribution of call frequencies.

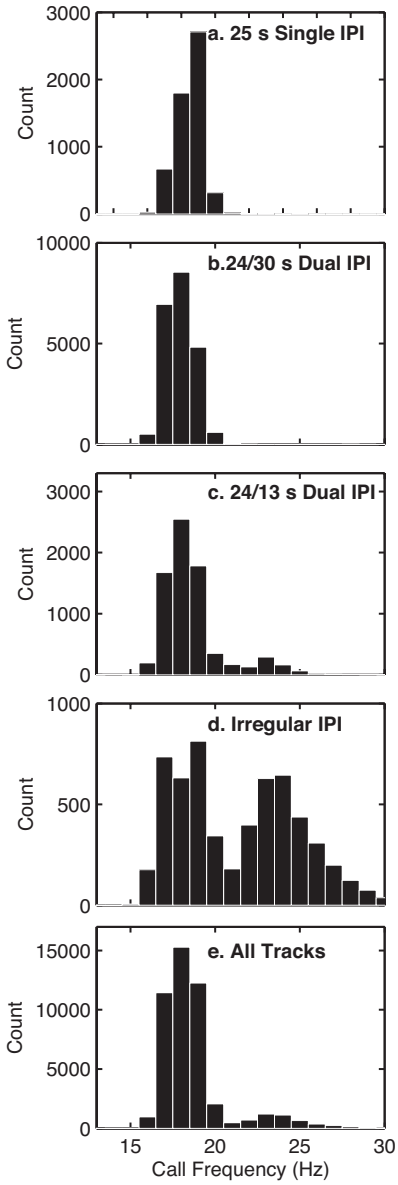

Figure 3.5 - Histogram showing the distribution of frequencies from the non-corrupted portions of calls in (a) the 25 s single IPI tracks (b) the 24/30 s dual IPI tracks (c) the 24/13 s dual IPI tracks (d) the irregular IPI tracks and (e) all tracks.

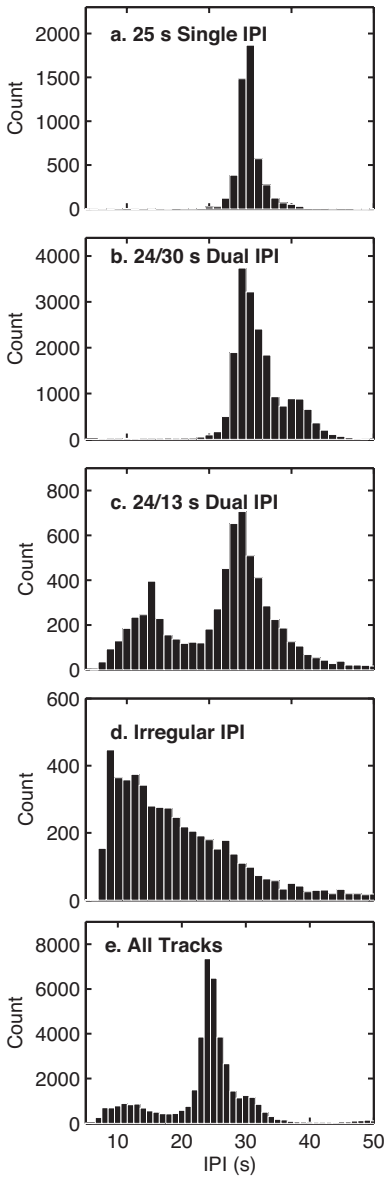

Figure 3.6 – Histograms showing the distribution of IPIs from portions of tracks that are not corrupted by off track calling for (a) the 25 s single IPI tracks (b) 24/30 s dual IPI tracks (c) the 24/13 s dual IPI tracks (d) the irregular IPI tracks and (e) all tracks.

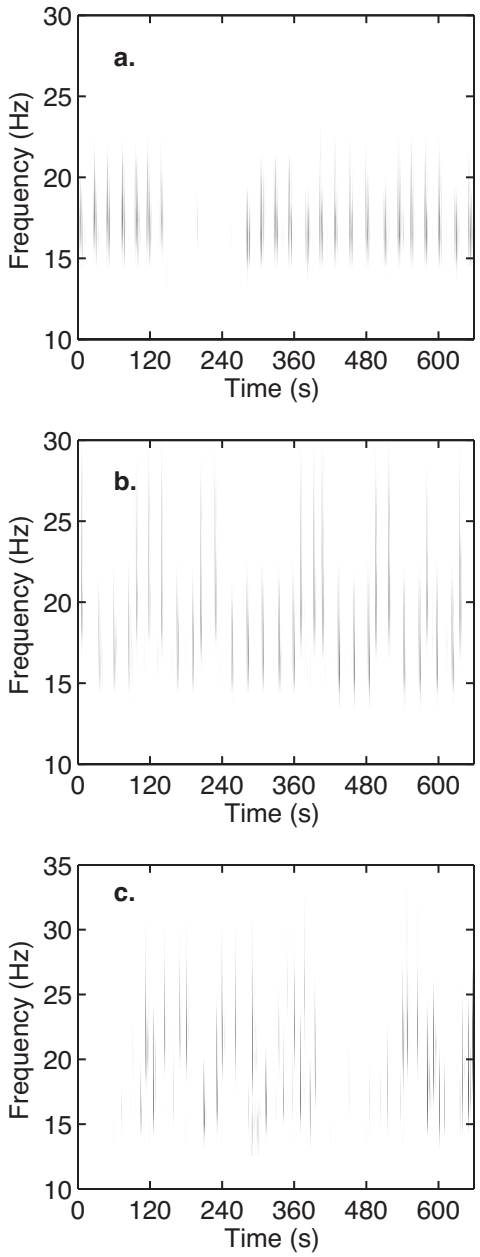

Figure 3.7 – Example modified spectrograms of 650 seconds of data for (a) a 24/30 dual IPI on 4 February 2004 showing both a resting interval from ~145 s to 285 s and two longer inter-pulse intervals starting at ~360 s and ~480 s; (b) a 24/13 dual IPI on 14 January 2004 showing calls centered at two frequencies and the short IPI correlating with the change from the lower frequency call to the higher frequency call; (c) an irregular IPI on 19 September 2003 showing short inter-pulse intervals at two separate frequencies.

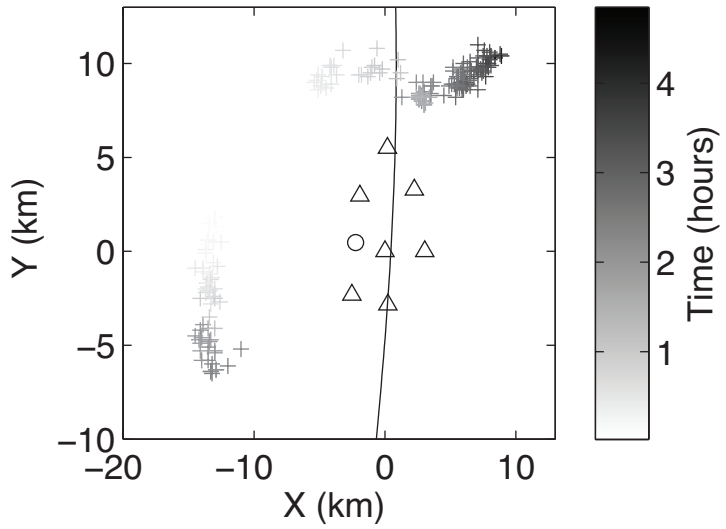

Figure 3.8 – Example of concurrent whale track from 10 November 2012 plotted with the same conventions as Figure 3.6.

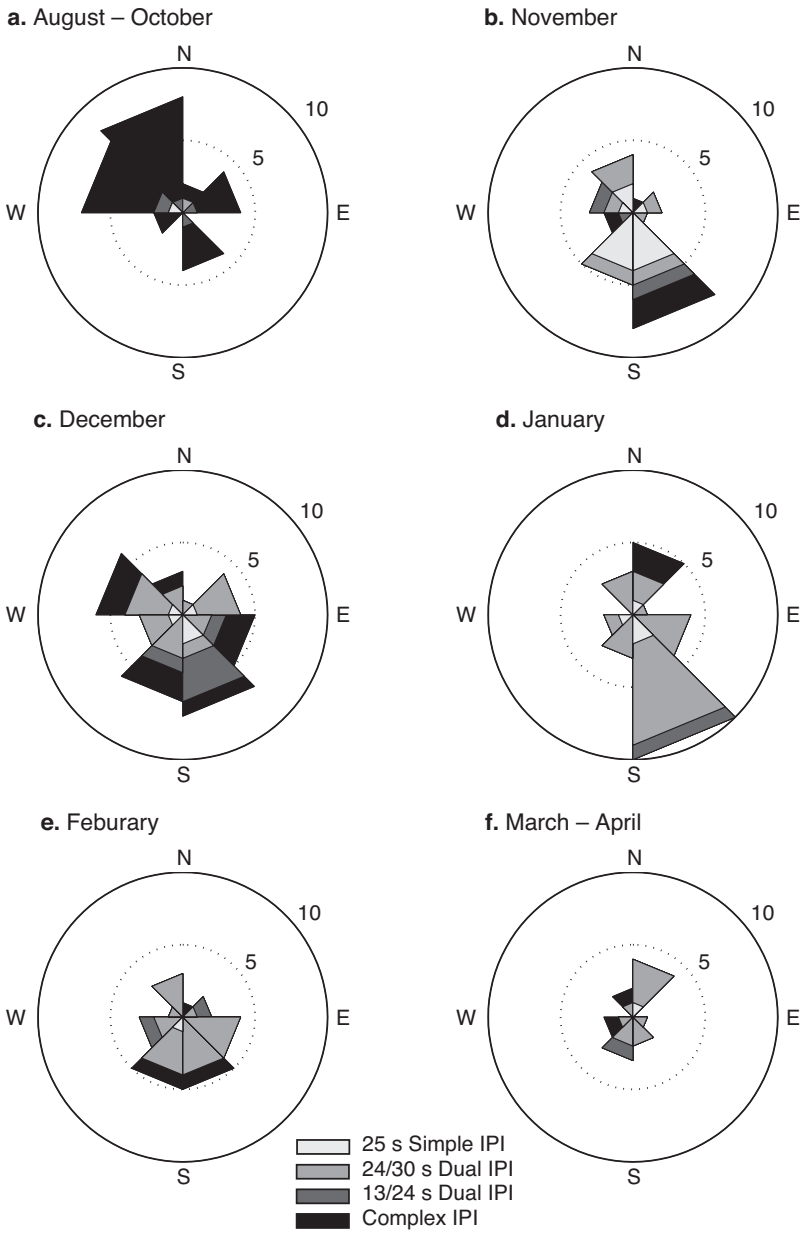

Figure 3.9 – Rose diagrams showing the temporal and directional distribution of whale tracks by category for (a) August through October, (b) November, (c) December, (d) January, (e) February and (f) March and April. Mixed IPI tracks are excluded from the plots

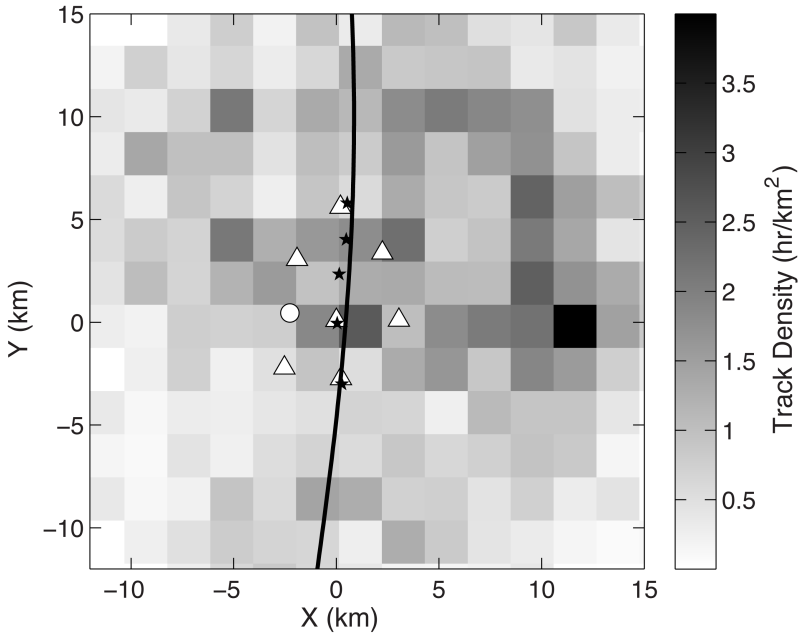

Figure 3.10 – Map showing the density of tracks on the rotated grid used for the locations (Figure 3.1) in units of hours per square kilometer. The position of the ridge axis, OBSs and vent fields are shown using the same convention as Figure 3.1.

Parameter	25s Single IPI	24/30s Dual IPI	24/13s Dual IPI	Irregular IPI	Mixed IPI	All Tracks
Tracks	24	74	16	27	13	154
Total duration (hr)	166	373	101	72	75	786
Uncorrupted (%)	31	66	64	70	91	73
Call count	5,542	21,477	7,395	5,765	6,843	47,022
Call Type						
18 Hz pulse (%)	94	85	80	39	–	81
Backbeats (%)	6	15	10	9	–	10
24 Hz pulse (%)	0	0	10	52	–	9
Tracks						
Mean length (km)	18	19	21	13	21	18
Mean net length (km)	12	13	13	11	13	13
Mean duration (hr)	6.9	5.0	6.3	2.7	5.7	5.1
Mean meander	1.7	1.8	2.0	1.2	2.4	1.8
Meander s.d.	1.3	2.7	1.9	0.3	2.2	2.1
Mean speed (km/hr)	3.0	4.3	4.0	5.9	3.9	4.3
Speed s.d. (km/hr)	1.7	2.0	1.8	2.5	1.5	2.1
Transiting (%)	17	36	38	60	31	37
Number of Call Frequencies						
1 frequency (%)	100	100	25	15	54	70
2 frequencies (%)	0	0	75	66	46	19
≥ 3 frequencies (%)	0	0	0	18	0	11
Swimming Direction						
Tracks to north	9	29	5	18	–	–
$P_{binomial}$	0.15	0.04	0.11	0.06	–	–
Random walk distance (km)	104	204	66	95	–	–
Random walk azimuth (°)	220	170	177	333	–	–
$P_{random\ walk}$	0.04	0.04	0.20	0.06	–	–

Table 3.1 – Characteristics of individual track categories and all tracks. Uncorrupted refers to the percentage of the total track duration that was not corrupted by calls from locations off the track. The call count is for the uncorrupted portions of the tracks. The percentages of 18 Hz and 24 Hz pulses are derived from the uncorrupted portions of tracks based on the number of calls with frequencies ≤20 Hz and ≥21 Hz, respectively. The percentage of backbeats was estimated from manual analysis of select track portions and subtracted from the percentage of 18 Hz pulse. Call type percentages were not calculated for the mixed IPI tracks and so the percentages in the All Tracks column are based on all tracks except the mixed IPI category. The mean length is the mean distance covered by the calling whale(s) and net length is the mean straight-line distance from the start to the end of each track. The meander parameter and criteria for classifying a track as transiting are described in the methods section. Tracks are assigned to 1, 2 or ≥ 3 frequency

classifications based on the number of distinct peaks at or above 18 Hz in the call frequency histogram. Tracks to north is the number of tracks in each category that has a northward component to their net distance traveled. $P_{binomial}$ is the one sided binomial probability that the north-south directionality of tracks is not southward for the 25 s single IPI, 24/30 dual IPI and 24/13 s dual IPI and not northward for the irregular IPI. Random walk distances and azimuths give the cumulative net length and direction obtained by putting tracks in each category end to end. $P_{random\ walk}$ is an estimate of the probability that randomly oriented tracks would travel at least as far as observed.

Chapter 4:

Large sensor-based datasets are effective learning tools for developing quantitative literacy and seismological understanding

Dax C. Soule[1], C. M. O'Reilly[2], Nickolas E. Bader[3], Thomas Meixner[4], Cathy Gibson[5], Russell E. McDuff[1] and Rebekka Darner Gougis[2]

[1]School of Oceanography, University of Washington, Seattle WA 98115
[2]Department of Geography-Geology, Illinois State University, Normal, IL 61790
[3]Department of Geology, Whitman College, Walla Walla, WA 99362
[4]Hydrology and Atmospheric Sciences, University of Arizona, Tucson, AZ 85721
[5]The Nature Conservancy, Albany, NY 122205

4.0 Abstract

EDDIE (Environmental Data-Driven Inquiry and Exploration) modules engage students in analysis of data collected by networks of environmental sensors, which are used to study various natural phenomena, such as nutrient loading, climate change, and stream discharge. We compared two approaches to EDDIE module implementation in an undergraduate time-series analysis course. Course goals were to use high-frequency and long-term environmental datasets to improve quantitative literacy, develop data manipulation and analysis skills, construct scientific knowledge about natural phenomena, and highlight the inherent variability in real data. In both instructional treatments, students explored data and developed skills through a scaffolded in-class analysis and then solved more complex problems in homework assignments. In Treatment 1, Engage and Explore lesson phases involved discussion of instructor-prepared plots using the think-pair-share method. Conversely, in Treatment 2's Engage and Explore lesson phases, students prepared graphs and completed activities in a computer lab, which required more guidance in data manipulation and thus contained less structured discussion of data analysis and interpretation. We administered a pre/post questionnaire to compare learning gains

between the two treatments in quantitative literacy, statistical reasoning, nature-of-science (NOS) understanding, and understanding of seismological concepts. Results indicate that EDDIE modules are sufficiently flexible to be effective in both learning environments.

4.1 Introduction

Today, students and researchers in the Earth and environmental sciences have unprecedented access to digital datasets from Earth-observing sensors. The characterization of dynamic environments, such as rivers or seafloor hydrothermal vents, requires temporally and spatially rich observations (Schimel et al., 2015) Sensor networks operated by U.S. Geological Survey (USGS), the National Ecological Observatory Network (NEON), the OOI Cabled Array and the Incorporated Research Institutes for Seismology (IRIS) all provide online access to data measuring a wide range of environmental parameters. The analysis of data from high-frequency sensors that range from multiple samples per day to thousands of samples per second require different skill sets than those currently taught in most undergraduate curricula (Brewer and Gross, 2003; Carey et al., 2015; Michener and Jones, 2012; Rubin and Abrams, 2015). However, these large datasets also create an opportunity to engage a broad student population in environmental investigations that both address authentic questions about Earth science and explore the skills and concepts of modern data science.

Digital data manipulation and analysis is a valued STEM (Science, Technology, Engineering and Mathematics) skill that is important both academically and in the workplace (Langen et. al, 2014; Rubin and Abrams, 2015). Data analysis can develop many skills, such as locate, retrieve, and synthesize data from diverse sources or the ability to formulate and test hypotheses (Rubin and Abrams, 2015). Specialized knowledge is needed to access compiled data that is available online and make decisions about how to deal with bad readings or gaps in the

record. Undergraduates are often unprepared and uncomfortable with the mechanics of sorting raw numbers into an interpretable database (Carey et al., 2015; Hernandez et al., 2012; Rubin and Abrams, 2015; Strasser and Hampton, 2012) and have difficulty manipulating and locating data. While student frustration with the "messiness" of real data may impede progress through curricula (Ellwein, 2014), it is important this knowledge be developed in the next generation of scientists because successful scientists must grapple with data regularly, and it is commonly the catalyst for more exploration. Evidence suggests that when they are comfortable with the mechanics of data analysis, students become more willing to use data to independently solve scientific problems and that using real data in the classroom starts a cycle in which exposure develops skills that lead to further exploration (Carey et al., 2015).

Data-centric research experiences using raw data sources, as opposed to procedure-driven lab experiences that examine fabricated and idealized data, engage students to demonstrate the intellectual connections and tools central to all science disciplines (Rubin and Abrams, 2015). Though teaching students statistics with Microsoft Excel creates the potential that students may plug numbers into the spreadsheet without fully understanding the resulting values or their assumptions and limitations (Rubin and Abrams, 2015; Whitford and Vieira, 2000), thoughtful analysis and interpretation of data requires the student to reason about variation to explain the patterns they observe (Gougis 2016; McCright, 2012). Thus, students engaged in data analysis have the opportunity to develop more sophisticated and intuitive scientific conceptions. For example, inquiry-based learning statistical learning has helped STEM students to improve their knowledge of scientific and statistical principles and processes, as well as hone their scientific research skills (McCright, 2012). Furthermore, when students envision data, create figures, and interpret data in figure captions, it requires reasoning about observations, which links technical

skill to conceptual understanding (Gougis et al., 2016). Students who learn statistical and scientific concepts in response to a need for descriptive statistics enhance their conceptual understanding when they analyze digital data that extend beyond the rote memorization of procedures (Eberlein et al., 2008; Fuller et al., 2011; Lim, 2009; McCright, 2012).

The use of real data is among the core recommendations of the American Statistical Association's Guidelines for Assessment and Instruction in Statistics Education (Gould, 2010). Variation, rate of change, uncertainty, and the exclusion of data are all concepts that students and scientists confront in order to make sense of raw data. Examining variation in real data, along with structured discussion of observed variation, has the potential to develop statistical conceptions about variation, randomness, and regression because such discussions can compel students who conceive of variation as merely a calculation or as superficial differences in form, toward understanding the need to capture variation in a dataset (Gougis et al., 2016). Bad data and outliers create opportunities to consider appropriate criteria for exclusion of data (Carey et al., 2015) and creates opportunities to build the statistical toolbox students need to correctly express significance and uncertainty (McCright, 2012).

Challenges remain regarding how to best teach analytical skills using digital data to students from diverse computational backgrounds (Moriarty et al., 2003, Hancock and Manduca, 2005, Hardin et al., 2015). Teaching in a computer lab overcomes the challenges inherent to data manipulation because it allows for hands-on experience with the data, but class time is limited and therefore teaching students to sort and manipulate data creates a tradeoff between hands-on exploration and the amount of conceptual information that could be covered in a lecture environment with no computer access (Eberlein et al., 2008). STEM classes do not typically scale well because computing facilities that offer hands-on experience are limited in size and

students in data-driven courses often need more time-intensive support than those in a traditional lecture environment (Davies et al., 2013; Langen et al., 2014). Additionally, it is challenging to coordinate the interaction of large groups typical of a lecture-based course while achieving meaningful contribution from all students when there are disparities in data manipulation and analysis skills (Hancock and Manduca, 2005).

Traditional lecture has been shown to have disadvantages for teaching STEM material in numerous studies across a variety of STEM fields (Hake, 1998, Knight and Wood, 2005, Eberlein et al., 2008, Freeman et al., 2014). Even the best passive lectures have limited effectiveness in achieving STEM learning objectives because they lack the active engagement needed to achieve meaningful understanding of new concepts (Knight and Wood, 2005). These challenges are only amplified when developing analytical skills that often involve complex manipulations with diverse data sets (Davies et al., 2013). Conversely, using pedagogical techniques that engage students in STEM content by having them collaboratively develop or invent difficult concepts have the advantages found in the large lecture environment with the learning success and gains in long-term retention of information associated with an active learning format (Eberlein et al., 2008, Chase et al., 2013, Freeman et al., 2014, Hake, 1998, Knight and Wood, 2005, Vanags et al., 2013). When using active learning techniques, the instructor can structure activities to provide class-wide discussions that control the pace of the class and address difficulties before any group gets too far behind (Beichner, 2000).

4.2 EDDIE

EDDIE (Environmental Data-Driven Inquiry and Exploration; www.projecteddie.org) seeks to develop students' process skills through cooperation and reflection by using digital datasets that help students examine an environmental phenomenon through inquiry (Bader et al.,

2016). EDDIE is focused on improving quantitative reasoning, building data manipulation skills, and highlighting the inherent variability in real data in the environmental sciences. The EDDIE team has created ten teaching modules based on the analysis of high-frequency and long-term datasets. Modules are designed to be scalable across different skill levels, both within and across different types of institutions. Each exercise has a flexible modular "A-B-C" structure that is loosely based on the 5E learning cycle (Bybee et al., 2006). In an EDDIE module, part A engages students in initial data exploration and skill development using simple analyses that bypass some of the technical challenges associated with the manipulation of data. Part B asks the student to *e*xplore and explain through more detailed analysis that requires the student to independently discuss and decide what analyses are appropriate for the data and explain the implications of results. In part C, students expand on the developed ideas by exploring data from sites of their choosing and/or by exploring questions that that they have developed (Carey et al., 2015). Modules are successful in improving quantitative literacy and increasing appreciation for the predictive power of large datasets (Carey et al., 2015). EDDIE modules provide opportunity for students to practice sophisticated cognitive tasks, such as data visualization and discussion of how spatial and temporal resolution affects ability to detect environmental changes.

Of particular interest in this study is EDDIE's Spectral Seismology module, which engages students in the use of spectral analysis to describe the frequency content of seismic arrivals. Seismology is an area of geoscience education that is understudied, particularly undergraduate students' conceptual development in this subdiscipline. Only 60% of geophysics and seismology items on the National Association of State Boards of Geology examination are answered correctly (Williams et al., 2004). To support undergraduates' geotechnical skills, several teaching resources have been provided (e.g., IRIS website; www.iris.edu/hq/). Other

examples are provided in the literature. For example, Hornbach (2004) constructed a multi-channel seismic device to conduct classroom experiments, and Wysession and Baker (2002) provided computer-generated animations to visualize seismic wave propagation. Although seismology instruction commonly engages students in analysis of authentic seismological data, this is less true for lower-level undergraduate seismology instruction due to coding barriers to many seismological analysis tasks, thus highlighting the need for EDDIE's Spectral Seismology module. This module is based on a conceptual presentation of waveforms and filters (Transnational College of LEX, 2012). The goal is for students to go beyond the basic terminology used to describe waveforms and develop the ability to relate a signal presented in the time domain to its conjugate in the frequency domain. The EDDIE module begins exploring this concept with students constructing complex waveforms using Excel and progressing to the use of seismic and acoustic signals available through IRIS to develop the vocabulary needed to describe spectrograms qualitatively. Using seismic data presents challenges based on the size of the data files and the difficulty of implementing some of the required calculations in Excel. To address this, our module uses Seismic Canvas (Kroeger, 2015; https://seiscode.iris.washington.edu/projects/seismiccanvas), which is a graphically interactive application for accessing, viewing and analyzing waveform data which we use to plot earthquake data in the time domain. Once students are familiarized with the general components of the waveform (i.e. frequency, wavelength, amplitude and period), they use Seismic Canvas to transform the data into the frequency domain. Bypassing the mathematics of Fourier Series allows us to focus on conceptual understanding by plotting and manipulating seismic data in both the time and frequency domain.

4.2.1 Purpose & Questions

A primary goal of this study is to elucidate the flexibility of EDDIE modules for different learning environments. Across the broad spectrum of active learning techniques (e.g. POGIL (Vanags et al., 2013), flipping the classroom (Davies et al., 2013)), it is common for instructors to adapt a given strategy by incorporating key aspects from another established technique (Chase et al., 2013). Instructors typically choose pedagogical strategies based on perceived effectiveness and difficulty of implementation. Knowing if EDDIE modules lose effectiveness when taught using different pedagogical strategies will allow educators to determine if the modules are sufficiently flexible to be adapted to a wide range of teaching strategies, depending on the specific educational setting (e.g., lecture hall, computer lab). In this study, we asked whether EDDIE modules are sufficiently flexible to be effectively taught in these two distinct learning environments, by documenting learning gains observed in each instructional setting. The focal conceptual areas are statistical understanding, quantitative literacy, and nature-of-science understanding.

A second question asked in this study was: What are the observed gains in students' understanding of seismology, presumably due to engagement with EDDIE's Spectral Seismology module, which seems to be the only teaching resource for lower division undergraduates currently available that engages students with real seismological data?

4.3 Methods

This study utilized a randomized experimental design to compare two instructional treatments, both implementing EDDIE (Environmental Data-Driven Inquiry and Exploration) modules. Goals of both treatments were to engage students in analysis of authentic data by exploring a variety of environmental phenomena. The EDDIE modules implemented were

Climate Change, Streamflow, Nutrient Loading and Spectral Seismology, which incorporate a range of statistical concepts (Table 4.1).

4.3.1 Participants

Students participating in this study were sophomore, junior, and senior science majors enrolled at a large, highly selective, public university located in the Pacific Northwest. All students were enrolled in a special topics course advertised to students as an Introduction to Data Analysis and Seismology data. Students who registered for the course were randomly assigned to an instructional treatment. Both treatments contained 10 students and met once per week for one hour.

4.3.2 Treatments

Each lesson plan was based on EDDIE's conceptual structure for creating modules that engage students in authentic data analysis using the 5E learning cycle (Bybee et al., 2006). In both treatments, part A of each module consisted of initial data exploration and skills development using simple analyses. Statistical concepts were both implicitly explored through practical application and explicitly presented in the form of vignettes consisting of brief lectures for the topics of linear regression, the R-squared value, standard deviation, probability, and the geometric distribution. Parts B and C of the modules were homework assignments that guided students through the subsequent three phases of the learning cycle. In both treatments, feedback is provided on the graded homework assignments and common misconceptions were debriefed in subsequent class meetings.

The two treatments differed in location and how Part A was structured for the in-class portion of the modules (Table 4.2). Treatment 1 took place in a traditional classroom, and students engaged in Part A without computers using worksheets that included instructor-

produced graphs and relevant statistics. The lecture presentation in Part A was punctuated with questioning and discussion among students or between students and instructor in the form of think-pair-share questions (King, 1993). Part A worksheets engaged students in initial data exploration and prepared them for homework (Parts B-C) using simple analyses that bypass all of the technical challenges associated with the manipulation of data. Data-manipulation skills were left for the student to develop while completing the homework.

In contrast, students in Treatment 2 met in a computer lab and engaged in all the steps of Part A's data analysis, including navigating, downloading, processing, and plotting the data during the first class meeting in which a module was covered. A brief lecture presentation is followed by students working in pairs to complete worksheets that tell students how to access the data for Part A and create appropriate graphs (Table 4.2). In short, treatments differed in that Treatment 1 removed data manipulation from Part A and focused on data interpretation, while Treatment 2 engaged students in data manipulation from the beginning of the module.

4.3.3 Data Collection

Quantitative data was collected using a 6-part questionnaire administered at the beginning and end of the course to all participants. Part I focused on seismology understanding that was used to address the second research question, which measured observed gains in students' understanding of seismology. It consisted of 5 open-ended items that measured skills in analyzing a Seismology record for a teleseismic earthquake plotted as both a traditional seismogram and as a spectrogram. Each open-ended item was scored on a scale of 1-6, with 6 being the highest level of understanding. Because each item examined a different aspect of understanding that will be discussed separately, Part I scores were not aggregated for statistical analysis. Seismology Item 1 asked students' to use the seismogram (Figure 4.1a) and the

spectrogram (Figure 4.1b and 4.1c) to estimate the frequency content of the primary wave. This tested the students' understanding of frequency and how the data being displayed on the spectrogram are related to the data being displayed on the seismogram. Seismology Item 2 built on question one by asking students to identify the time and frequency of the largest amplitude arrival. This measured students' understanding of amplitude and their ability to use the spectrogram (Figure 4.1b and 4.1c) as an analysis tool. Seismology Item 3 asked students to estimate the frequency range with the most energy for this earthquake, which tested students' ability to use the spectrogram and their understanding of frequency and amplitude. Seismology Item 4 asked students to estimate the background frequency, which indicated students' ability to differentiate between the signal pre- and post- arrival of the primary wave and use the spectrogram to estimate frequency content. Seismology Item 5 was designed to test students' understanding of how frequency content can be removed from a signal in the spectral domain. Students were asked to compare plots of raw data (Figure 4.1) and the same data filtered with a high-pass filter (Figure 4.2), and identify the filter used to create the second plot.

Part II consisted of Watson et al.'s (2003) distributional variation scale (DVS), modified to have close-ended answer choices that were derivatives of prototypical students' responses to the original open-ended items documented by Gougis et al. (2016). The DVS measures students' ability to identify probable and improbable variation in a dataset (Watson et al., 2003). Responses on the modified DVS were summed to yield a DVS score (0 -10).

Part III consisted of three close-ended items that asked students to define variation, sample, and random in the context of science. These items were close-ended, with answer choices formulated from prototypical students' responses to the original open-ended items documented by Gougis et al. (2016). Each item's answer choice was ranked according to levels

of sophistication (Gougis et al., 2016). Variation (0 - 2), sample (0 - 2), and random (0 - 3) items' responses were summed to yield an overall score (0 - 7) for conceptual understanding of statistical ideas.

Part IV consisted of the Student Understanding of Science and Scientific Inquiry (SUSSI) instrument, which is a 20-item instrument answered on a 5-point Likert scale that measures students' understanding of the nature of science and scientific methods (Liang et al., 2006).

Part V contained 6 close-ended items measuring students' ability to distinguish r-squared from slope when making inferences from regression analyses, which were summed to yield an overall score of ability to distinguish r-squared from slope. Part VI contained 11 items prompting students to rank their Excel comfort and skills on a 5-point Likert scale.

To address the first research question in which we ask do the instructional treatments differ in the degree to which students learn statistical concepts and skills and nature-of-science understanding, separate split-plot analyses of variance (ANOVA) were used to compare pre/post scores across treatments on the DVS, conceptual understanding of statistical ideas, the SUSSI, ability to distinguish r-squared from slope, and Excel comfort and or ability. In the second research question in which we ask if engagement in EDDIE modules (Climate Change, Streamflow, Nutrient Loading and Spectral Seismology) supports learning of seismological concepts, a separate split-plot ANOVA was performed on each Part I item.

4.4 Results

The interaction of time (pre versus post) and treatment was not statistically significant for any of the measures, indicating that students reacted similarly to both instructional treatments. Comparison of pre- and post-course scores on the DVS (Part II) exhibited significant gains ($F(1,14) = 4.5$, $p = 0.05$, Figure 4.3), and students' ability to provide scientific definitions of "variation," "random," and "sample" also significantly improved ($F(1,14) = 4.9$, $p = 0.04$, Figure 4.4). Students demonstrated significant improvement in differentiating r-squared from slope between pre- and post-course ($F(1,15) = 4.6$, $p = 0.05$, Figure 4.5). Similarly, students' comfort and self-reported ability using Excel significantly improved between pre- and post-course ($F(1,15) = 72.9$, $p < 0.0001$, Figure 4.6).

For the Seismology item 1, the pre/post comparison was statistically significant ($F(1,15) = 6.1$, $p = 0.03$), indicating both treatments positively increased between pre- and post-course (Figure 4.7). This same result was observed on Seismology item 2, in which the pre/post comparison was statistically significant ($F(1,15) = 8.7$, $p = 0.01$, Figure 4.8), as well as Seismology item 5 ($F(1,15) = 7.5$, $p = 0.02$, Figure 4.7) Seismology items 3 and 4 showed no statistically significant pre/post changes.

Nature of science understanding, as measured by the SUSSI (Liang et al., 2006), showed no statistically significant changes between pre- and post-course, although treatment 2 demonstrated a negative trend in nature of science understanding (Figure 4.10).

4.5 Discussion

The widespread adoption of data-intensive course work is slowed both by limitations in infrastructure and the lack of preparation in both instructors and students (Hampton et al., 2013). Though many studies have compared traditional lecture to active learning environments for STEM material (Hake, 1998, Knight and Wood, 2008, Eberlein et al, 2008, Davies et al., 2013, Freeman et al., 2014), and studies have varied the implementations of pedagogical models (Chase, 2013), less study has been devoted to comparing the active learning lecture environment to a computer lab for the purposes of using digital data as a pedagogical tool, perhaps because it is assumed that the lab environment is needed to achieve optimal results? Our results indicate that EDDIE modules are effective when implemented in active learning strategies, particularly think-pair-share, and flexible enough to teach students data analysis skills without access to a computer lab. Positive outcomes in quantitative literacy are achievable in either the active learning environment or the computer laboratory environment. This flexibility in choice of learning environment should help eliminate obstacles based on infrastructure and facilitate participation across a wider range of class environments.

Treatment 1 and Treatment 2 shared many key features. Both presented a brief slide-based introduction to the general topic explaining the attributes of the datasets in an exercise. Both treatments operated on the premise that basic science concepts will be learned when they are discussed and applied in a practical, real-world context (Hake et al., 1998; Eberlein et al., 2008). In both cases the instructional style was dynamic and the instructor carefully tracked the students' progress as they worked on in-class exercises (Langen et al., 2014). The instructor clarified or modified material as needed, and common misconceptions were addressed to the whole class. Both treatments were assigned identical homework. After the introductory

presentation, Treatment 1 transitioned to worksheet-guided collaborative activities that engaged them in Part A of an EDDIE module. Instructor-produced graphs were incorporated in the activity and included in slides used to discuss problem-solving strategies as a class (Eberlein et al., 2008). As Beichner (2000) suggests, this approach provided ample opportunities to supplement the small collaborations with large class discussions that addressed misconceptions and points of difficulty.

In contrast, Treatment 2, which took place in a computer lab, used identical introductory slides, but in Part A of the module, students worked collaboratively to access, plot, and analyze the data. Discussions about individual graphs occurred in small groups as the instructor circulated among the students. This created a tradeoff in which the time spent accessing and plotting the data in Treatment 2 was spent on additional conversation and reflection in Treatment 1. It also created challenges dealing with varying rates at which students worked through the activities (Carey, 2015).

4.5.1 Improving students' statistical understanding

As suggested in Manduca and Mogk (2002), each module uses multiple datasets to look at different aspects of a central problem. The EDDIE modules on climate change, streamflow and nutrient loading all share common themes of variation on both short and long timescales. Together they present opportunities to use data in the context of multiple environmental questions. The modules explore environmental topics including the determinants of global temperature, the modern rate of change versus historical rate of change of both temperature and carbon dioxide, modern and historical patterns of stream discharge and peak flow in both pristine and urban environments, nutrient loading, and water pollution. Students are introduced to and frequently revisit the statistical topics of r-squared, slope, probability, geometric distributions,

covariation, and sampling. Analysis is supplemented through discussion of the social aspects of these datasets, and student responses to the modules indicated that they were engaged in controversial aspects such as science denial, the effects of urbanization on discharge events, eutrophication, and the difficult policy choices we face regarding agriculture and water quality. This study documents the first case in which measurable improvement in statistical understanding was observed when teaching EDDIE modules, indicating that implementation of multiple EDDIE modules can be used to successfully teach statistical concepts.

Prior studies suggest that the statistical vignettes, in conjunction with practical applications, are among the most effective ways to build conceptual understanding of difficult topics (Gould et al., 2010). In this study, we observed improvements in the following areas of statistical knowledge: Ability to distinguish plausible variation from unlikely variation in a dataset; more sophisticated definitions of variation, random, and sample; ability to distinguish between r-squared and slope; and comfort and self-reported skill using Excel. In our approach, problems were presented to students first, which allowed for students to construct the concept before it was operationalized during the statistical vignette (Eberlein et al., 2008). It is likely the vignettes contributed to conceptual development of statistical concepts because they linked analytical tasks (e.g., creating a trendline in Excel and retrieving an r-squared value) to conceptual understanding of the statistical meaning and purpose behind those tasks. In other words, the problem presented in Part A of the EDDIE module provokes an intellectual need compelling the statistical learning (Fuller et al., 2011; Lim, 2009).

4.5.2 Spectral Seismology Module

A secondary goal of this study was to document the learning of seismological concepts during EDDIE's Spectral Seismology module. Because our pre/post questionnaires were

administered before and after the course, we acknowledge that a limitation of this study is that we cannot claim for certain that learning of seismological concepts was due solely to the Spectral Seismology module. However, the other course content (EDDIE's Climate Change, Streamflow, and Nutrient Loading modules) included absolutely no frequency-time representations, so we feel comfortable concluding that positive changes in seismology understanding was due to instruction during the Spectral Seismology module.

The Spectral Seismology module uses seismic events as a context to explore the properties of a wave. Previous research examining the teaching of seismology in an active learning environment has focused on using data to teach students about Earth properties (Bobbio et al., 2007). Other studies (Denton et al., 2008) have shown that physics can be taught using earthquakes and seismology as a hook to grab students' attention. This approach can also extend to analysis. The relationship between the time and frequency domain are most often explored in the context of the mathematical procedures that are required to make the mathematical transformation between the two (Whitford et al., 2001; Vogt, 2011; Miller et. al., 2016). Due to the procedural manner in which this material is often presented, it is common for students to still lack a conceptual understanding of the relationship between the time and frequency domain, despite having used the mathematical formula to make the transformation many times (Moriarty, 2003).

Student performance on Seismology Item 1 demonstrated that students in both treatments developed their ability to use the seismogram and the spectrogram to estimate the frequency content of the primary wave. This finding indicates that the module developed students' conceptual understanding of frequency and how the spectrogram is related to the seismogram. A similar pre/post improvement was observed on Seismology Item 2, which measured the students'

ability to differentiate seismic arrivals based on their amplitude, indicating the module likely developed their understanding of amplitude and their ability to use the spectrogram as an analysis tool. Similarly, significant improvement was observed on Seismology Item 5, which asks the student to observe both a filtered and unfiltered signal and describe the likely filter based on the observed change in waveform in the time and frequency domain. Students' improvement on Seismology Item 5 demonstrates the module's efficacy in developing students' conceptual understanding of waveforms as the sum of simpler components that can be filtered based on frequency.

Seismology Items 3-5 required more sophisticated understanding of seismological content, and significant improvement was only observed on one of these items. Student performance on Seismology Items 3 and 4 indicated the module's effectiveness at developing the ability to use the spectrogram and to measure frequency and amplitude. Upon reflection, the instructor (first author) speculates that in order to elicit significant learning gains on these items two modifications should be explored. First, more time must be devoted to developing the Fast Fourier Transform (FFT), which converts the time series information to the frequency domain. Second, the lesson would be more effective if we provided the students with a web-based widget that would enable them to create their own spectrograms and manipulate the time-series that created it.

4.5.3 Nature of Science Understanding

Nature of science (NOS) understanding, as measured by the SUSSI (Liang et al., 2006), showed no statistically significant changes between pre- and post-course, although Treatment 2 demonstrated a negative, albeit nonsignificant, trend in nature of science understanding. This interesting result is consistent with prior studies using EDDIE modules that have struggled to

achieve this learning objective. Lederman (1992) points out that although instructors' understanding of NOS does not translate to the ability to teach it effectively, many instructors across all backgrounds do not possess adequate conceptions of the nature of science and thus cannot effectively teach what they do not understand. We suspect that our result is due to the implicit nature of the NOS instruction contained in the EDDIE modules (Khishfe, and Abd-EL-Khalick, 2002). Separate vignettes could be created that explore the amoral, tentative, empirically-based product of human creativity or parsimonious aspects of NOS, distinctions between observations and inference, and relationships between scientific theories and laws (Lederman et al., 1992; Khishfe and Lederman, 2006), along with suggestions as to where these might best fit with respect to any given EDDIE module. Explicit NOS instruction in the form of a vignette would serve the dual purpose of developing the instructor's NOS understanding while also providing a pedagogically sound format for explicit NOS instruction.

4.5.4 Assumptions and Limitations

There are several limitations to this study that should temper extrapolation of these findings to other student populations. One key limitation of this study is the small sample size, which may have played a role in our ability to achieve statistically significant results. Also, all participants chose to take this course as an elective, which may have resulted in a class that was more motivated than typical undergraduate students. This enthusiasm may have eventually been overwhelmed by the low credit-to-work ratio; the course was taught as a 1-credit credit/no credit course. Students' most common complaint was the length of the modules and in the later part of the term, students almost certainly made economic decisions with their time that resulted in effort being directed away from the analysis and report for each module towards other courses in which there was a grade at stake, thus reducing the learning opportunity in later modules. As

mentioned earlier, we are basing claims about the Spectral Seismology module's efficacy on a pre/post comparison that encompassed implementation of EDDIE's Climate Change, Streamflow, and Nutrient Loading modules, in addition to the Spectral Seismology module. However, since the other modules contained no seismological content, we feel confident in assuming these gains were due to the Spectral Seismology module.

4.6 Conclusions

In this study we compared students' learning gains in two instructional approaches, both implementing EDDIE modules (projecteddie.org). One approach began with guidance through instructor-generated graphs and analyses before students completed data manipulation, analysis, and interpretation independently. The other approach engaged students in all phases of authentic science, from data acquisition through analysis, from the beginning of each module. Positive pre/post learning gains were observed in both instructional approaches, and no differences in learning gains were observed across instructional treatments. Specifically, students experienced gains in understanding of statistical concepts (i.e., randomness, variation, sampling, r-squared, slope), comfort and self-reported ability using Excel, and ability to differentiate plausible variability from unlikely variability in a dataset. Students also exhibited significant gains in understanding of seismological concepts, presumably due to EDDIE's Spectral Seismology module. While not significant, a negative trend was observed in nature of science understanding in the treatment that engaged students in all phases of authentic science, indicating an explicit approach to teaching NOS concepts is needed if EDDIE modules are to be used to address this learning objective.

This study demonstrates the flexibility of EDDIE modules in supporting a variety of learning goals related to quantitative literacy and statistical understanding. Follow-on studies are planned to develop additional seismology modules focused on earthquake location and focal mechanisms as well as exploring the use of explicit instruction on either statistics or NOS in the form of a modular "vignettes" that could supplement any lesson plan. We would also like to examine the effects of more than one Project EDDIE module on both Excel skills and the conceptual understanding of the scientific principles under study to determine if students' attention shifts from spreadsheet manipulation to the learning of scientific concepts and principles, as they feel increasingly comfortable.

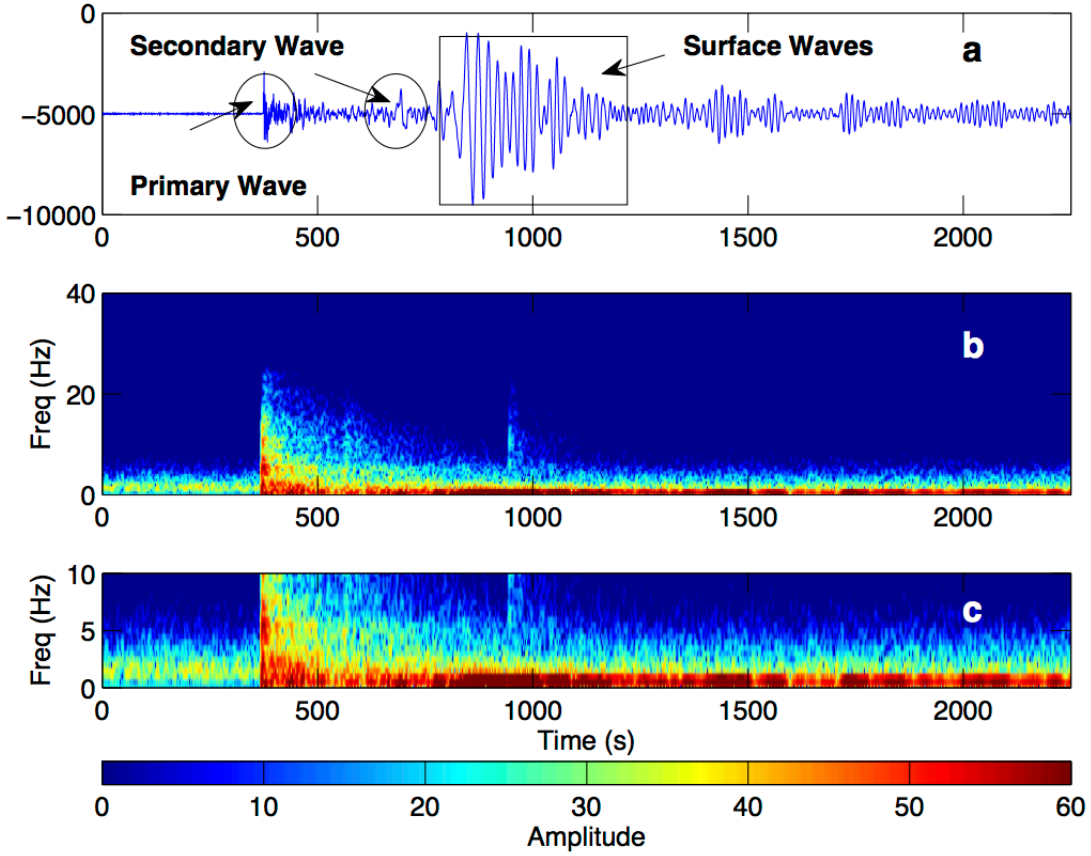

Figure 4.1 – (a) Example seismogram plots time on the X-axis versus displacement on the Y-axis for a distant teleseismic earthquake. (b) Example spectrogram plots the same data in the frequency domain with time on the X-axis versus frequency on the Y-axis. (c) Example spectrogram plots the same data in the frequency domain from 0-10 Hz with time on the X-axis versus frequency on the Y-axis.

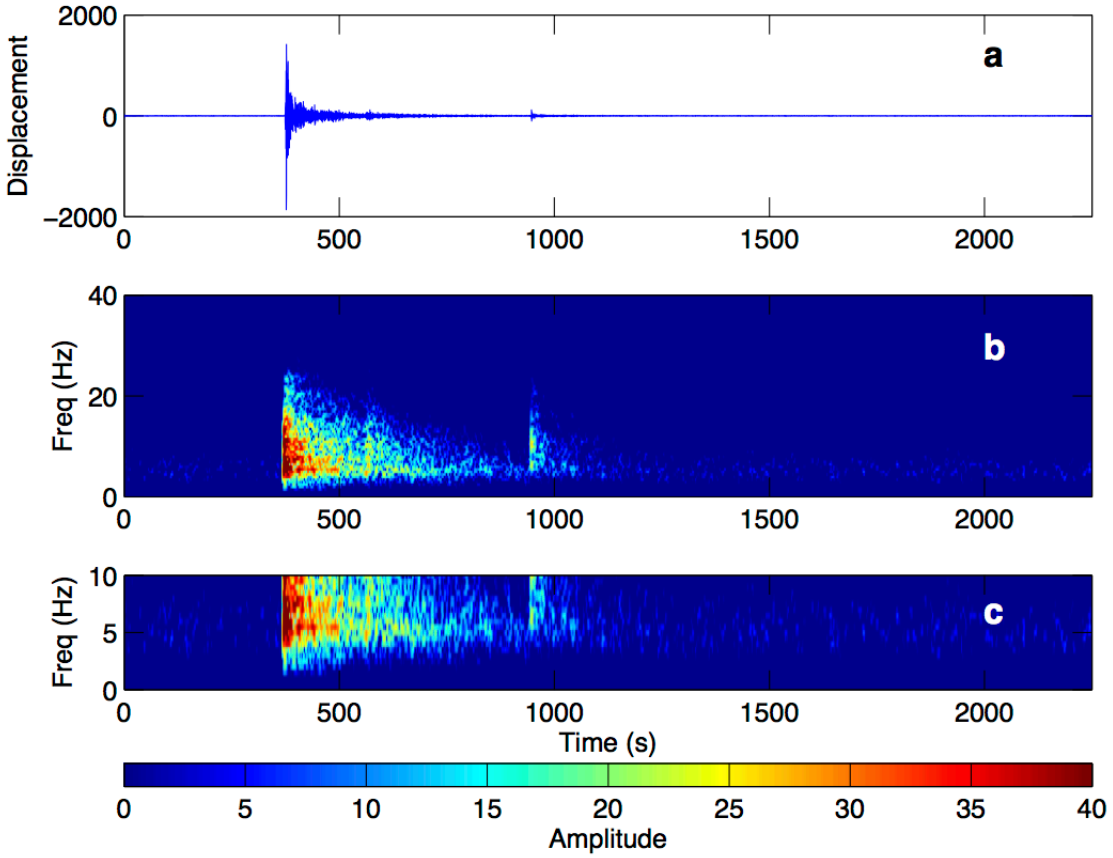

Figure 4.2 - (a) Example seismogram with a 1 Hz high-pass filter plots time on the X-axis versus displacement on the Y-axis for a distant teleseismic earthquake. (b) Example spectrogram plots the same data in the frequency domain with time on the X-axis versus frequency on the Y-axis. (c) Example spectrogram plots the same data in the frequency domain from 0-10 Hz with time on the X-axis versus frequency on the Y-axis.

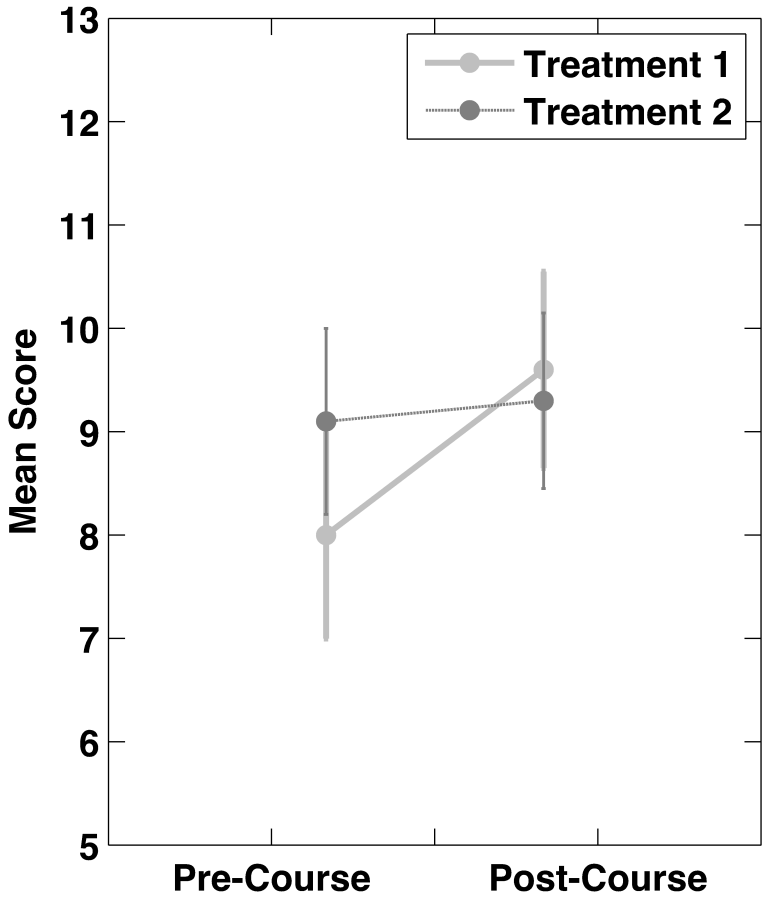

Figure 4.3 – There was no significant interaction between treatments on the distributional variation scale (DVS) (Watson et al. (2003)), which measures students' ability to identify probable and improbable variation in a dataset. With treatments pooled into a single sample, there was a significant pre- and post-course gain ($F(1,14) = 4.5$, $p = 0.05$). The F statistic measures the ratio between the between group variability and the within group variability. Here we measure both if the mean variation between treatments is significantly less than or greater than the mean variation within each treatments. The mean is considered significantly different between treatments if the test statistic is in the top 2.5% or bottom 2.5% of its probability

distribution, resulting in a p-value less than 0.05.

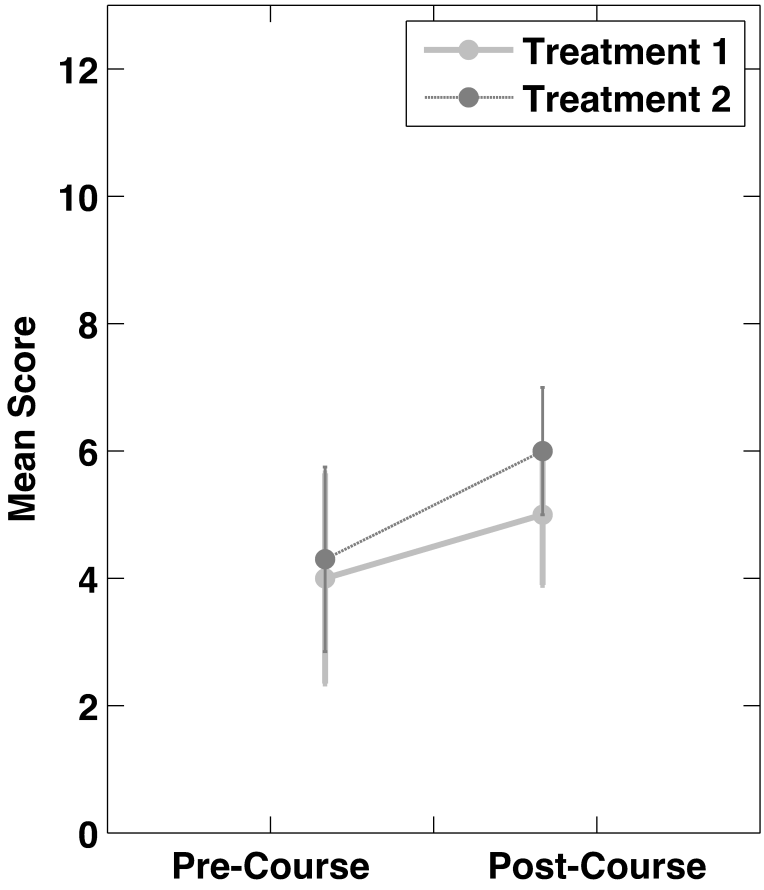

Figure 4.4 – Measure of Statistical Reasoning - the measure of conceptual understanding of "variation," "random," and "sample" significantly improved for both Treatment 1 (classroom learning environment) and Treatment 2 (computer lab learning environment) between pre- and post-course ($F(1,14) = 4.9$, $p = 0.04$) questionnaires.

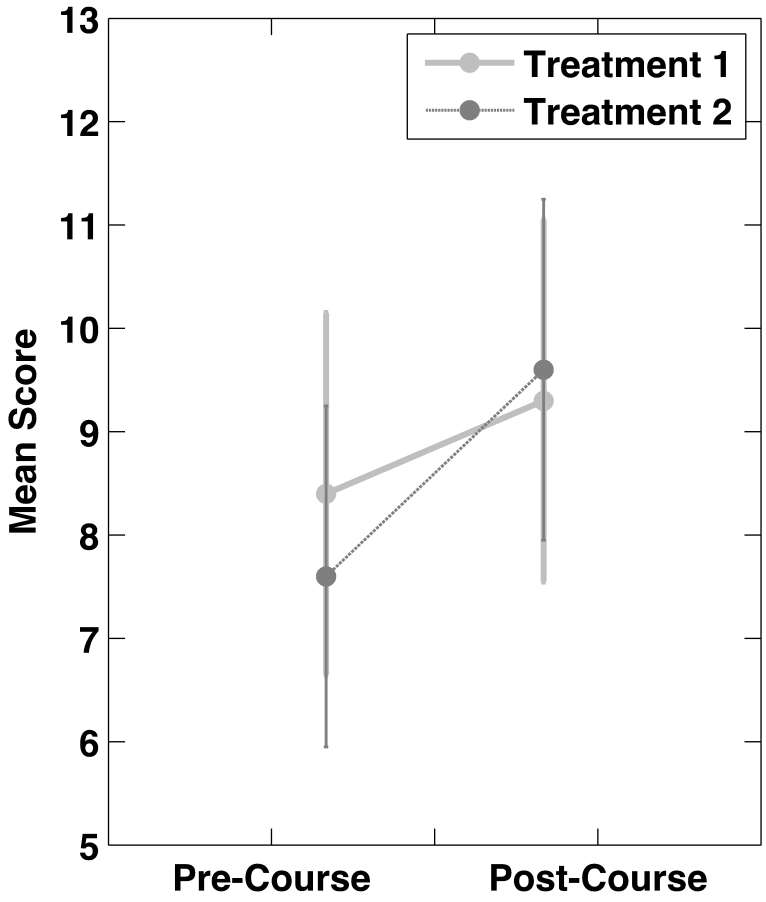

Figure 4.5 – Students demonstrated significant improvement for both Treatment 1 (classroom learning environment) and Treatment 2 (computer lab learning environment) in differentiating r-squared from slope between pre- and post-course questionnaires ($F(1,15) = 4.6$, $p = 0.05$).

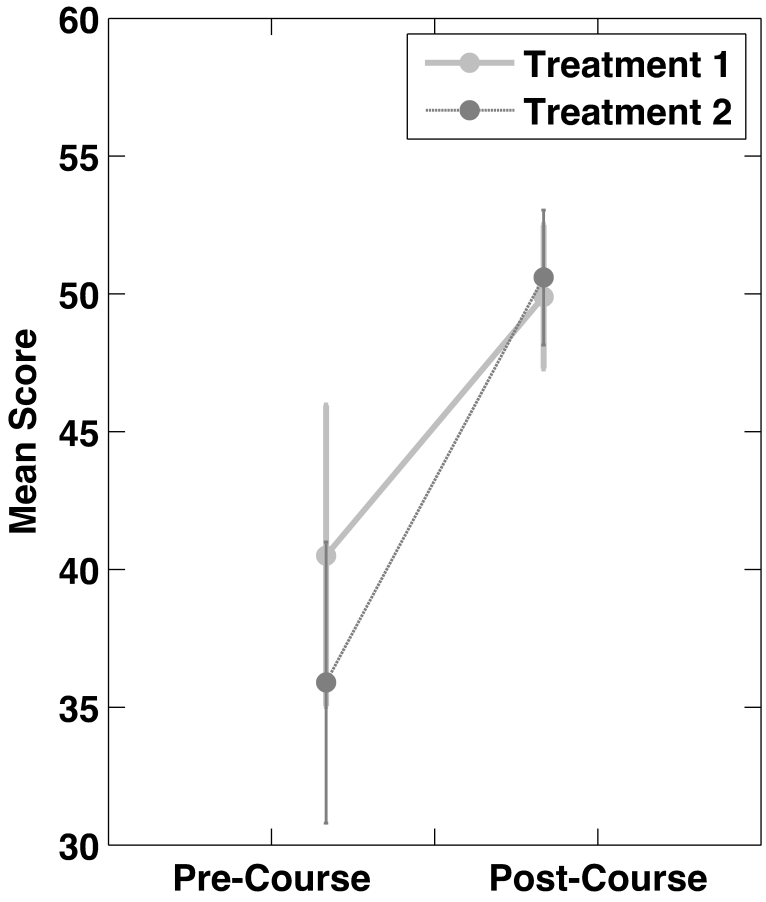

Figure 4.6 – Change between pre- and post-course in students' comfort and self-reported ability using Excel. The pre/post comparison was statistically significant ($F(1,15) = 72.9$, $p < 0.0001$, $n = 16$) for both Treatment 1 (classroom learning environment) and Treatment 2 (computer lab learning environment).

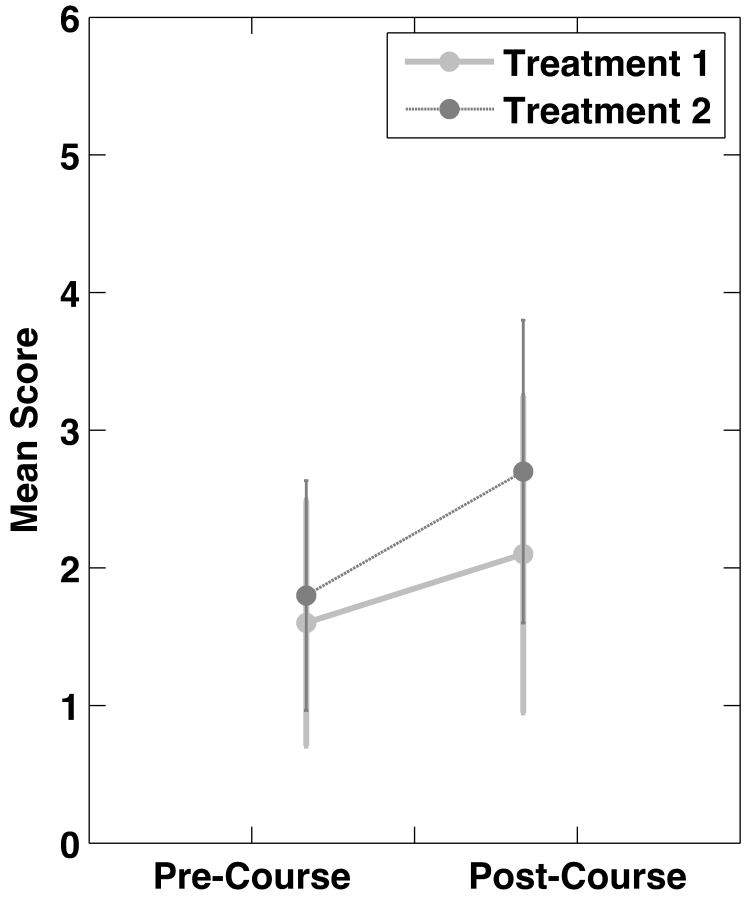

Figure 4.7 – Change between pre- and post-course in students' ability to use the seismogram and the spectrogram to estimate the frequency content of the primary wave, measured by Seismology Item 1. The pre/post change was statistically significant ($F(1,15) = 6.1$, $p = 0.03$, $n = 16$) for both Treatment 1 (classroom learning environment) and Treatment 2 (computer lab learning environment).

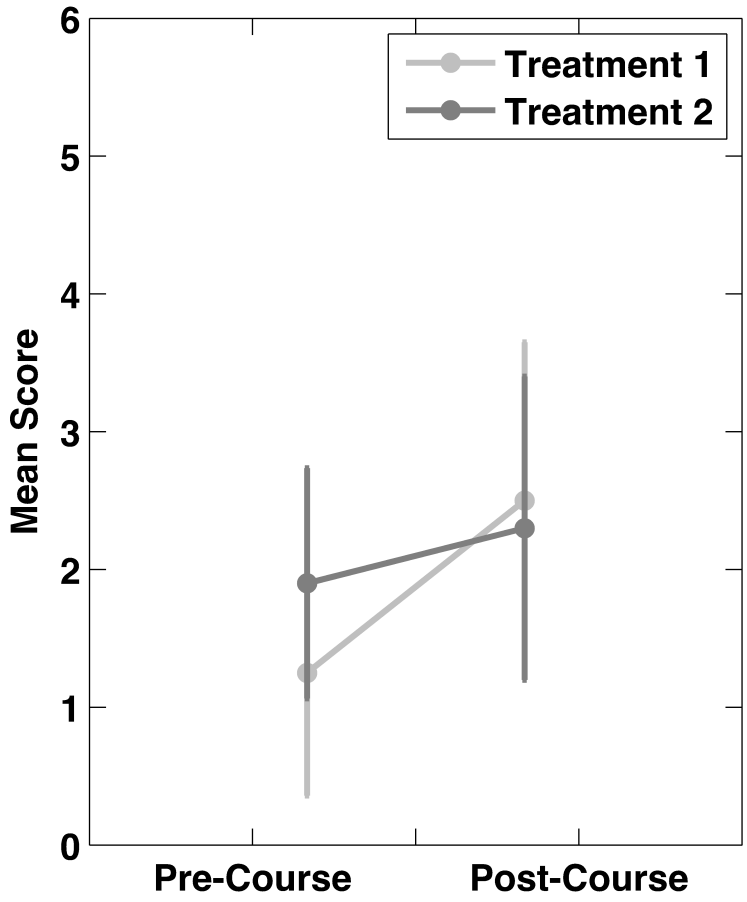

Figure 4.8 – Change between pre- and post-course in students' ability differentiate seismic arrivals based on their amplitude, measured by Seismology Item 2 the pre/post change was statistically significant $F(1,15) = 8.7$, $p = 0.01$, $n = 16$) for both Treatment 1 (classroom learning environment) and Treatment 2 (computer lab learning environment).

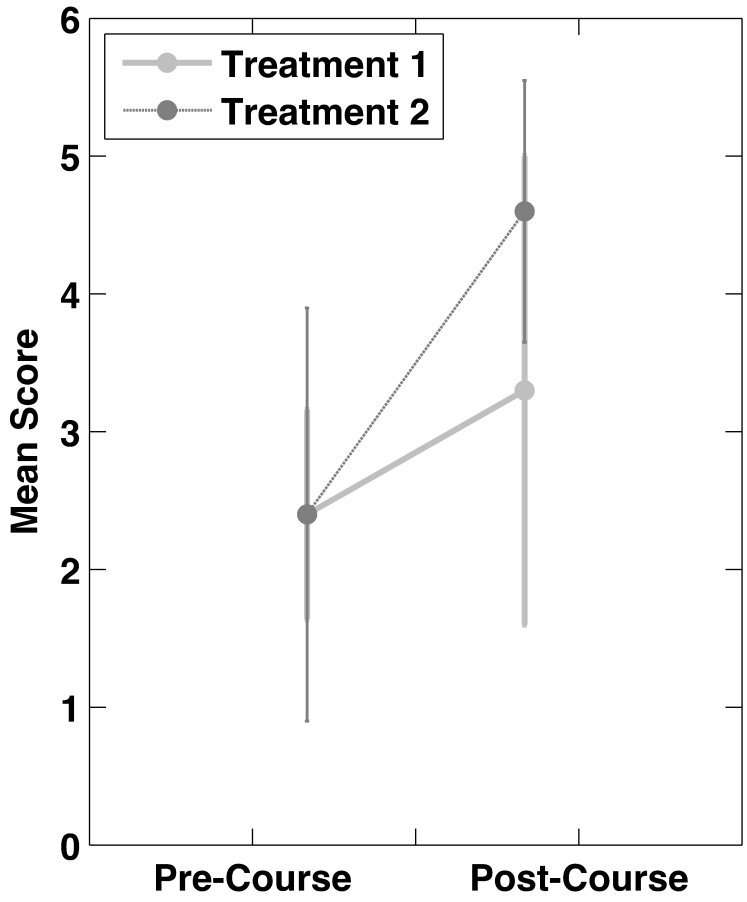

Figure 4.9 – Change between pre- and post-course in students' ability to observe both a filtered and unfiltered signal and describe the likely filter based on the observed change in waveform in the time and frequency domain, measured by Seismology Item 5; the pre/post change was statistically significant ($F(1,15) = 7.5$, $p = 0.02$, $n = 16$) for both Treatment 1 (classroom learning environment) and Treatment 2 (computer lab learning environment).

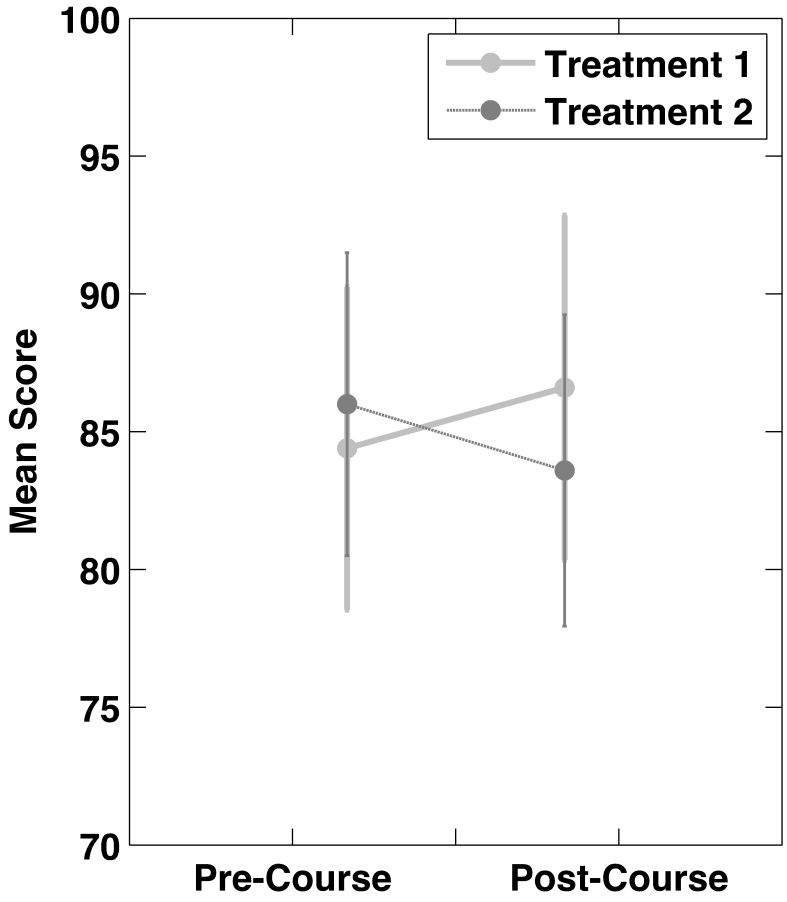

Figure 4.10 – Students' nature of science (NOS) understanding, as measured by the SUSSI (Liang et al., 2006), showed no statistically significant changes between pre- and post-course for both Treatment 1 (classroom learning environment) and Treatment 2 (computer lab learning environment).

Table 4.1. This table summarizes the EDDIE modules taught in this study, the amount of in class time devoted to each topic and the statistical concepts addressed in each lesson.

Module Name	Description	Class time used (h)	Concepts Addressed
Climate Change	This module explores how climate is changing by examining both air temperature and CO2 records. These modern rates of change will be compared to changes in the Vostok ice core data.	1.5	Linear Regression, r-squared, natural variation, rates of change
Stream Discharge	This module explores real-time stream discharge data available from the United States Geologic Survey to assess changes in discharge with time, calculate flood frequency, and see the effects of urbanization and food control.	1.5	Variability and trends, r-squared, peak event probability
Nutrient Loading	This module uses real-time nitrate data from the US Geological survey to investigate the interplay of concentration and discharge and explore nitrogen loading to streams in the context of drinking water regulatory standards.	1.5	Covariation, averaging, sampling
Spectral Seismology	This module uses seismic data to learn basic seismology concepts by exploring time series data qualitatively in both the time and frequency domain.	3	Sampling, filtering, frequency, amplitude

Table 4.2. This table summarizes the differences between treatment 1 and treatment 2. The columns represent the range of pedagogical features applied to the instructional environments in Treatment 1 and Treatment 2. A "x" indicates that the given pedagogical feature was not used in the given Treatment, while a checkmark represents that the feature was used.

Instructional environment	Student acess to computers during instructioal period	Slide-based introduction to the general topic	Introductory worksheet	Students plotted and analyzed data during instructioal period	Students analyzed data using instructor produced plots during instructional period	Statistcal vignettes
Treatment 1	✖	✔	✔	✖	✔	✔
Treatment 2	✔	✔	✔	✔	✖	✔

Chapter 5:

Summary and Conclusions

This study demonstrates the utility of seafloor networks in both instruments of primary data collection and tools for teaching Earth science to students as they develop Science, Technology, Engineering, and Mathematics (STEM) skills. Larger data sets and increased bandwidth offer opportunities to explore multiple questions with individual data streams that would be expensive to duplicate in a dedicated experiment. OBS data from an experiment that was designed to target small seafloor earthquakes were used to identify important acoustic and swimming behaviors in an endangered whale population. Linking the acoustic behavior of fin whales to their swimming behavior in this manner hints at the potential for long term *in situ* measurements to address questions that range far beyond the intended scope of any specific experimental design. This work has led to follow on studies exploring various aspects of fin whale vocalizations and behaviors. Call location data have facilitated estimation of fin whale call source levels (Weirathmueller et al., 2013) and calling depth and have been used to verify single-station estimates of range using the multipath structure of received vocalizations (Weirathmueller and Wilcock, 2015). The analysis of vocalization and swimming patterns continues to be used as a baseline for similar studies applied to both fin and blue whale calls (Wade et al., 2015) recorded at larger regional networks (Cascadia Initiative, Ocean Networks Canada, OOI Cabled Array).

Our model of crustal thickness and lower crustal velocities on the Endeavour Segment of the Juan de Fuca Ridge is the first segment scale model of crustal thickness and lower crustal velocity in young crust produced at an intermediate spreading rate ridge with substantial contrasts in seafloor morphology and upper crustal structure between the segment center and the

segment ends. Our results contribute to the understanding of the magmatic processes that form the oceanic crust and in particular the processes that control the thickness and structure of the lower crust. This study confirms that an elevated plateau at the segment center is underlain by thickened crust. We infer that at the segment ends the lower crust cools by hydrothermal circulation on axis while at the segment center it cools within 5 km of the spreading axis.

The Endeavour velocity model is an important part of ongoing studies examining the composition of the lower crust and upper mantle and provides important new constraints that are needed for further analysis of lower crustal densities and the nature of the Moho interface both beneath the spreading center and off axis. The broad implications of these results are that along-axis melt transport is ineffective in the lower crust and that hydrothermal circulation is effective at cooling young crust away from the axial magma chambers.

Though seafloor data has historically been accessible to only a few students at universities with seagoing scientist, major advancements in oceanographic data collection and fiber optic connectivity create an opportunity to incorporate the Ocean Networks Canada (ONC), OOI Cabled Array and Argo programs into undergraduate training in a way that will both provide early analytical skills and promote a more diverse scientific community for the future. These programs represent a paradigm shift from the model in which data is primarily collected small groups of scientists on oceanographic cruises to one in which data is available in real time and is freely available to anyone. In order to engage students with diverse backgrounds, it is incumbent upon institutions like the University of Washington to lead by developing pedagogical techniques that use these innovations to facilitate the use of oceanographic data at a broad range of institutions.

This dissertation contributes a new pedagogical application of ocean bottom seismometer data that engages students using both seismic and acoustic signals developed in the context of an EDDIE module (projecteddie.org) and will lead to follow-on studies developing additional seismology modules and exploring the use of explicit statistical instruction in the form of a "vignette". The effectiveness of these modules in supporting a variety of learning goals related to quantitative literacy and statistical understanding demonstrate the successful use of digital data in either a lecture setting or a computer laboratory. The flexibility of EDDIE modules makes them an ideal platform for the seismic and earth science communities in the construction of lesson plans that use oceanographic data.

References

Arai, R. and Dunn, R. A. (2014), Seismological study of Lau back arc crust: Mantle water, magmatic differentiation, and a compositionally zoned basin, Earth Planet. Sci. Lett., 390, 304-317, doi:10.1016/j.espl.2014.01.014.

Bader, N. E., Soule, D. and Castendyk, C. (2016), Students, meet data: Using publicly available, high-frequency sensor data in the classroom. Submitted Eos 2016. DOI: http://dx.doi.org/10.1029/2016EO047175

Barclay, A. H., D. R. Toomey, and S. C. Solomon (1998), Seismic structure and crustal magmatism at the Mid-Atlantic Ridge, 35°N, J. Geophys. Res., 103 (B8), 17827–17844, doi:10.1029/98JB01275.

Beichner, R. J., Saul, J. M., Allain, R. J., Deardorff, D. L., and Abbott, D. S. (2000), Introduction to SCALE-UP: Student-centered activities for large enrollment university physics. American Society For Engineering Education, Proceedings of the Annual Meeting.

Bobbio, A., Cantore, L., Miranda, N., and Zollo, A. (2007), New tools for scientific learning in the EduSeis project: The e-learning experiment. Annals of Geophysics, 50 (2): 283-290.

Bowlin, J. B., Spiesberger, J. L., Duda, T. F., and Freitag, L. F. (1993), Ocean Acoustics Ray-Tracing Software RAY, Technical Report WHOI-93-10, WHOI.

Brewer, C. A., and Gross, L. J. (2003), Training ecologists to think with uncertainty in mind. Ecology, 84:1412–1414. DOI:10.1890/0012-9658(2003)084 (1412:TETTWU) 2.0.CO;2

Bybee, R. W., Taylor, J. A., Gardner, A., Van Scotter, P., Power, J. C., Westbrook, A., and Landes, N. (2006), BSCS 5E instructional model: Origins and effectiveness. A report prepared for the Science Education, National Institute of Health. BSCS.

Burd, B. J., Thompson, R. E., and Jamieson, G. S. (1992), Composition of a deep scattering layer overlaying a mid-ocean ridge hydrothermal plume, Mar. Bio. 113, 517–526.

Burd, B. J. and Thomson, R. E. (1994), Hydrothermal venting at Endeavor Ridge – effect on zooplankton biomass throughout the water column, Deep-Sea Res. Part I-Ocean. Res. Papers 41, 1407–1423.

Burd, B. J. and Thomson, R. E. (1995), Distribution of zooplankton associated with the Endeavour Ridge hydrothermal plume, J. Plankton Res. 17, 965–997.

Canales, P. J., Detrick, R. S., Toomey, D. R. and Wilcock, W. S. D. (2003), Segment-scale variations in the crustal structure of 150 – 300 kyr old fast spreading oceanic crust (East Pacific Rise, 8°15′N–10°5′N) from wide-angle seismic refraction profiles. Geophys. J. Int., 152, 766–794, doi: 10.1046/j.1365-246X.2003.01885.x.

Carbotte, S. M., R. S. Detrick, A. Harding, J. P. Canales, J. Babcock, G. Kent, E. Van Ark, M. Marjanović, and J. Diebold (2006), Rift topography linked to magmatism at the intermediate spreading Juan de Fuca Ridge, Geol. Soc. Am. Bull, 34, 209-212. doi: 10.1130/G21969.1.

Carbotte, S. M., M. R. Nedimović, J. P. Canales, G. M. Kent, A. J. Harding, and M. Marjanović (2008), Variable crustal structure along the Juan de Fuca Ridge: Influence of on-axis hot spots and absolute plate motions, Geochem. Geophys. Geosyst, 9, Q08001, doi: 10.1029/2007GC001922.

Carbotte, S. M., M. Marjanović, Helene Milena, J. C. Mutter, J. P. Canales, M. R. Nedimović, S. S. Han and M. R. Perfit (2013), Fine-Scale segmentation of the crustal magma beneath the East Pacific Rise, Nat. Geosci., 6, 866-870. doi: 10.1038/ngeo1933.

Carey, C. C. et al. (2015), A model for using environmental data-driven inquiry and exploration to teach limnology to undergraduates. Limnology and Oceanography Bulletin, 24 (2): 32-35. DOI: 10.1002/lob.10020

Carlson, R. L., and C. N. Herrick (1990), Densities and Porosities in the Oceanic Crust and Their Variations With Depth and Age, J. Geophys. Res., 95 (B6), 9153-9170. doi: 10.1029/JB095iB06p09153.

Carlson, R. L., and J. D. Miller (2004), Influence of pressure and mineralogy on seismic velocities in ocean gabbros: Implications for the composition and state of the lower crust, J. Geophys. Res., 109, B09205, doi: 10.1029/2003JB002699.

Carlson, R. L., J. D. Miller, and J. Newman (2009), Olivine enigma: Why alteration controls the seismic properties of oceanic gabbros, Geochem. Geophys. Geosyst., 10, Q03O16, doi:10.1029/2008GC002263.

Castellote, M., Clark, C. W., and Lammers, M. O. (2011), Fin whale (Balaenoptera physalus) population identity in the western Mediterranean Sea, Mar. Mamm. Sci. DOI: 10.1111/j.1748- 7692.2011.00491.x, 1–19.

Charif, R. A., Mellinger, D. K., Dunsmore, K. J., Fristrup, K. M., and Clark, C. W. (2002), Estimated source levels of fin whale (Balaenoptera physalus) vocalizations: Adjustments for surface interference, Mar. Mamm. Sci. 18, 81–98.

Chase, A., Pakhira, D. and Stains, M. (2013), Implementing process-oriented, guided-inquiry learning for the first time: Adaptations and short-term impacts on students' attitude and performance. Journal of Chemical Education, 90: 409-416. DOI: 10.1021/ed300181t

Christensen, N. I. (1979), Compressional wave velocities in rocks at high temperatures and pressures, critical thermal gradients, and crustal low-velocity zones, J. Geophys. Res., 84 (B12), 6849–6857, doi:10.1029/JB084iB12p06849.

Cotte, C., Guinet, C., Taupier-Letage, I., Mate, B., and Petiau, E. (2009), Scale-dependent habitat use by a large free-ranging predator, the Mediterranean fin whale, Deep-Sea Res. Part I-Oceanographic Res. Papers 56, 801–811.

Croll, D. A., Acevedo-Gutierrez, A., Tershy, B. R., and Urban-Ramirez, J. (2001), The diving behavior of blue and fin whales: Is dive duration shorter than expected based on oxygen stores?, Comparative Biochem. and Physiol. Part A Mol. and Integrative Physiol. 129A, 797– 809.

Croll, D. A., Clark, C. W., Acevedo, A., Tershy, B., Flores, S., Gedamke, J., and Urban, J. (2002), Only male fin whales sing loud songs, Nature 417, 809.

Davies, R. S., Dean, D. L. and Ball, N. (2013), Flipping the classroom and instructional technology integration in a college level information systems spreadsheet course. Education Technology Research and Development, 61: 563-580. DOI: 10.1007/s11423-013-9305-6

Davis, E. E. and J. L. Karsten (1986), On the cause of the asymmetric distribution of seamounts about the Juan de Fuca ridge: ridge-crest migration of a heterogeneous asthenosphere, Earth Planet. Sci. Lett., 79 (3-4), 385-396, doi:10.1016/0012-821X(86)90194-9.

Delarue, J., Todd, S., Parijs, S. V., and Iorio, L. D. (2009), Geographic variation in Northwest Atlantic fin whale (Balaenoptera physalus) song: Implications for stock structure assessment, J. Acoust. Soc. Am. 125, 1774–1782.

Denton, P. (2008), Seismology in schools: 10 years on. Astronomy and Geophysics, 49 (6): 13-14. DOI: 10.1111/j.1468-4004.2008.49613.x

Detrick, R. S., H. D. Needham, and V. Renard (1995), Gravity anomalies and crustal thickness variations along the Mid-Atlantic Ridge between 33°N and 40°N, J. Geophys. Res., 100 (B3), 3767–3787, doi:10.1029/94JB02649.

Dunn, R. A., D. R. Toomey, and S. C. Solomon (2000), Three-dimensional seismic structure and physical properties of the crust and shallow mantle beneath the East Pacific Rise at 9°30'N, J. Geophys. Res., 105 (B10), 23537–23555, doi:10.1029/2000JB900210.

Dunn, R. A., V. Lekić, R. S. Detrick, and D. R. Toomey (2005), Three-dimensional seismic structure of the Mid-Atlantic Ridge (35°N): Evidence for focused melt supply and lower crustal dike injection, J. Geophys. Res., 110, B09101, doi:10.1029/2004JB003473.

Dziak, R. P. (2006), Explorer deformation zone and reorganization of the Pacific-Juan de Fuca-North American tripple junction, Geology, 34 (3), 213-216, doi: 10.1130/G22164.1

Eberlein, T., Kampmeier, J., Minderhout, V., Moog, R.S., Platt, T., Varma-Nelson, P., and White, H.B. (2008), Pedagogies of engagement in science. Biochemistry and Molecular Biology Education, 36(4): 262-273. DOI: 10.1002/bmb.20204

Ellwein, A. L., Hartley, L. M., Donovan, S., and Billick, I. (2014), Using rich context and data exploration to improve engagement with climate data and data literacy: Bringing a field station into the college classroom. Journal of Geoscience Education, 62: 578-586.

Freeman, S., Eddy, S. L., Mcdonough, M., Smith, M. K., Okoroafor, N., Jordt, H., and Wenderoth, M. P. (2014), Active learning increases student performance in science, engineering, and mathematics. Proceedings of the National Academy of Sciences of the United States of America, 111(23), 8410-5. DOI: 10.1073/pnas.1319030111

Fuller, E., Rabin, J. M., and Harel, G. (2011), Intellectual need and problem-free activity in the mathematics classroom. International Journal for Studies in Mathematics Education, 4(10), 80-114.

Gougis, R.D., Stomberg, J.F., O'Hare, A.T., O'Reilly, C.M., Bader, N.E., Meixner, T., and Carey, C.C. (2016), Post-secondary science students' explanations of randomness and variation and their implications for science learning. In press in International Journal of Science & Mathematics Education, 1-18.. DOI: 10.1007/s10763-016-9737-7

Gould, R. (2010), Statistics and the modern student. International Statistical Review, 78 (2): 297-315. DOI: 10.1111/j.1751-5823.2010.00117.x

Hake, R.R. (1998), Interactive-engagement versus traditional methods: A six-thousand-student survey of mechanics test data for introductory physics courses. American Journal of Physics, 66: 64–74. DOI: 10.1119/1.18809

Hampton, S. E., Strasser, C. A., Tewksbury, J. J., Gram, W. K., Budden, A. E., Batcheller, A. L., Duke, C. S., and Porter, J. H. (2013), Big data and the future of ecology. Frontiers in Ecology and the Environment, 11 (3): 156-162. DOI: 10.1890/120103

Hancock, G. C., and Manduca, C. (2005), Developing quantitative skills activities for geoscience students. Eos Transactions American Geosciences Union, 86(39): 354-355. DOI: http://dx.doi.org/10.1029/2005EO390003

Hardin, J., Hoerl, R., Horton, N. J., and Nolan, D. (2015), Data science in statistics curricula: preparing students to think with data . The American Statistician 69(4): 343-353.

Hatch, L. T. (2004), Acoustic differentiation among fin whales, Balaenoptera physalus, in the North Atlantic and North Pacific Oceans, and integration with genetic estimates of divergence, Dissertation, Cornell University, Ithaca, N. Y.

Hatch, L. T. and Clark, C. W. (2004), Acoustic differentiation between fin whales in both the North Atlantic and North Pacific Oceans, and integration with genetic estimates of divergence, Int. Whal. Comm. document SC/56/SD6, 37.

Hernandez, R. R., Mayernik, M. S., and Murphy-Mariscal, M. (2012), Advanced technologies and data management practices in environmental science: Lessons from academia. Bioscience, 62 (12): 1067-1076. DOI:http://dx.doi.org.offcampus.lib.washington.edu/10.1525/bio.2012.62.12.8

Hooft, E. E. E., R. S. Detrick, D. R. Toomey, J. A. Collins, and J. Lin (2000), Crustal thickness and structure along three contrasting spreading segments of the Mid-Atlantic Ridge, 33.5°–35°N, J. Geophys. Res., 105 (B4), 8205–8226, doi:10.1029/1999JB900442.

Hooft, E. E. E., H. Patel, W. S. D. Wilcock, K. Becker, D. Butterfield, E. Davis, R. Dziak, K. Inderbitzen, M. Lilley, P. McGill, D. R. Toomey, and D. Stakes (2010), A seismic swarm and regional hydrothermal and hydrologic perturbations: The northern Endeavour segment February 2005, Geochem. Geophys. Geosyst, 11, Q12015, doi: 10.1029/2010GC003264.

Hornbach, M. J. (2004), Development of a Low Cost, Portable Multi-Channel Seismic Data Acquisition System for Classroom Experiments and Independent Studies. Journal of Geoscience Education, 52(4):386-390. DOI: http://dx.doi.org/10.5408/1089-9995-52.4.386

Johnson, H. P., J. L. Karsten, J. R. Delaney, E. E. Davis, R. G. Currie, and R. L. Chase (1983), A detailed study of the Cobb Offset of the Juan de Fuca Ridge: Evolution of a propagating rift, J. Geophys. Res., 88 (B3), 2297–2315, doi:10.1029/JB088iB03p02297.

Iturrino, G. J., N. I Christensen, S. Kirby and M. H. Salisbury (1991), Seismic velocities and elastic properties of oceanic gabbroic rocks from hole 735B, Proc. Ocean Drill. Prog. Sci. Results. 118, 227-244, doi:10.2973/odp.proc.sr.118.151.1991.

Karsten, J. L., S. R. Hammond, E. E. Davis, and R. G. Currie (1986), Detailed geomorphology and neotectonics of the Endeavour Segment, Juan de Fuca Ridge: New results from Seabeam swath mapping, Geo. Soc. Am. Bul., 97 (2), 213-221, doi: 10.1130/0016-7606(1986)97<213:DGANOT>2.0.CO;2.

Khishfe R. and Abd-El-Khalick, F. (2002), Influence of explicit and reflective versus implicit inquiry-oriented instruction on sixth graders' views of nature of science. Journal of Research in Science Teaching, 39 (7): 551-578. DOI: 10.1002/tea.10036

Khishfe, R. and Lederman, N. (2006), Teaching nature of science within a controversial topic: Integrated versus nonintegrated. Journal of Research in Science Teaching, 43 (4): 395-418. DOI: 10.1002/tea.20137

King, A. (1993), From sage on the stage to guide on the side. College Teaching, 41(1), 30-36. DOI: 10.1080/87567555

Knight, J. K., and Wood, W. B. (2005), Teaching more by lecturing less. Cell Biology Education, 4 (4): 398-410. DOI: 10.1187/05-06-0082

Kroeger, G. (2015), Seismic Canvas: Evolution as a Data Exploration and Analysis Tool. American Geophysical Union Fall Meeting, San Francisco

Langen, T. A., Mourad, T., Grant, B.W., Gram, W.K.,Abraham, B. J., Fernandez, D.S., Carroll, M., Nuding, A., Balch, J. K., Rodriguez, J., Hampton, S. E. (2014), Using large public datasets in the undergraduate ecology classroom. Frontiers in Ecology and the Environment, 12: 362–363. DOI: 10.1890/1540-9295-12.6.362

Lederman, N. G. (1992), Students' and teachers' conceptions of the nature of science: A review of the research. Journal of Research in Science Teaching, 29 (4): 331-359.

Liang, L. L., Chen, S., Chen, X., Kaya, O.N., Adams, A. D., Macklin, M., and Ebenezer, J. (2006), Student understanding of science and scientific inquiry (SUSSI): Revision and further validation of an assessment instrument. Presented at the annual conference of the National Association for Research in Science Teaching (NARST), San Francisco, CA, April 3-6, 2006.

Lim, K. H. (2009), Provoking intellectual need. Mathematics Teaching in the Middle School, 15(2), 92-99. DOI: 10.1080/00207391003605239

Lin, J., G. M. Purdy, H. Schouten, J. C. Sempere, and C. Zervas (1990), Evidence from gravity data for focused magmatic accretion along the Mid-Atlantic Ridge, Nature, 344, 627-632, doi: 10.1038/344627a0.

Lin, J. and J. Phipps Morgan (1992), The Spreading Rate Dependence of 3-Dimensional Midocean Ridge Gravity Structure, J. Geophys. Res. Lett., 19 (1), 13-16, doi: 10.1029/91GL03041.

Magde, L. S., and D. W. Sparks (1997), Three-dimensional mantle upwelling, melt generation, and melt migration beneath segment slow spreading ridges, J. Geophys. Res., 102 (B9), 20571–20583, doi:10.1029/97JB01278.

Magde, L. S., A. H. Barclay, D. R. Tommey, R. S. Detrick and J. A. Collins (2000), Crustal magma plumbing within a segment of the Mid-Atlantic Ridge, 35°N, Earth Planet. Sci. Lett., 175 (1-2), 55-67, doi: 10.1016/S0012-821X(99)00281-2.

Manduca, C. A., and Mogk, D. W. (2002), Using data in undergraduate classrooms. Northfield, MN, Science Education Resource Center, Carleton College: 36.

Marjanović, M., S. M. Carbotte, M. R. Nedimović, and J. P. Canales (2011), Gravity and seismic study of crustal structure along the Juan de Fuca Ridge axis and across pseudofaults on the ridge flanks, Geochem. Geophys. Geosyst., 12, Q05008, doi: 10.1029/2010GC003439.

McCright, A. M., (2012), Enhancing students' scientific and quantitative literacies through an inquiry-based learning project on climate change. Journal of the Scholarship of Teaching and Learning, 12(4), 86-102.

McDonald, M. A. and Fox, C. G. (1999), Passive acoustic methods applied to fin whale population density estimation, J. Acoust. Soc. Am. 105, 2643–2651.

McDonald, M. A., Hildebrand, J. A., and Webb, S. C. (1995), Blue and fin whales observed on a seafloor array in the Northeast Pacific, J. Acoust. Soc. Am. 98, 712–721.

McKenzie, D., J. Jackson, and K. Priestley (2005), Thermal structure of oceanic and continental lithosphere, Earth Planet. Sci. Lett., 223, 337-349, doi:10.1016/j.epsl.2005.02.005.

Michener, W. K., and Jones, M. B. (2012), Ecoinformatics: Supporting ecology as a data-intensive science. Trends in Ecology and Evolution, 27 (2): 85-93. DOI: 10.1016/j.tree.2011.11.016

Miller, T. C., Richardson, J. N., and Kegerreis, J. S. (2016), Using mathematical software to introduce Fourier transforms in physical chemistry to develop improved understanding of their applications in analytical chemistry. Journal of Chemical Education, 93: 299-303. DOI: 10.1021/acs.jchemed.5b00493

Mizroch, S. A., Rice, D.W., and Breiwick, J. M. (1984), The fin whale, Balaenoptera physalus, Mar. Fish. Rev. 46, 20–24.

Mizroch, S. A., Rice, D. W., Zwiefelhofer, D., Waite, J., and Perryman, W. L. (2009), Distribution and movements of fin whales in the North Pacific Ocean, Mamm. Rev. 39, 193–227.

Moore, S. E., Stafford, K. M., Dahlheim, M. E., and Braham, W. (1998), Seasonal variation in reception of fin whale calls at five geographic areas in the North Pacific, Mar. Mamm. Sci. 14, 617–627.

Morgan, J., M. Warner, G. Arnoux, E. E. E. Hooft, D. R. Toomey, B. VanderBeek and W. S. D. Wilcock (2016), Next-generation seismic experiments – II: wide-angle, multi-azimuth, 3-D, full-waveform inversion of sparse field data, Geophys. J. Int., 204, 1342-1363, doi: 10.1093/gji/ggv513.

Moriarty, P. J., Gallagher, B. L., Mellor, C. J., and Baines, R. R. (2003), Graphical computing in the undergraduate laboratory: Teaching and interfacing with LabVIEW. American Journal of Physics, 71: 1062. DOI: 10.1119/1.1582189

Mutter, C. Z. and J. C. Mutter (1993), Variations in thickness of layer 3 dominate oceanic crustal structure, Earth Planet. Sci. Lett., 117, 295-317, doi:10.1016/0012-821X(93)90134-U

Oleson, E. M. (2005), Calling behavior of blue and fin whales off California, Ph.D. thesis, University of California, San Diego, California.

Payne, R. and Webb, D. (1971), Orientation by means of long range acoustic signaling in baleen whales, Ann. (N. Y.) Acad. Sci. 188, 110–141.

Rankin, S., Barlow, J. (2007), Vocalizations of the sei whale balaenoptera borealis off the Hawaiian Islands, Bioacoustics, 16:2, 137-145

Rayleigh, L. (1919), On the problem of random vibrations and of random flights in one, two, or three dimensions, Phil. Mag. J. Sci., 37, 321-346

Rebull, O. G., Cusi, J. D., Fernandez, M. R., and Muset, J. G. (2006), Tracking fin whale calls offshore the Galicia Margin, North East Atlantic Ocean, J. Acoust. Soc. Am. 120, 2077–2085.

Rice, J. A. (1994), Mathematical Statistics and Data Analysis, 2nd Edition, (Duxbury Press, Pacific Grove, CA), pp. 672.

Romanowicz, B., Stakes, D. S., Uhrhammer, R., McGill, P. R., Neuhauser, D., Ramirez, T. M., and Dolenc, D. (2003). The MOBB experiment: A prototype permanent off-shore ocean bottom broadband station, Eos Trans. AGU 84, 331–332.

Rubin, S. J., and Abrams, B. (2015), Teaching fundamental skills in Microsoft Excel to first-year students in quantitative analysis. Journal of Chemical Education, 92: 1840-1845. DOI: 10.1021/acs.jchemed.5b00122

Schimel, D. and Keller, M. (2015), Big questions, big science: Meeting the challenges of global ecology. Oecologia, 177(4): 925-34.

Sempere, J. C., Macdonald, K. C. and Miller, S. P. (1984), Overlapping spreading centres: 3-D inversion of the magnetic field at 9°03′N on the East Pacific Rise. Geophys. J. Roy. Astron. Soc., 79: 799–811, doi: 10.1111/j.1365-246X.1984.tb02869.x

Shaw, P. R., and J. A. Orcutt (1985), Waveform inversion of seismic refraction data and applications to young Pacific crust, Geophys. J. R. Astr. Soc., 82, 375-414, doi:10.1111/j.1365-246X.1985.tb05143x

Shoberg, T. S. Stein and J. Karsten (1991), Constraints on rift propogation history at the Cobb offset, Juan de Fuca Ridge, from numerical modeling of tectonic fabric, Tectonophysics 197, 295-308, doi:10.1016/0040-1951(91)90047-V

Simon, M., Stafford, K. M., Beedholm, K., Lee, C. M., and Madsen, P. T. (2010), Singing behavior of fin whales in the Davis Strait with implications for mating, migration and foraging, J. Acoust. Soc. Am. 128, 3200–3210.

Sirovic, A., Hildebrand, J. A., and Wiggins, S. M. (2007), Blue and fin whale call source levels and propagation range in the Southern Ocean, J. Acoust. Soc. Am. 122, 1208–1215.

Stafford, K. M., Citta, J. J., Moore, S. E., Daher, M. A., and George, J. E. (2009), Environmental correlates of blue and fin whale call detections in the North Pacific Ocean from 1997 to 2002, Mar. Ecol. Prog. Ser. 395, 37–53.

Stafford, K. M., Mellinger, D. K., Moore, S. E., and Fox, C. G. (2007), Seasonal variability and detection range modeling of baleen whale calls in the Gulf of Alaska, 1999-2002, J. Acoust. Soc. Am. 122, 3378–3390.

Stakes, D. S., McClain, J., Zandt, T. V., McGill, P. R., and Begnaud, M. (1998), Corehole seismometer development for low-noise seismic data in a long-term seafloor observatory, Geophys. Res. Lett. 25, 2745–2748.

Strasser, C. A., and Hampton, S. E. (2012), The fractured lab notebook: Undergraduates and ecological data management training in the United States. Ecosphere, 3 (12): 1-18. DOI: 10.1890/ES12-00139.1

Strub, P. T. and James, C. (2002), Altimeter-derived surface circulation in the large–scale NE Pacific Gyres. Part 1. seasonal variability, Pro. Ocean. 53, 163–183.

Thompson, R. E., Burd, B. J., Dolling, A. D., Gordon, R. L., and Jamieson, G. S. (1992), The deep scattering layer associated with the Endeavour Ridge hydrothermal plume, Deep-Sea Res. 39, 55–73.

Thompson, P. O. and Friedl, W. A., (1982), A long term study of low frequency sounds from several species of whales off Oahu, Hawaii, Cetology. 45,1-19.

Tolstoy, M., A. J. Harding and J. A. Orcutt (1993), Crustal thickness on the Mid-Atlantic Ridge: Bull's-eye gravity anomalies and focused accretion, Science, 262, 726-729, doi: 10.1126/science.262.5134.726.

Toomey, D. R., D. Jousselin, R. A. Dunn, W. S. D. Wilcock and R. S. Detrick (2007), Skew of mantle upwelling beneath the East Pacific Rise governs segmentation, Nature, 446, 409-414, doi:10.1038/nature05679.

Toomey, D. R., and E. E. E. Hooft (2008), Mantle upwelling, magmatic differentiation, and the meaning of axial depth at fast-spreading ridges, Geology, 36 (9), 679-682, doi: 10.1130/G24834A.1.

Transnational College of LEX (2012), Who is Fourier? : A mathematical adventure. Cambridge, Massachusetts : Language Research Foundation.

Turcotte, D., and G. Schubert (2002), Geodynamics, 2nd ed., pp. 219, Cambridge Univ. Press, New York.

Van Ark, E. M., R. S. Detrick, J. P. Canales, S. M. Carbotte, A. J. Harding, G. M. Kent, M. R. Nedimovic, W. S. D. Wilcock, J. B. Diebold, and J. M. Babcock (2007), Seismic structure of the Endeavour Segment, Juan de Fuca Ridge: Correlations with seismicity and hydrothermal activity, J. Geophys. Res., 112 (B2), B02401, doi: 10.1029/2005JB004210.

Vanags, T., Pammer, K. and Brinker, J. (2013), Process-oriented guided-inquiry learning improves long-term retention of information. Advances in Physiology Education, 37: 233-241. DOI: 10.1152/advan.00104.2012

VanderBeek, B., D. R. Toomey, E. E. E. Hooft and W. S. D. Wilcock (2014), Segment-Scale Seismic Structure of Slow-, Intermediate-, and Fast-Spreading Mid-Ocean Ridge: Constraints on the Origin of Ridge Segmentation and the Geometry of Shallow Mantle Flow, Abstract V23E-07 presented at the 2014 Fall Meeting, AGU, San Francisco, CA., 15-19 Dec.

Vogt, F. (2011), Data filtering in instrumental analyses with applications to optical spectroscopy and chemical imaging. Journal of Chemical Education, 88(12): 1672-1683. DOI: 10.1021/ed100984c

Wade, R. S., Fredrickson, E., Wilcock. W. S. D., Mellinger, D.K, Nieukirk, S.L., Weirathmueller, M.J., (2015), Tracking blue whales (Balaenoptera musculus) in the Northeast Pacific with seafloor seismometers. Presentation at the 21st Biennial Conference on the Biology of Marine Mammals, San Francisco, December 13-18, 2015.

Watkins, W. A. (1981), Activities and underwater sounds of fin whales, Sci. Rep. Whales Res. Inst. 33, 83–117.

Watkins, W. A., Daher, M. A., Reppucci, G. M., George, J. E., Martin, D. L., DiMarzio, N. A., and Gannon, D. P. (2000), Seasonality and distribution of whale calls in the North Pacific, Oceanography 13, 62–67.

Watkins, W. A., Tyack, P., Moore, K. E., and Bird, J. E. (1987), The 20-hz signals of finback whales (Balaenoptera physalus), J. Acoust. Soc. Am. 82, 1901–1912.

Watson, J. M., Kelly, B. A., Callingham R. A., and Shaughnessy, J. M. (2003), The measurement of school students' understanding of statistical variation. International Journal of Mathematical Education in Science and Technology, 34(1): 1-29. DOI: 10.1080/0020739021000018791

Weekly, R. T., W. S. D. Wilcock, Hooft, E. E. E., Toomey, D. R., McGill, P. R., and Stakes, D. (2012), Termination of a decadal-scale ridge-spreading event observed using a sea floor

seismic network on the Endeavour Segment, Juan de Fuca Ridge, in press, Geochem. Geophys. Geosyst.

Weekly, R. T., W. S. D. Wilcock, E. E. E. Hooft, D. R. Toomey, P. R. McGill, and D. S. Stakes (2013), Termination of a 6 year ridge-spreading event observed using a seafloor seismic network on the Endeavour Segment, Juan de Fuca Ridge, Geochem. Geophys. Geosyst., 14, 1375–1398, doi:10.1002/ggge.20105.

Weekly, R. T., W. S. D. Wilcock, D. R. Toomey, E. E. E. Hooft, and E. Kim (2014), Upper crustal seismic structure of the Endeavour segment, Juan de Fuca Ridge from travel time tomography: Implications for oceanic crustal accretion, Geochem. Geophys. Geosyst., 15, 1296–1315, doi:10.1002/2013GC005159.

Weirathmueller, M. J., Wilcock, W. S., & Soule, D. C. (2013). Source levels of fin whale 20 Hz pulses measured in the Northeast Pacific Ocean. *The Journal of the Acoustical Society of America*, *133*(2), 741-749.

Weirathmueller, M. and Wilcock. W.S.D. (2015). Range estimation using multipath arrivals from 20 Hz fin whale vocalizations recorded in the NE Pacific Ocean. Presentation at the 7th DCLDE Workshop, La Jolla, July 13-16, 2015.

Whitford, D. J., Vieira, M. E. C., and Waters, J. K. (2001), Teaching time-series analysis. I. Finite Fourier analysis of ocean waves. American Journal of Physics 69, 490. DOI: 10.1119/1.1331300

Wilcock, W. S. D., Hooft, E. E. E., Toomey, D. R., McGill, P. R., Barclay, A. H., Stakes, D. S., and Ramirez, T. M. (2009), The role of magma injection in localizing black smoker activity, Nature Geosci. 2, 509–513.

Wilcock, W. S. D, (2012), Tracking fin whales in the Northeast Pacific Ocean with a seafloor seismic network, J. Acoust. Soc. Am. 132(4), 2408-19.

Williams, J. W., Warner, J. L., and Warner, S. P. (2004), Subject-Area knowledge measured by scores on the National Association of State Boards of Geology (ASBOG) Fundamentals Examination and the implications for academic preparation. Journal of Geoscience Education, 52(4): 374-378. DOI: http://dx.doi.org/10.5408/1089-9995-52.4.374

Wysession, M. E. and Baker, S. (2002), An educational animation of the propogation of earthquake-generated seismic shear waves across the mantle. Journal of Geoscience Education, 50(2):186-194. DOI: http://dx.doi.org/10.5408/1089-9995-50.2.186